2022

Design and Analysis of Soft Actuator with Enhanced Stiffness with Granular Jamming

Abbishek Manoj Patel
University of Windsor

Design and Analysis of Soft Actuator with Enhanced Stiffness with Granular Jamming

By

Abhishek Manoj Patel

A Thesis

Submitted to the Faculty of Graduate Studies

through the Department of Mechanical, Automotive & Materials Engineering

in Partial Fulfilment of the Requirements for

the Degree of Master of Applied Science

at the University of Windsor

Windsor, Ontario, Canada

2022

Design and Analysis of Soft Actuator with Enhanced Stiffness with Granular Jamming

by

Abhishek Manoj Patel

APPROVED BY:

_____
M. Khalid
Department of Electrical and Computer Engineering

_____
BA. Schuelke-Leech
Department of Mechanical, Automotive and Materials Engineering

_____
L. Oriet, Co-Advisor
Department of Mechanical, Automotive and Materials Engineering

_____
E. Lang, Co-Advisor
Department of Mechanical, Automotive and Materials Engineering

September 13, 2022

Declaration of Originality

I hereby certify that I am the sole author of this thesis and that no part of this thesis has been published or submitted for publication.

I certify that, to the best of my knowledge, my thesis does not infringe upon anyone's copyright nor violate any proprietary rights and that any ideas, techniques, quotations, or any other material from the work of other people included in my thesis, published or otherwise, are fully acknowledged in accordance with the standard referencing practices. Furthermore, to the extent that I have included copyrighted material that surpasses the bounds of fair dealing within the meaning of the Canada Copyright Act, I certify that I have obtained a written permission from the copyright owner(s) to include such material(s) in my thesis and have included copies of such copyright clearances to my appendix.

I declare that this is a true copy of my thesis, including any final revisions, as approved by my thesis committee and the Graduate Studies office, and that this thesis has not been submitted for a higher degree to any other University or Institution.

Abstract

The field of soft robotics has been increasing popularity and importance in last decade with its groundbreaking applications in the field of delicate food handling industry and rehabilitation of limbs and fingers of stroke affected patients. The area of soft robotics seeks to improve robot safety, allowing them to function in circumstances where standard robots cannot.

This research is focused on pneumatically actuated soft robots as they are efficient, easily controlled, affordable, and well researched. These robots consist of one or more soft actuators, made of silicone elastomers with low material hardness. Low hardness silicone actuators are structurally weak and cannot generate functional forces, which can be rectified by simply increasing the hardness of the material, resulting in compromising softness of the robot. This research attempts to provide a solution to increase structural stability and force output of soft actuator without compromising softness of the material. These were achieved in two ways; one, by improving the cross-sectional profile of the actuator, with an addition of vacuum functionality which increases degree of freedom by one. Two, by attaching a granular jamming component to the actuator, which can change its stiffness actively based on the vacuum applied to it.

In this research, the soft actuator was made of Eco-Flex 00-30 silicone and ground coffee was used as granular material for jamming. The actuator was designed on CATIA, and simulation analysis was carried out in ANSYS. A simulation study is conducted to optimize the design parameters to improve bending angle. The jamming components are attached on either side of the actuator and filled with ground coffee which provides controlled stiffness. The actuator was fabricated by molding, all molds are 3D printed with polylactic acid. The actuator was powered by an electric air pump. The actuator is evaluated for bending angle and blocking force at the tip. 280% more bending was achieved under vacuum when compared to conventional design. The blocking force was increased by 270% upon implementing jamming component. The force output obtained per unit pressure applied when compared to present literature increased by 4 times. Lastly, these methods can be implemented to improve the performance of any soft pneumatic actuators.

Dedication

I would like to completely dedicate this work to my parents, Malini and Manoj Patel. I cannot imagine this journey without their love and support. They always inspire me and are source of my strength.

I would also like thank my friends who helped me in any way possible, emotionally, and academically.

Acknowledgement

Gratitude to all my committee members for taking out their valuable time to read my manuscript and giving crucial suggestions. I would like to thank my thesis advisors, Dr Leo Oriet and Dr Edward Lang, at the University, for their invaluable support and trust in the decisions I made. I would also like to thank my committee members Dr Beth-Anne Schuelke-Leech and Dr Mohammed Khalid, for their important insights and suggestion in this research. I would also like to thank my classmates and colleagues for their support and assistance during this research.

Table of Contents

List of Tables

List of Figures

xvii

List of Appendices

List of Abbreviations

STEM	Science, Technology, Engineering, Mathematics
DoF	Degree of Freedom
CAD	Computer Aided Designing
SPA	Soft Pneumatic Actuator
PAM	Pneumatic Artificial Muscle
PBA	Pneumatic Balloon Actuator
PneuNet	Pneumatic Network
sPN	slow Pneumatic Network
fPN	fast Pneumatic Network
SMA	Shape Memory Alloy
ERF	Electrorheological Fluid
EAP	Electro-active Polymer
MRE	Magnetorheological Elastomer
IPMC	Ionic Polymer-metal Composite
MEMS	Microelectromechanical Systems
STEP	Standard for the Exchange of Product Data
PLA	Polylactic Acid
FDM	Fused Deposition Modeling
PWM	Pulse-width Modulation
ANSYS	Analysis of Systems

Chapter 1 Introduction

Robotics is a collaboration of many fields not only from STEM but also from Arts, which include design, mechanical engineering, electronics engineering, and computer engineering. These fields combine to make automatic machines that help perform repetitive tasks with more precision and repeatability and can also help in a dangerous working environment. Many of these robots are inspired by mammalian limbs, which have an arm-like structure analogous to the human hand with joints like the shoulder, elbow, and wrist.

Scientists keep going back to nature for inspiration to develop something which can achieve the best abilities from the best living examples. Therefore, we try to make robots that can fly like a bird, think, and solve problems like humans, run as fast as a cheetah, and end effectors perform tasks as dexterously as a human hand and as flexible as an octopus. All of these are notable examples and evidence of biomimicry and whether we can achieve them or not.

1.1 What is "Soft Robotics"?

Soft robotics is a new field of robotics, the goal of which is to make robots from a soft and flexible materials like silicone, rubber, plastic, fabric, and other polymers, which allows greater freedom of movement, instead of conventional robots with a hard body. Distinguishing properties of hard and soft robots are shown in Table 1. Soft robots are also made from hard materials which are deformable like spring and origami structures. Soft robotics is broadly in the same field as biology-inspired robotics, which aims to mimic organisms in nature. To be classified as a soft robot, a machine must be made primarily of soft material or consist of soft actuator working with hard robotic components in a way that the interaction of the robot with its environment is soft in characteristic which provides safe interaction with objects or humans. Soft actuators are devices mainly made of soft materials which produces motion which can be linear, rotational, tortional, or

1

a combination of these motions in one of more planes. In this research, we have focused on soft

pneumatic actuators (SPA) which are made of compliant material like rubber, silicone, or a flexible

polymer. Usually, SPAs are inspired from human fingers and produces continuous bending when

actuated with air pressure.
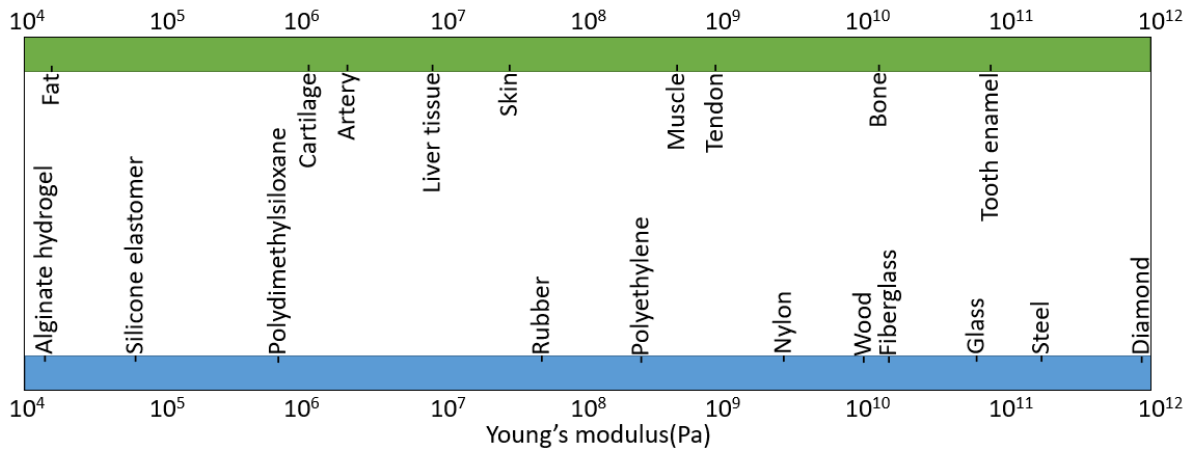
Figure 1. Approximate tensile modulus (Young's modulus) of selected engineering
(blue) and biological (green) materials [1]

To understand the soft nature of the material in accordance with biological and manmade materials,

a comparison is drawn in Figure 1 on a spectrum of young's modulus. The young's modulus shown

in the figure are approximate as most of the material related to human body are non-linear materials.

Table 1. Distinguishable features of soft and hard robotics.

Soft Robotic System	Hard Robotic System
Made from soft, flexible, and stretchable material	Made from hard/conventional engineering material
Compliance nature facilitates ease in environment adjustment	Requires advanced feedback control system for safe operation within the environment
Continuum in nature with infinite degree of freedom	Discrete topology with finite degree of freedom

Soft Robotic System	Hard Robotic System
Inherently safe, adaptive, and tolerant in unknown environments, and human-machine interaction	Unsafe and intolerant with limited adaptability to operate in unknown environments unless intricate control measures are applied.
High level of bio-inspiration	Low level of bio-inspiration
Very diverse	Very specific types of motion
Low accuracy can be tolerated.	Requires very high accuracy
Low speed and low force applications	High speed and high force application
Lightweight and economical	Heavy and expensive

1.2 Soft Pneumatic Actuator

Soft actuators are devices that converts one form of energy into useful dynamic movements like push, pull, rotation, revolution, expand and contract. SPA uses pneumatic pressure energy as source and converts it into useful energy. Pneumatic pressure energy is generated by a pump or an air reservoir. Most common SPAs, like Pneumatic network actuators, balloon actuators, pneumatic artificial muscle, etc. uses air pressure to inflate pneumatic chamber to generate motion, usually, bending. These soft actuators are continuous actuators, meaning the actuation do not take place at one particular point instead, this happens continuously along a line or surface and therefore, these actuators act as a combination of an actuator and link. Silicon elastomers are the most common material for manufacturing SPAs.

The need of grasping function is undeniably important, and it is essential to carry out multitude of tasks from holding a chopstick to holding a surgical tool. Soft actuator's primary function is to gasp, hold and release an object by itself or by combining two or more actuators. Engineers have found a way to use SPAs in the field of rehabilitation. Stroke survivors around the globe suffers from some kind of disability, including losing partial motor control on their limbs [2]. In disabilities

related to hand and finger, a physiotherapy is needed from a professional, which could lead to huge financial problem. Researchers have developed a SPA, which could be attached to the wrist and help move fingers in given direction upon use. This would help patients greatly in getting their treatment on time and whenever necessary. Similar application can be found in the field of surgical robotics, where researchers have developed mini soft actuators to handle small surgical tools and living tissues to impart minimal damage [3]. Also, soft actuators or soft grippers when used in food industry, provides greater feasibility in handling delicate food products, fresh produce, etc. with less complicated control system.

Silicone used for SPA is very soft and can deform easily. Because of it having a high strain rate and elasticity, the material regains its original form on removal of external load. The softness of the material causes the SPA to deform on its own weight. To overcome soft material deformation problem, we can increase the hardness of the material, but doing so defies the soft nature of the soft actuator. In this thesis, we have discussed about ways to improve the performance of the soft actuator without changing its hardness. One of the focuses is on the improving design of the conventional soft actuator and obtain better load carrying capacity without changing initial pressure requirement.

1.3 Problem Statement

The primary characteristic of a soft actuator is the soft nature. Soft nature can roughly be defined as soft or safe interaction of the actuator with external environment with soft material [4]. These soft materials, usually silicone elastomers have very low hardness. However, as the hardness of the silicone decreases, the actuators start losing their structural integrity which in turn reduces force imparting capability. To avoid these, silicone with higher hardness is used, which compromises on the softness of the actuator.

To improve the performance, the importance is given to two main criteria – bending angle and holding force [5-8]. Bending angle is a measure of how much movement can be obtained for a given pressure and holding force is a measure of how much an actuator can carry for a given pressure.

1.4 Thesis Objectives

This research was aimed to achieve performance improvement of bending angle, bending under vacuum, force exerting capabilities through design improvement and implementing granular jamming component.

Aims of this research includes:

- Studying current literature on soft actuators to learn current methods and designs and their advantages and disadvantages.
- Evaluating material properties of Eco-Flex 00-30 for material modelling, which is used for simulation studies.
- Conceptualizing and designing on CAD, evaluating design parameters and their effects on bending angle.
- Fabricating the soft actuator with molding and designing molds for 3D printing.
- Fabricating granular jamming components and attaching it to achieve stiffness enhancement by controlling the degree of vacuum.
- Building experimental setup for actuator operation and performance evaluation. Comparing theoretical, simulation, and experimental data.

1.5 Thesis Outline

Chapter 2 contains a detailed literature review on different types of soft robotic actuators and their actuation methods. A number of manufacturing methods are also discussed in this chapter followed

by granular jamming. It also includes comparisons between different types of actuators and actuation methods. Lastly, it discusses on evaluation parameters used in this research. Chapter 3 describes the methodology followed in this thesis. Chapter 4 contains the material modelling of Eco-flex 00-30 for simulation study. Selection of best hyperelastic model for the silicone elastomer. Chapter 5 discusses on design of the actuator. It includes discussion on geometry, simulation study, and parameter optimization from simulation study. A brief discussion on theoretical model is also drawn. Chapter 6 includes method of fabricating the soft actuator and jamming component. Description on an electric and pneumatic setup for operating soft actuator and conducting experimentation is also made in this chapter. A discussion is made on the research findings. A gripper is also developed in this study. Chapter 7 contains concluding statements with summary on the contribution of this research. it also explains potential applications of this actuator and future work.

Chapter 2 Literature review

2.1 Introduction

Actuators are devices that convert one form of energy into useful mechanical output. Soft actuators can move more flexibly when compared with conventional actuators [1]. Human muscles are the most efficient and versatile actuators, and scientists have been trying to develop something on par with them [9]. Soft actuators can be classified into the following categories based on their actuation method:

- smart material actuators (shape memory alloy, electrorheological, electro-active polymers, and magnetorheological elastomers)
- soft fluidic actuators (pneumatic and hydraulic actuators)
- compliance-based actuators

This chapter entails a comprehensive literature review on the prior art, which includes several types of soft actuators, their design requirements and discusses the challenges and limitations of current devices. This helps in better understanding of their working and potential to improve. It also reviews some of the common manufacturing techniques which leads to choosing a suitable manufacturing technique for this study.

2.2 Soft Fluidic Actuators

Soft fluid actuators are the starting point for the field of soft robotics. Though the first actuation method, it is still being used widely in a multitude of applications because of a number of advantages like ease of fabrication, cost-effectiveness, robust nature of materials, affordability of the materials, versatility, and biocompatibility. There are two types of fluidic actuators: hydraulic and pneumatic.

2.2.1 Soft Pneumatic Actuators

The basic design of a soft pneumatic actuator (SPA) consists of a chamber-like structure made with highly deformable materials. The bending motion of such actuators is obtained by keeping the geometry asymmetric or the materials anisotropic. The difference in the degree of expansion can be achieved by constraining the shape of the chamber with geometry or by using a different material [10]. The range of motion obtained by pneumatic actuators is also impressive as some the actuators can extend twice its length [15] and make a 360 degrees of rotation [27]. Not only that, but the forces obtained compared to supplied power are also exceptionally high, meaning a high power density [10, 11]. For example, studies have found that with a pressure of 300 kPa, a force of 80 N, and with 200 kPa, 112 N can be obtained [2, 12]. The limitations on the bending angle are implemented by the maximum allowable strain of the materials. Some soft pneumatic actuators can also perform at high speeds, achieving a bending angle of 300 degrees in a reaction time of approximately 0.05 to 0.1 seconds [3, 13]. Various factors affect response time like pump/compressors characteristics (pressure-flow rate characteristics), material stiffness, and chamber's internal volume. The SPAs are usually driven by positive pressure, but they can also be actuated with vacuum. The vacuum can provide an extra degree of freedom to the actuator. These SPAs are actuated through pneumatic pump of an air pressure reservoir.

2.2.1.1 Pneumatic Artificial Muscles

Pneumatic artificial muscles or PAMs are developed and researched to obtain human muscle-like actuators. The actuator consists of an inflatable chamber which is restricted with the help of pleated material. The pleating is performed in a way that would restrict the expansion of the surface area. When this entity is inflated under a restricted surface area, the expansion of volume forces the chamber to attain a shape of maximum volume for a given surface area, and that is a sphere [14]. Resulting in achieving contraction linearly as shown in Figure 2.

Figure 2. PAM in inflated and deflated state [15]

One of the most known PAM is McKibben muscle shown in Figure 3. This muscle type has been researched for over 50 years [16, 17]. McKibben invented this muscle as an orthotic device and was successful in using it in a prosthetic device [18]. McKibben type muscle had a braided sleeve on inflated chambers which were powered by compressed air. The braided sleeved over a rubber diaphragm concept was derived from the patented design by Morin (1953) [19]. The implementation of this sleeve not only made the entire procedure simple but also added structural integrity to the actuator. The braided sleeve is connected to both ends of the enclosure. The volume enclosed can be obtained by using equation (1). Where V is the volume of the inflated chamber, l_s is the length of each thread of the braid, n is the number of times each thread is encircled about the tube, and θ is the pitch angle of the thread.

$$V = \frac{l_s^3}{4\pi n^2} \cos \theta \sin^2 \theta \qquad (1)$$
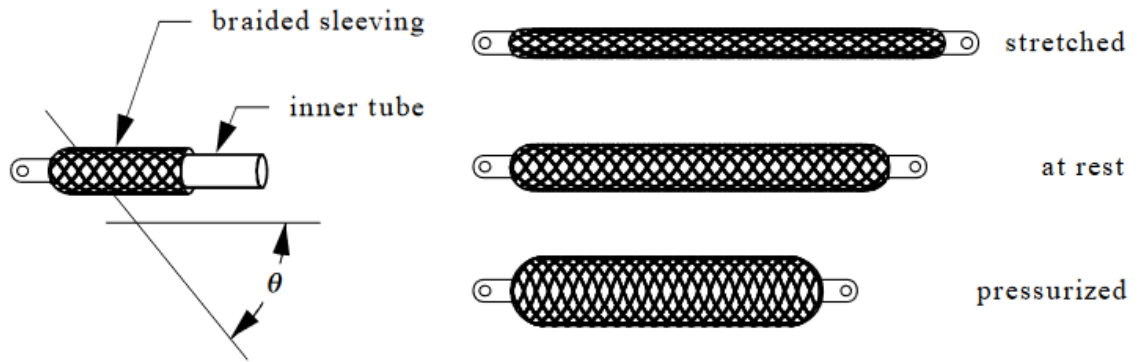
Figure 3. McKibben Muscle [18]

Many scientists have applied McKibben muscle actuators as principal actuators in their research and produced devices like 'Blackfinger' [9], prosthetic glove [20] and 'shadow hand' [21].

2.2.1.2 Pneumatic Balloon Actuator

Pneumatic balloon actuator or (PBA) are widely used in micro soft robotics because of its features like light weight, intricate structure development and flexibility. The basic concept of PBA is having a balloon like structure on the actuator which swells up, usually with pressurized air and with one wall constrained. This leads to bending in the opposite wall and making the entire actuator bend. This was perfectly demonstrated by Satoshi Konishi et al. [22, 23] with flexible layers made up of silicone and constraint layers made of polyimide.
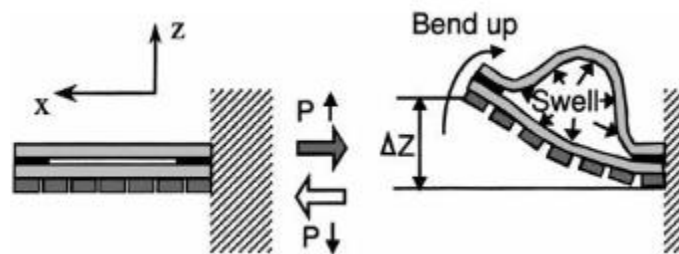
Figure 4. Working principle of Pneumatic balloon actuator [22]
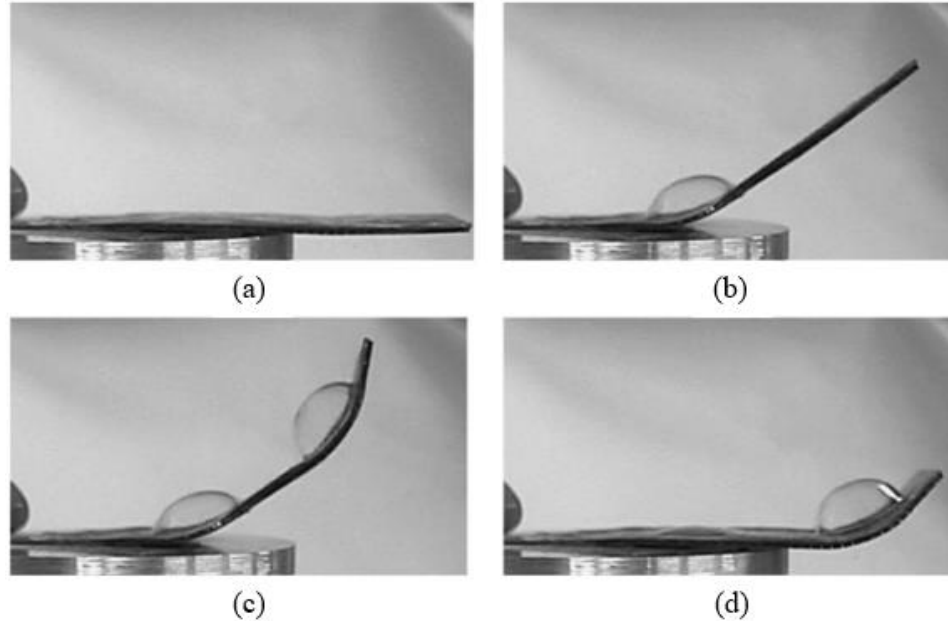
Figure 5. Sequence of working of 2-DoF actuator; (a) not in operation, (b) balloon 1
is in operation, (c) balloons 1 and 2 are in operation, (d) balloon 2 is in operation
[22]

Scientists who focus their work on micro actuators have taken a liking to PBAs and therefore a significant number of micro actuators and sensing systems are developed using principle of PBA [24, 25]. Also, as depicted in Figure 5, with introducing more joints, in this case the joint being another balloon (actuator) make it more feasible to be used as a gripping mechanism. The dual-actuator system, which is inspired by human finger can also be used as mechanical levers and valves in micro-mechanical systems. It also has potential in surgical robotics technologies [24].

2.2.1.3 Pneumatic Network Actuators

Pneumatic network actuators or commonly known as PneuNet actuators are the most researched and widely used actuators. PneuNet actuator are a network of small pneumatic chambers connected, usually in a linear fashion to form a structure that gives bending actuation when pneumatically actuated. The pneumatic actuation can be positive pressure or negative pressure depending on design parameters and requirements. These actuators are similar to pneumatic balloon actuators in

principle. They can be described as a chain of PBA, which in turn gives better actuation. PneuNets are usually made from silicone-based polymers. The individual chambers in these networks can be actuated individually by miniature pump, to obtain specific actuations such as spider like soft robot developed for rigidity and resilient remote operation [26].
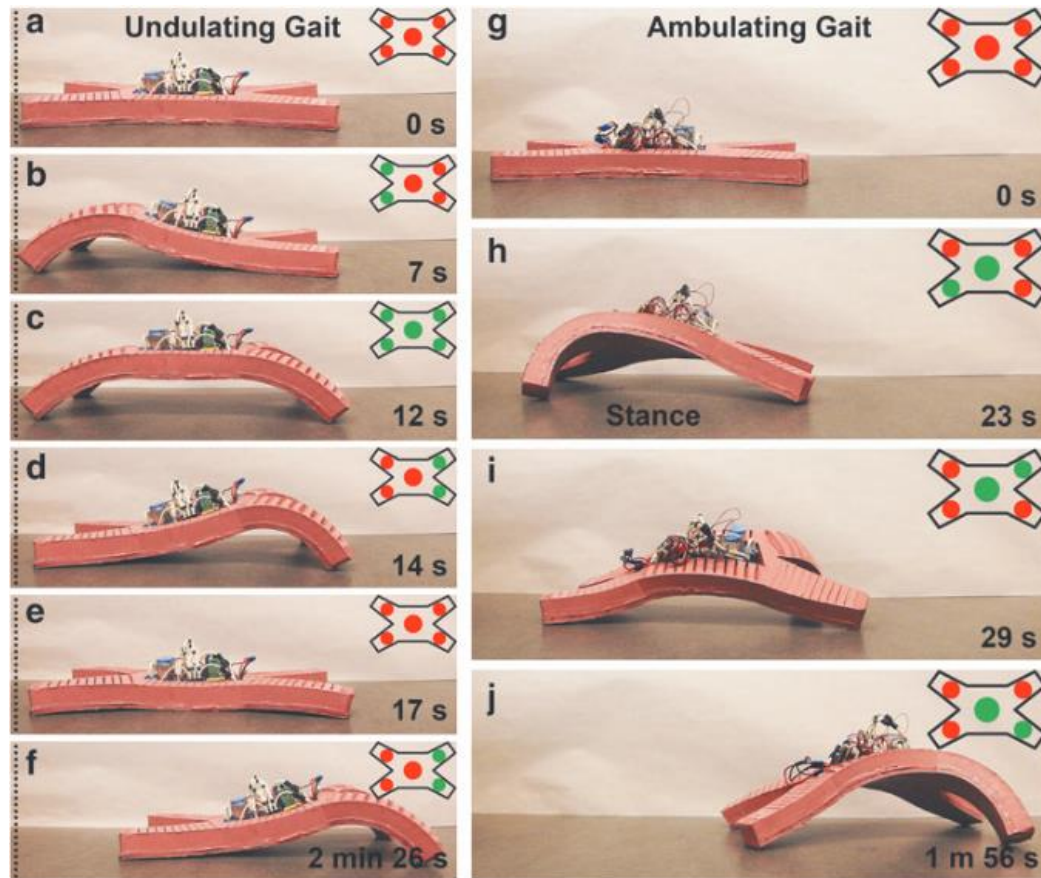
Figure 6. Undulating and ambulating gait locomotion obtained by individually controlling different networks with onboard compressor [26]

The study done by Mosadegh B. et al., [27] has performed an interesting study where they have compared two types PneuNet actuators and based on the outcome they were named as slow pneumatic network and fast pneumatic network. These studies were done for high-speed actuations (multiple actuations in one second). The construction of slow PneuNet actuator is shown in Figure 7 (A). the individual chambers were connected to each other whereas in fast PneuNet actuators the

12

chambers were separated from one end as shown in Figure 7 (B). When the chambers are connected to each other, the stress developed in one chamber is exerted by the chambers adjacent to it, which in turn slows down the expansion and increases the pressure required for obtaining a particular expansion volume when compared to fast pneumatic network actuator.
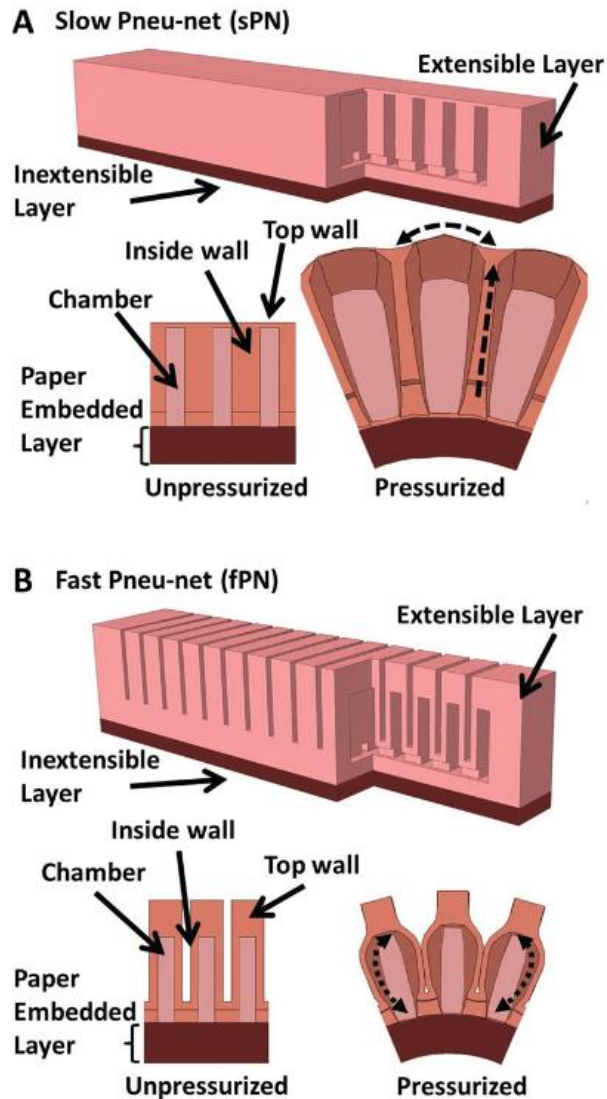
Figure 7 . Construction and working of slow (A) and fast (B) pneuNet soft actuators [27]
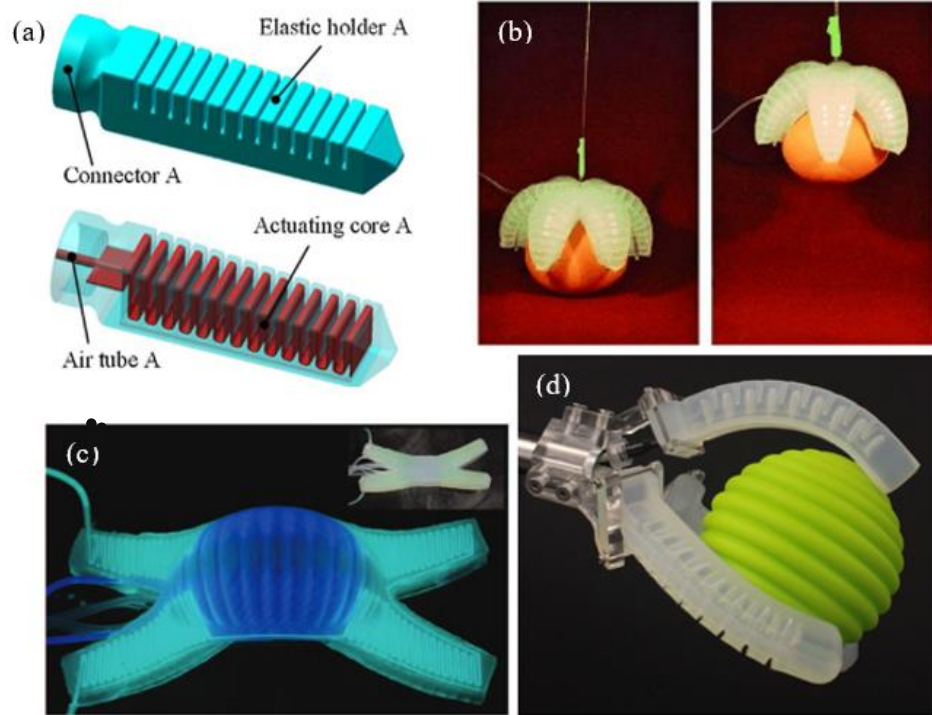
Figure 8. (a) A soft robot with hard actuating core and soft shell [28], (b) soft robotic gripper made from a single actuator [29], (c) Spider-like soft robot made with camouflage properties to blend in the environment [30], and (d) Three fingered soft robotic actuator [31].

There are other types of PneuNets actuators with novel designs which provides them with unique abilities and applications. A SPA is developed by a combining fiber-reinforced inner core which is responsible for generating motions for the actuator and a soft shell made of silicone elastomer to provide softness [28] as shown in Figure 8 (a). This actuator is larger in size compared to most of the developed actuators and has by far, the highest force delivering capabilities. Gripper is developed by combining multiple actuators [31] or can be made from a single actuator [29] as shown in Figure 8 (b), (d). These grippers can be used as pick and place end-effectors for robots. The soft nature of the grippers allows it to handle delicate objects. The gripper which itself is an actuator is a unique idea and shows the potential of soft robotics. The SPAs have advantages such as affordability, easy manufacturability, and compatibility with the environment. They are also very

versatile and can be adapted and modified according to the problem statement. This research focuses on one of a kind pneumatic network actuator.

2.2.2 Hydraulic Actuators

Hydraulic actuators work similarly in principle to pneumatic actuators. The major difference in the working of the hydraulic actuators is the use of the principal fluid. The liquid medium is incompressible in nature and has different properties. The hydraulic actuators can give precise actuation and are also capable of delivering actuation with high force output. Okayasu et al. have developed a soft surgical robot with five degrees of freedom. This robot was developed to perform in a very precise way, and they were able to obtain good results with hydraulic actuators [32]. Biomimetic fish robots are very useful in monitoring marine life and operations like deploying sensors and collecting data from an aquatic environment. Researchers are developing such robots with the help of hydraulically actuated soft robots, as shown in Figure 9 [33, 34].

The fish-inspired robot is completely mobile and fully actuated hydraulically [34]. It has an onboard pump and valve system to move the fluids in the required directions. This soft-bodied robot is completely autonomous and can swim in 3 directions. This robot also has a battery and a control system on board. The fins are also powered hydraulically. The oscillating motion of the rear fish body is achieved by circulating water in the internal channels of the fish body. This motion provides forward propulsion and yaw motion to the robot. Similarly, a soft robot inspired by cephalopods is designed around hydraulic actuation [33]. This robot uses a soft propeller and soft tentacles to generate thrust. The steering is achieved by four soft actuators placed inside the main body.

There have been various studies of developing hydraulic actuators for the application in surgical robotics like hydraulic forceps for minimally invasive surgery [35] and catheter [36]. The hydraulic actuation is very commonly used in industries and has a very wide range of applications with one major disadvantage which is working pressure as high as 30 MPa [37].

15
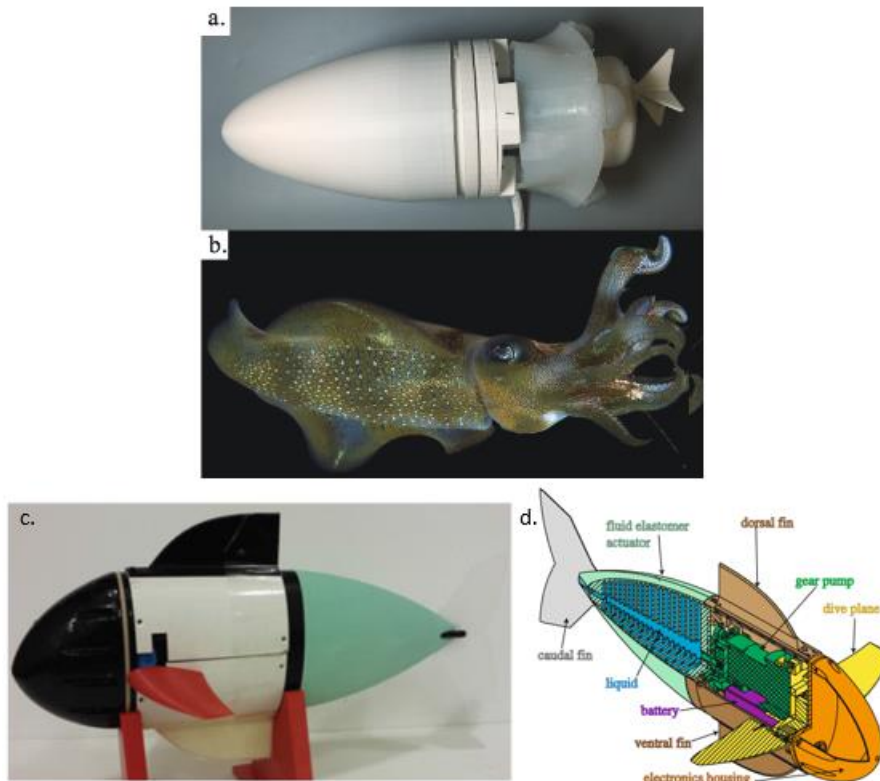
Figure 9. A biomimetic soft robot inspired by Cephalopod (a, b) [33] and a soft robot inspired by fish (c, d) [34]

2.3 Tendon-Driven Soft Actuators

Tendon driven actuator also known as tension cable actuators are inspired by mammalian fingers, the working mechanism comprises of multiple links, these links are connected together usually with the help of pin joints and that makes in more like fingers. These links are connected to base with cables or tendons to perform actuation. The links can be connected to the base individually or all together depending on the design requirement. When connected individually, all links can be controlled separately, and this can be helpful in achieving multi-dimensional maneuvers whereas, when entire finger is connected with one cable it gives underactuated motion which is more like human finger. This allows for simpler cable actuation methods and controls. The joints are also

equipped with a spring like mechanism for retracting links of this finger to its home position. This type of actuators is easy to build and cheaper but less versatile when compared to soft fluidic actuators.
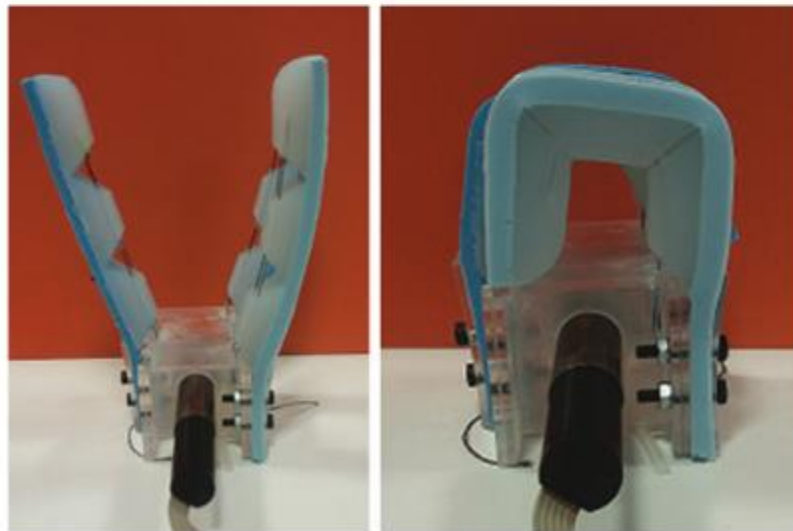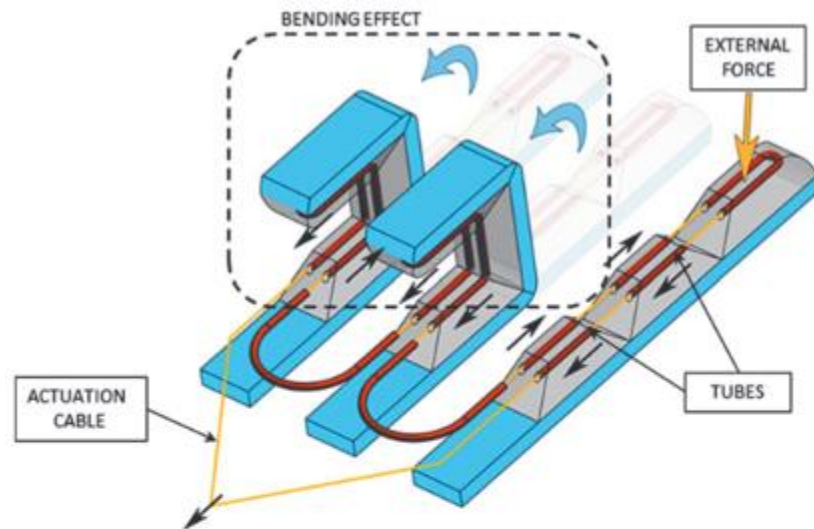
Figure 10. Tendon driven soft actuator and gripper [38]

One of the examples of tendon driven actuator given by Manti et al., is shown in Figure 10. This design uses two materials for fingers, one is harder rubber which is shown in blue color and the softer silicone elastomer is translucent. The softer part provides larger surface area on contact which

results in better gripping whereas, the harder part provides strength to the body of the actuator. There are many developments in making a tendon driven human hand like grippers, which are made with molding or 3D printed with hinges integrated monolithically into the molding process [38, 39].

2.4 Smart Material Actuators

Actuators made from smart materials like shape memory alloys (SMAs), electrorheological fluids (ERFs), electro-active polymers (EAPs), and magnetorheological elastomers (MREs) are discussed in this section. Their advantages and limitations are also described.

2.4.1 Shape-memory Alloy Actuator
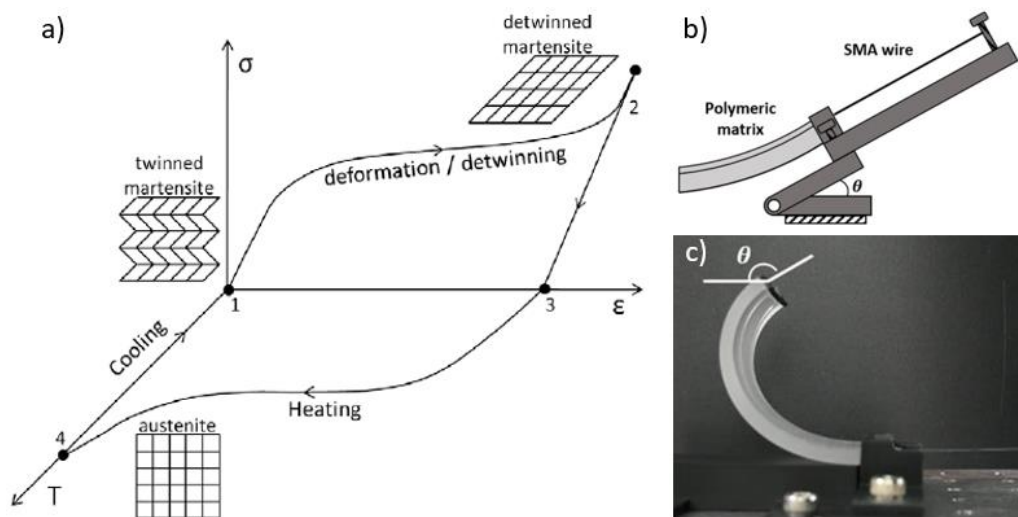
Figure 11. a) Shape memory effect with twinned martensite phase at point 1, deformation is created with external load (1-2), plastic deformation retained (detwinning) after removing load (2-3). Increasing temperature changes the phase to austenite and original shape is obtained (3-4), which remains same even when temperature reduces (4-1), b) a soft actuator using SMA as a tendon to for actuation, c) SMA driven actuator in action [40].

18

SMA has unique property of returning to its shape after plastic deformation. When enough force is applied, the material deforms plastically and regains its shape when heat is applied. The main characteristic of SMA is, it can remember the original shape even after deformation and can get back to its original shape with simple mechanism. This actuation can be exploited to be used in locomotion and grasping techniques [41]. The locomotion can be achieved by using inchworm like movement [42]. SMAs unlike, other metals have two different phases, and they are temperature dependent. There is a high temperature phase called austenite and low temperature phase called martensite.

Working concept of SMA is described well in Figure 11. Most commonly used SMA is nickel titanium alloy with high active stress and strains up to 5% [43]. The metallic property of this alloy allows it to be drawn in a wire with diameter of 25-500 μm, which can be further coiled to transform it into a spring. This spring exhibit compliance and large actuation with up to 50% linear contraction [44]. SMA are very versatile in nature but when it comes to performance, the efficiency of this actuators is relatively low. When heating most of the energy is consumed by the wire and if heated to higher temperatures, the wire can easily be damaged. Therefore, researchers are focusing on improving efficiency of this actuators.

2.4.2 Electro-active Polymers

Electro-active polymers or EAPs are smart materials, which are stimulated electrically. This is a very attractive option for soft actuators and sensors as these are very flexible, economical, bio-compatible, noiseless, and easy to fabricate and power efficient [45]. These features are ideal for soft robotics applications and EAPs are also suitable for artificial muscle [46]. EAPs deform its shape or size when under electric fields and can produce large displacement under high forces. Because of these, EAPs are used in actuators and sensors.

Another classification of EAPs, is ionic EAPs, where the actuation is driven by movement of ions. Ionic EAPs are operated under low voltage and are very suitable as micro soft actuators. Also, these actuators are found to be very similar to human muscle and are getting more attention because of that [47]. However more research is required to obtain efficiency, and reliability. Ionic polymer-metal composites (IPMC) also fall under this category. IPMC actuators are used getting popular with researcher working on bio-mimetic underwater soft robots [48-51].
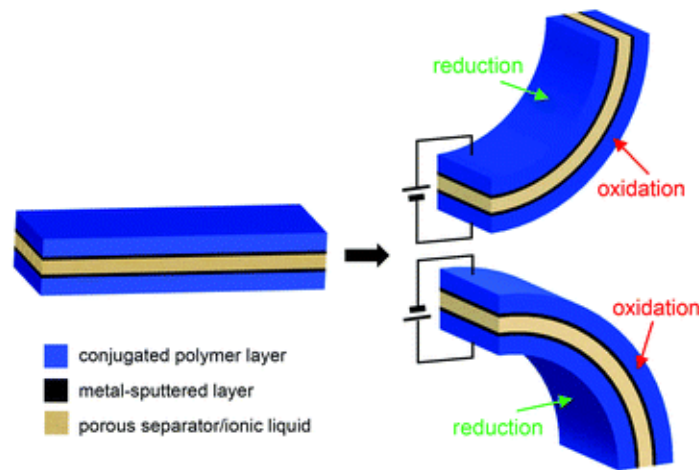
Figure 12. Oxidation-reduction based EAP [52]
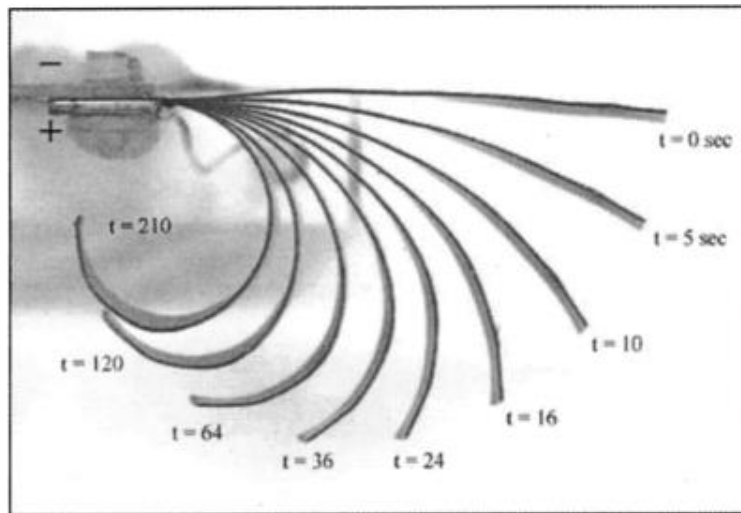
Figure 13. Compiled photo of successive movement of Flemion-based IPMC; the movement is continuous [53].

2.4.3 Electrorheological Fluids

Electrorheological fluids or ERFs can be classified into two types, homogenous and heterogenous. The mechanism of working of homogenous fluids are not known with certainty. The heterogenous ERFs consists of non-conductive but electronically active very fine particles of up to 50 micrometers in diameter, suspended in electrically non-conductive fluid. An external electric field is used to induce dipoles in the fluid. the particles align themselves with the field lines of the electric field making chain-like structures. This so-called chain model according to Winslow [54] is the simplest structural model for explaining the electrorheological effect. The rheological behavior of such fluids can be explained macroscopically using the Bingham model. As a result of this the viscosity of the fluid changes drastically on an application of external electric field.
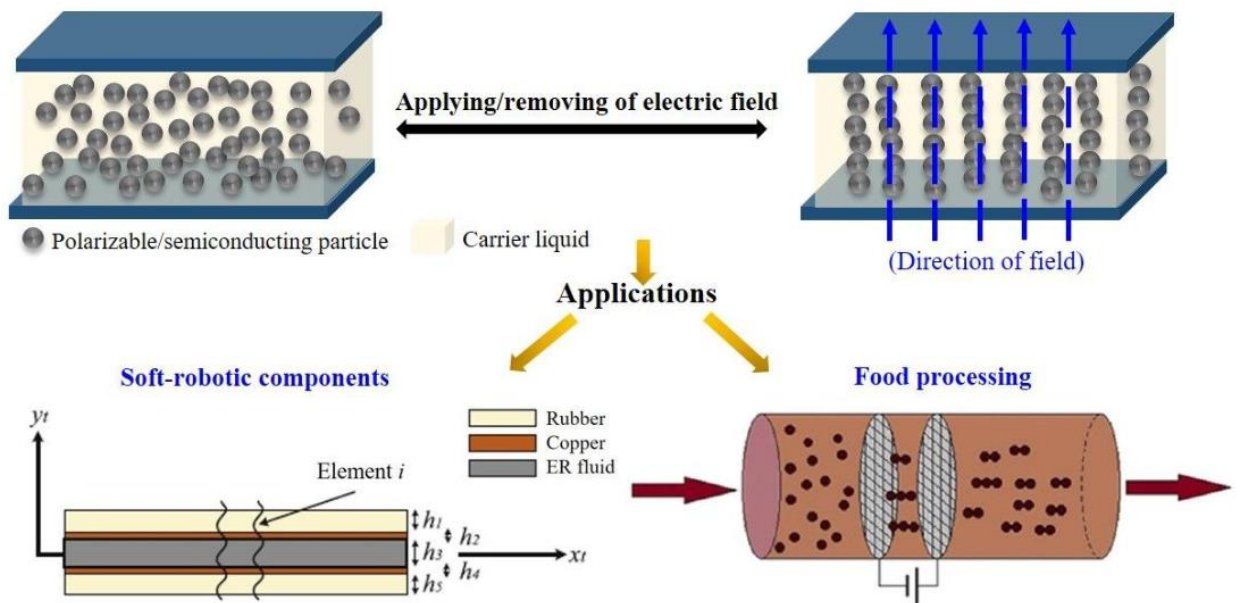
Figure 14. Effect of ERFs in active electric field and its application as a soft robotic component and food processing component [55]

In Figure 14, it can be interpreted that the suspended ERF in the soft robotic component can have varying stiffness with change in viscosity, which can be controlled by altering electric field across the component. In food processing, Tao et al. introduced a very innovative idea of applying electric

field in the direction of flow (liquid chocolate), which reduced the viscosity and by aligning

particles as shown in Figure 14 and it resulted in decreasing fat by 10-20 % [56].

2.4.4 Magnetorheological Elastomers

Magnetorheological elastomers (MREs) are magnetorheological fluid or particles embedded in

elastomers to obtain the magnetorheological effect. This is comparatively new branch in the field

of smart material and has very limited studies that are related to soft robotics. The control of

viscoelastic properties with the help of magnetic field applied externally is called

magnetorheological effect [57]. This effect shares similarities with electrorheological effect.
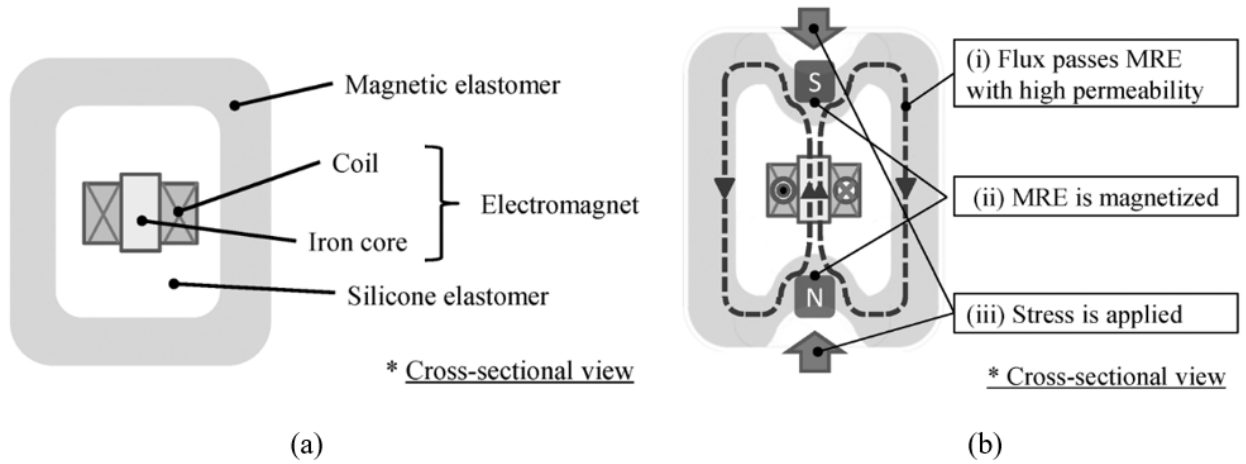
Figure 15. (a) cross-section view of the structure of the actuator, (b) operating
principle of the actuator [58]

Figure 15 shows a novel design of MRE based actuator. In Figure 15 (a) shows the cross-sectional

view of this actuator where the silicone elastomer is covered by magnetorheological elastomer. The

silicone elastomer encapsulates the ferrous core which is covered by electromagnetic coil. The

electromagnetic coil is activated to magnetize the ferrous core. The magnetized ferrous core

produces magnetic flux which passes through MRE and produces stress to dynamically control the

compression on the silicone elastomer as shown in Figure 15 (b).

2.5 Granular Jamming

2.5.1 Introduction

Granular or particle jamming is a very unique property of granular material. When particles of a granular material are filled in a sac or bladder and placed under vacuum, the particles tend to come close to each other. This leads them to fall them into the voids between the particles, and as the voids are filled with particles pulling towards each other, the space between these particles reduces. This allows them to fall into crystal like formation and act like solid as shown in Figure 16. Because of that, the particles in a sac under vacuum is also known as pseudo solid.
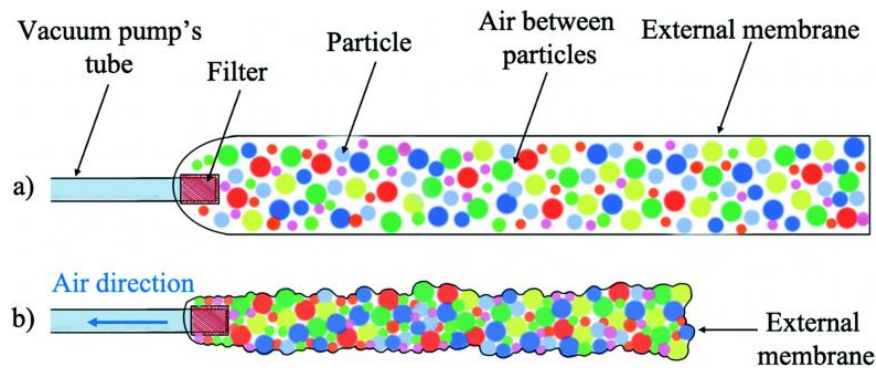
Figure 16. Granular particles in a sac, a) without vacuum, b) under vacuum [59]

Granular jamming has found its way to the field of soft robotics in a very unique invention as a universal gripper. The particles when put in a sac has no definite shape or structure, it is more like fluid than solid. But when it is put under vacuum, it acts like solid with increased stiffness. This also applies for its shape and structure. The sac can be shifted to any shape when in normal, unactuated state and acquires and remains in that shape upon application of vacuum.

2.5.2 Passive Particle Jamming
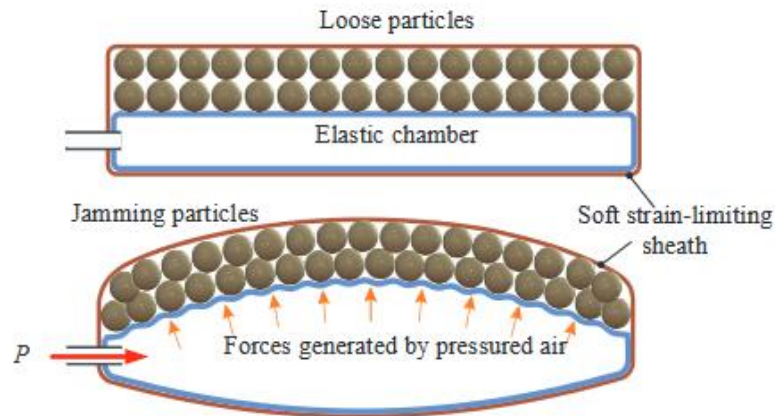
Figure 17. Particle jamming through positive pressure (passive jamming) [60]

Vacuum is not the only method of obtaining particle jamming. As the principle behind the jamming is making all the particles to getting close to each other and forming a crystal-like structure. This can be achieved passively by putting granular particles in a chamber, which is attached to the pneumatic chamber parallelly as shown in Figure 17. When the pressure in the pneumatic chamber is increased, it inflates. This inflation of the chamber imparts pressure on the particle chamber through expansion and bending, which causes particle jamming. This principle is used to design novel soft actuators [60,61]. The working of this actuators is very simple. As the actuator is pressurized and bend, the stiffness of the actuator increases, leading to dynamic change is stiffness. But as the stiffness increases, the actuator needs more pressure to bend itself, which limits the bending capabilities.

2.5.3 Ball Joint with Particle Jamming

Granular jamming enables the controlled stiffness, as its stiffness can be controlled by varying the degree of vacuum. Taking advantage of this property Wei Y et al., in their research of "a soft robotic spine with tunable stiffness" develops a unique spine made from a number of small links connected together with ball joints as shown in Figure 18. This spine is enclosed by a flexible membrane and

filled with granular material as shown in Figure 18 c). The jamming action provides the spine with

increased stiffness so that the spine can retain its position when active.
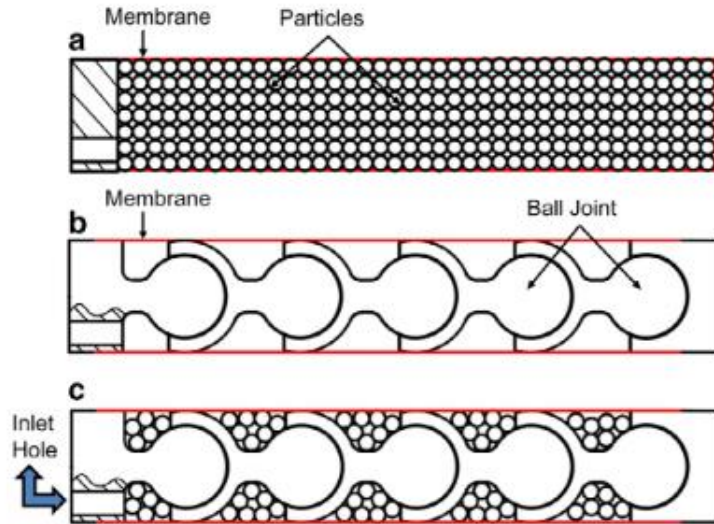
Figure 18. a) particle in a membrane in normal state, b) a series of ball joints acting like a backbone, c) integrated design of ball joints and granular particles [62].

2.5.4 Universal Gripper
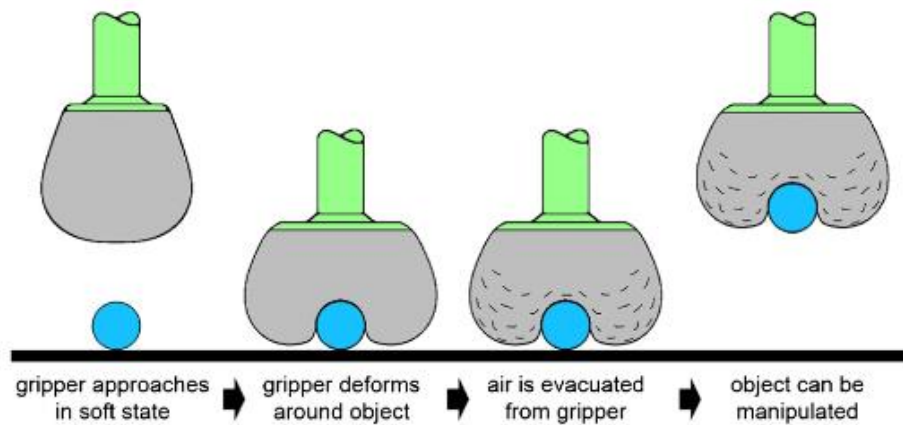
Figure 19. Universal gripper using granular jamming [63].

Universal gripper based on jamming of granular material works on a shape retaining property of

the granular material in a sac under vacuum. As shown in Figure 19, a gripper in a shape of sphere,

contains granular particles. This gripper touches the object to be manipulated, in a manner to get

hold of it. After positioning the inactive gripper, vacuum is activated, which leads to temporarily solidifying the gripper and letting it "grab" the object. The object can be released by simply deactivating vacuum. This gripper requires does not require many parts and it is very simple to operate. Also, it can grasp most of the objects that fits into the size range and weight capacity because of its nature to grip almost everything.

2.6 Summary on Types of Soft Actuators

Table 2 summarizes important literatures studied above which is divided by type of actuation. It gives measure of different qualities of a soft actuator which are: Responsiveness – a measure of time between input signal and output, Displacement – maximum displacement that can be achieved by an actuator compared to its own size, Force – degree of force that can be implied on an object, Flexibility – degree to achieve various movements, Ease of control and how economical it is. Each of these categories are rated out of five, five being the most effective and are represented by "●" in the table.

Table 2. Summary of various soft actuator based on type of actuation.

Type Of Actuation	Studies	Features	Responsiveness	Displacement	Force	Flexibility	Ease Of Control	Economical
Pneumatic Artificial Muscle	[16], [17], [18], [19], [20], [21], [22]	A flexible bladder covered with sleeve made of a cloth. Usually provides extension and retraction	○ ● ● ● ●	○ ○ ● ● ●	○ ● ● ● ●	○ ○ ○ ● ●	○ ○ ○ ● ●	○ ● ● ● ●
Pneumatic Balloon	[22], [23], [24], [25]	balloon like structure at joints, when inflated, uses only one side of material, resulting in differential motion	○ ● ● ● ●	○ ○ ○ ● ●	○ ○ ○ ○ ●	○ ○ ● ● ●	○ ● ● ● ●	○ ○ ● ● ●

Type Of Actuation	Studies	Features	Responsiveness	Displacement	Force	Flexibility	Ease Of Control	Economical
Pneumatic Network	[26], [27], [28], [29], [30], [31]	a network of chambers connected to pneumatic source with one or multiple lines.	●	○	○	●	●	●
			●	●	○	●	●	●
			●	●	●	●	●	●
			●	●	●	●	●	●
			●	●	●	●	●	●
Hydraulic	[32], [33], [34], [35], [36], [37]	actuating with the help of hydraulic pump.	●	○	●	○	○	○
			●	○	●	●	○	○
			●	●	●	●	●	●
			●	●	●	●	●	●
			●	●	●	●	●	●
Tendon Driven	[38], [39]	fingerlets connected with a joint or a flexible material acting like a joint, operated with one or multiple tendons	○	○	○	●	○	●
			●	○	○	●	○	●
			●	●	●	●	●	●
			●	●	●	●	●	●
			●	●	●	●	●	●
Shape-Memory Alloy	[41], [42], [43], [44]	SMA changing the shape of the actuator with change in temperature	○	○	○	○	○	○
			○	●	●	○	○	○
			○	●	●	●	○	●
			○	●	●	●	●	●
			●	●	●	●	●	●
Electro-Active Polymers	[45], [46], [47], [48], [49], [50], [51], [52]	Electrically activated polymers, actuation achieved with differential voltage	○	○	○	○	○	○
			●	●	○	○	●	○
			●	●	○	○	●	○
			●	●	●	●	●	●
			●	●	●	●	●	●
Electrorheological Fluids	[54], [55], [56]	electrically controlled viscosity of the fluid	●	○	○	○	○	●
			●	○	○	○	○	●
			●	○	○	○	○	●
			●	●	●	○	○	●
			●	●	●	○	●	●
Magnetorheological Elastomers	[57], [58]	magnetically controlled viscosity of the fluid	●	○	○	○	○	●
			●	○	○	○	○	●
			●	○	○	○	○	●
			●	●	●	○	○	●
			●	●	●	○	●	●

Type Of Actuation	Studies	Features	Responsiveness	Displacement	Force	Flexibility	Ease Of Control	Economical
Granular Jamming	[60], [61], [62], [63]	granular material packed in a flexible sac, which changes its stiffness based on degree of vacuum	○ ● ● ● ●	○ ○ ● ● ●	○ ● ● ● ●	○ ○ ○ ○ ●	○ ● ● ● ●	○ ● ● ● ●

From the Table 2, it was observed that the SMA actuators have a responsiveness rating of 1/5 because it takes more time (10-15 minutes) to reach the temperature gradient required to achieve phase change. Whereas other actuators take significantly less time (< 1 min) to actuate. Pneumatic network actuators were found to be actuated in less than 1 second.

In terms of displacement, MRFs and ERFs performs significantly less (< 50 % of their size) because of their bulky sizes due to electrical and magnetic components being directly attached to the actuator. PneuNets and SMAs can deform more (> 90%) and therefore can produce more displacement.

Hydraulic actuators provide best performance in terms of force, as the force can be as high as the hydraulic pressure depending on the materials ability to retain the pressure without getting damaged. Granular jamming actuators also performs well because the amount of load carried by the actuator depends on the size of the actuator and the degree of vacuum.

PneuNet actuators provides higher degree of flexibility as the material used to manufacture these actuators are very compliant in nature. Also, PneuNet actuators are easy to control when compared to others, as they are controlled by pneumatic systems which requires a pump and can be controlled with a set of valves. As the number of components are reduced, the control becomes simpler. These

actuators are manufactured from readily available and common materials like silicone and rubber which makes them extremely accessible and affordable.

Table 3. Comparison of actuation methods [1, 10, 39, 55]

	Accessibility	Affordability	Safety	Control	Ease of Use
Pneumatic system	●●●●●	●●●●●	●●●●○	●●●●○	●●●●●
Hydraulic system	●●●○○	●●●●○	●●●○○	●●●○○	●●●○○
Tendon Driven	●●●●●	●●●●●	●●●●●	●●●○○	●●●●○
Smart Materials	●●○○○	●●●○○	●●●○○	●●○○○	●●○○○

Table 3 shows the comparison drawn between different actuation methods. From the different types of actuators discussed above, a few significant actuation methods are pneumatic system, hydraulic system, tendon driven and smart material. The pneumatic system was observed to be most accessible, affordable, and easy to use. The pneumatic system consists of an electric pump, which provides pressurized air. A pneumatic connection system consisting of valves and tubes. Whereas other systems require more components and complex control strategies. Therefore, pneumatic system is selected in this research.

2.7 Fabrication Techniques for Soft Actuators

In this section, we discuss about different manufacturing techniques required of soft actuator, the section mainly focuses on manufacturing techniques related to pneumatic soft actuators which helps to determine a suitable process for this research.

2.7.1 Molding Fabrication Methods

Molding is one of the most commonly used manufacturing technique known till date. The process is simple. A design is made in a soft but stable material with the help of carving or a pre-

manufactured part. After the part has its features embodied into the soft material like clay, the part is removed, and a mould is prepared. A molten material is poured into the mould and settled. Once it is settled, the outer mould is broken in some cases and reused in other. It is an economical manufacturing method.

2.7.1.1 Micro Molding Method

Micro-molding manufacturing method is well known technique in fabricating bio-inspired or biological devices. Also, it is particularly used in MEMS technology and fabrication. Injection molding has become very popular lately, and with increase in popularity, the interest of scientists has also risen. The increased interest has led them to use this technology in the field of micro manufacturing, leading to fabricating soft robots with injection molding. The fabrication of parts is on the scale of microns and with such precision, many new innovative ideas and concepts can be put into shape. Intricate manufacturing capability leads to designing micro mechanisms which can be used in medical field for the application in drug delivery [64].

2.7.1.2 Lost Wax Casting

Lost wax casting is one of the oldest manufacturing procedures. In this method, the required structure is made from wax by various methods like carving. Carving allows to produce intricate profiles and designs. After this, the wax part is inserted into the mold. Material used in molding process must not be exothermic and the temperature should not be higher than or equal to the melting point of the wax used. Molding material is then poured into the mold and let it set. After setting of molding material, the wax inside is then melted away, this leaves a cavity which replicated the wax structure. This cavity acts as a mold for different materials and now that the structure does not contain any part of wax, materials with higher operating temperature can also be used like molten metals. This technique can also be used in soft robotics, intricate and complicated pneumatic networks can be made with wax and then melted away with small temperature rise.

30

Figure 20 shows the use of this technique to produce intricate and complex structure, it entails fabrication of a fish like soft robot.
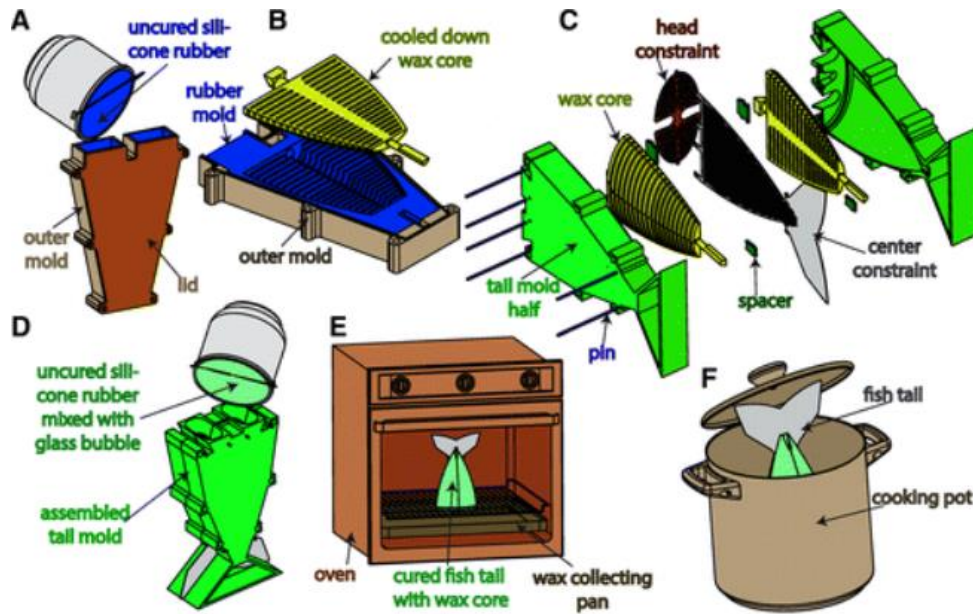
Figure 20. Manufacturing of a complicated fish-fin structure using lost wax method used by A. D. Marchese et. al., A) uncured silicone rubber is poured into a mold, B) cured silicone is used as a mold for creating wax structure, wax is poured and cooled down. C) cooled wax is used as a core and mold is assembled as shown. D) silicone is poured into the mold. E) after silicone is cured, the mold assembly is put in the oven to melt the wax out. Remaining wax is removed by putting the part into cooking pot [65].

2.7.1.3 Molding for Soft Actuator

Molding is a very simple, yet very effective manufacturing procedure. Also, it is one of the most common methods used for fabricating soft pneumatic actuators. Figure 21 shows the manufacturing process of soft actuator. the process is divided into six stages. The molds are usually manufactured using 3d printing, because it provides with facility of obtaining shapes and profile which would be rather difficult with conventional manufacturing methods. The molds are fabricated in two parts, a bottom tray, and a top mold. The top mold provides the main profile of the actuator and bottom tray helps in sealing the actuator with bottom layer as seen in Figure 21 a. A strain limiting layer is

embedded in some of the actuators at the bottom layer. This prevents elongation of the bottom layer.
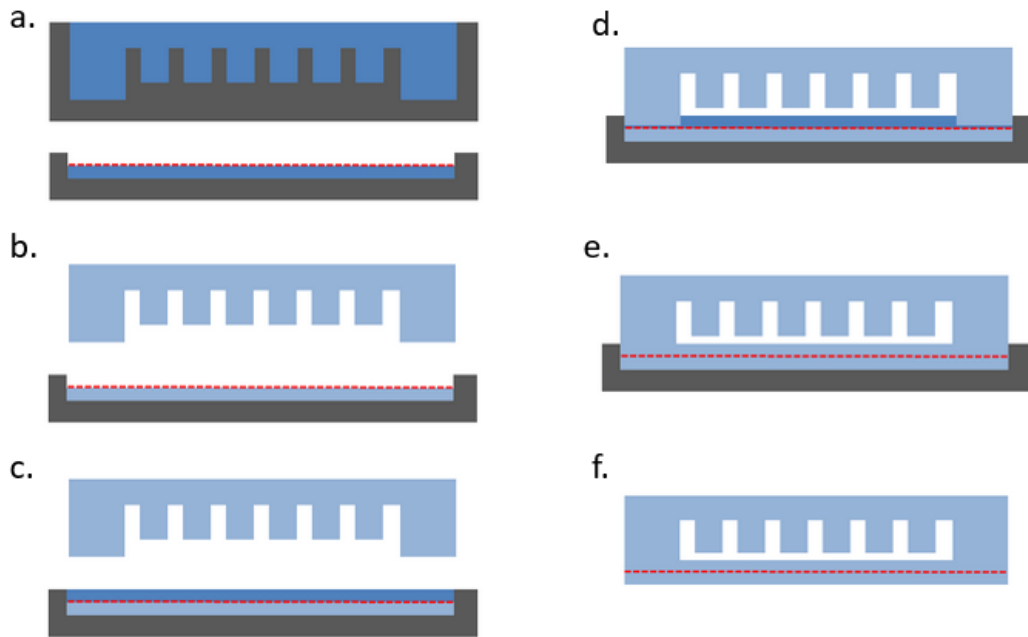
Figure 21. Manufacturing process of a soft actuator with molding, a) silicone elastomer is poured into the main mold and bottom tray mold. b) after setting, main mold is removed. c) a layer of uncured silicone is poured on the bottom tray as shown, which functions as a glue. d) top mold is placed in position for gluing. e) glue is set. f) actuator is removed from the mold [3].

2.7.1.4 3D Printing

3D printing is widely used technology in multitude of applications. It has found its way from biotech to aerospace industry. It is also known as additive manufacturing technique as it involves addition of material, layer by layer. In the field of soft robotics, as discussed in previous sub-section, the mold for manufacturing is also made using 3D printing. 3D printing can be done using many materials like plastics, metals, cements, etc. nowadays researchers are developing a 3D printing machine for making entire house [66]. A blend of specialized cement and building material is added into the hopper and mixed. The mixture comes down through nozzle of required diameter with controlled flow rate. Listed below are some of the types of most common 3D printing technologies.
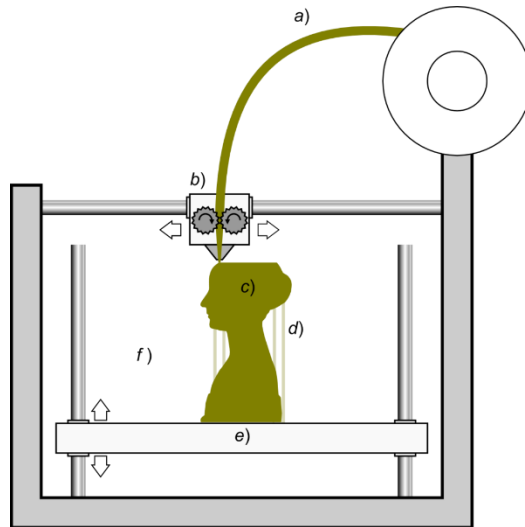
Figure 22. Schematic representation of Fused Filament fabrication, a 3D printing technique. a) material in a spool in the form of filament, b) extruder-melting of material and depositing it layer by layer, c) 3D printing part, d) supports for overhanging parts, e) build plate-base for 3D printing [67].

Jet Binder Application

The methods of free-jet binder application include additive manufacturing processes, in which a liquid binder is applied selectively to bind powdered material layer by layer.

Material Application with Directed Energy Input

Material application with directed energy input includes additive manufacturing processes in which bundled thermal energy is used to connect material where it is applied.

Material Extrusion

Material extrusion includes additive manufacturing processes in which material is selectively deposited through a nozzle or opening. Fused layer modeling falls into this category.

Free Jet Material Application

The methods of free-jet material application include additive manufacturing processes in which raw material is selectively deposited in the form of drops. This category includes poly-jet modeling and multi-jet modeling

33

Powder Bed-Based Melting

The methods of powder bed-based melting include additive manufacturing processes in which thermal energy selectively connects or fuses regions of a powder bed. Laser sintering, laser beam melting, electron beam melting, and thermal transfer sintering, among others, fall into this category.

Layer Lamination

Layer lamination methods include additive manufacturing processes in which layers (e.g., panels) of material are combined to form a component. Layer Laminated Manufacturing falls into this category.

Bath-Based Photopolymerization

Bath-based photopolymerization processes include additive manufacturing processes in which liquid photopolymer is selectively cured in a container, caused by light-activated polymerization. This category includes stereolithography and digital light processing [68].

2.8 Evaluation Parameters

This section discusses various parameters required to evaluate a pneumatic soft actuator design. The parameters are bending angle, force component, and pressure required. Table 5 contains the comparison of various SPAs based on above mentioned parameters.

2.8.1 Bending Angle

Bending angle is a measure of displacement for the soft pneumatic actuator as it shows how much an actuator can deform. Most of the soft actuators are rotational actuators and the actuation capacity for rotational actuators are measured in maximum angle achievable. Bending angle is measured as an angle between base of the actuator when not actuated and maximum angle achieved by the end

part of the base when actuated (with positive pressure or vacuum). P. Polygerinos et al., measured angle of their actuator by capturing images from single point. From which x and y coordinates were collected and used to measure the bending angle [69]. The bending angle also provides an estimate on holding capacity and degree of actuation because as the bending angle increases, the actuator can go around an object to grasp it like human fingers, tentacles, or elephant's trunk. Table 5 shows that the bending angle obtained in previous studies, irrespective of input pressure, were able to reach an average angle of 243° with a range of 45° to 350°. Also, withing SPA group, Pneu-Net actuators were able to obtain maximum bending angle [5, 8, 69, 73, 75]. To grasp objects successfully with an actuator, the actuator needs to reach an angle of 180° minimum [10].

2.8.2 Force Component

An actuator's ability to move, push or hold depends on the force exerted by the actuator on external object apart from force required by the object to actuate itself. In this study, we have measured this force in the terms of holding force/blocking force. Holding force is an amount of force required to deform an already actuated actuator at that given pressure. It can also be defined as the maximum force exerted by the actuator on the object at a given pressure. This method of force evaluation is relevant as it shows an actuator's ability to push or hold an object directly and therefore this can be observed in studies done by many researchers [5, 70, 71]. Figure 23 shows the most common method of measuring force component. In this method, an SPA is fixed with a clam and placed in such a way that the tip of the actuator is in contact with a force sensor [72]. As the SPA actuates, it starts to impart force on the sensor which gives the force output. From the previous art on SPAs made from a homogenous material, the maximum output force obtained was 3.5 N for the applied pressure of 120 kPa [76]. The objective is to increase the force outcome of the actuator with minimal pressure input.
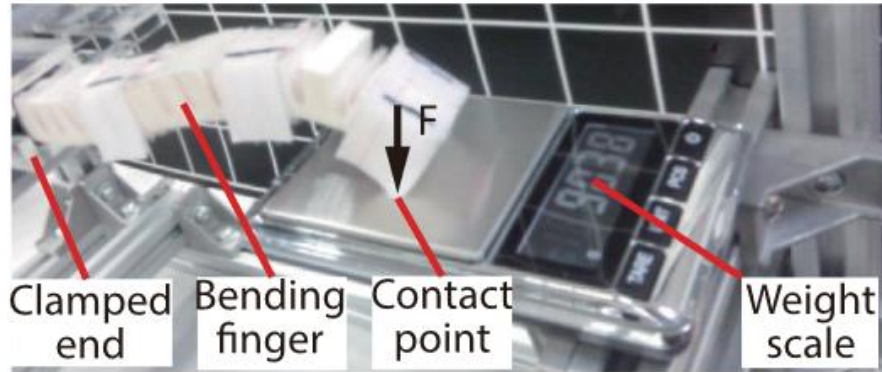
Figure 23. Measuring holding force/blocking force from tip of the actuator [72].

2.8.3 Pressure

Pneumatic soft actuators are powered by a pneumatic pump or a reservoir. Most of the pneumatic actuators operate on positive pressure [10,57,58]. These actuators inflate on application of pressure and deflates on its own when the source is disengaged. This pneumatic actuator uses vacuum as well to actuate the SPA in opposite direction to complement the retraction of the actuator and extend the retraction. The pressure provides the actuation ability to the actuator and the pressure energy is converted to force applied as seen in Figure 23. This experiment was conducted by J Wang et al. with the force output of 0.8 N with 80 kPa of applied pressure [72]. The pressure profile depends on the type of actuator, and it also depends on the material used to manufacture the actuator. Actuators developed with special reinforcements such as fiber-reinforcement, even when manufactured with soft material such as Eco-Flex 00-30, requires high pressure input of 195 kPa as shown by Y. Sun et al. [77]. As the pressure increases the force output increases but energy consumption also increases. Keeping the pressure values low and increasing force for corresponding pressure is the key, and therefore effectiveness is added to the evaluation parameters.

2.8.4 Effectiveness

Effectiveness is measured as output–generated force per unit of input–applied pressure. The output force from the current literature cannot be compared directly as the pressure at which they deliver

are very different (refer to Table 5). The material used for manufacturing plays a role in pressure requirement. Apart from these factors, other factors such as size of the actuator, type of the actuator, reinforced actuators or actuators with special features affects the force output. Therefore, to measure how effectively pressure is converted to output force, effectiveness is measured as force per unit pressure.

The materials used to manufacture SPAs are different, but it was observed that silicone elastomers, 'Elastosil M 4601' and 'Eco-Flex 00-30' have been used the most in past literature [5,8,69,73,75,76,77] as listed in Table 4. The Eco-Flex 00-30 has a shore hardness of 00-30, whereas the Elastosil M 4601 has a shore hardness of 00-70.

Table 4. Material used for previous SPAs.

Author		Material
P. Polygerinos et al.	[73]	Elastosil M 4601
K. M. de Payrebrune et al	[5]	Elastosil M 4601
T. Noritsugu et al	[6]	Composite
S. Konishi et al.	[74]	KE 1606
B. Mosadegh et al.	[75]	Ecoflex 00-30
H. Li et al.	[70]	Composite
Y. Li et al.	[7]	Composite
P. Polygerinos et al.	[69]	Elastosil M 4601 (fibre reinforced)
G. Alici et al. (A1 model)	[76]	Elastosil M 4601
G. Alici et al. (A2 model)	[76]	Soft Translucent
J. Wang et al.	[72]	Composite
Z. Sun et al.	[8]	Ecoflex 00-30 (reinforced)
Y. Sun et al. (with Fabric)	[77]	Ecoflex 00-30 (reinforced)
Y. Sun et al. (Ecoflex 0030)	[77]	Ecoflex 00-30
This Research		Ecoflex 00-30

2.9 Evaluation Metrics

Table 5. Summary of maximum bending angle, maximum force and pressure of soft actuators.

Author		Max. Bending angle (°)	Force (N)	Pressure (kPa)	Effectiveness Force/Pressure
P. Polygerinos et al.	[73]	320	1.2	45	0.0267
K. M. de Payrebrune et al	[5]	332	0.275	66	0.0042
T. Noritsugu et al	[6]	200	14	500	0.0280
S. Konishi et al.	[74]	75	1.72	80	0.0215
B. Mosadegh et al.	[75]	340	1.4	72	0.0194
H. Li et al.	[70]	270	15	400	0.0375
Y. Li et al.	[7]	45	18	500	0.0360
P. Polygerinos et al.	[69]	300	10	250	0.0400
G. Alici et al. (A1 model)	[76]	270	3.5	120	0.0292
G. Alici et al. (A2 model)	[76]	270	0.9	35	0.0257
J. Wang et al.	[72]	270	0.8	80	0.0100
Z. Sun et al.	[8]	350	2.5	120	0.0208
Y. Sun et al. (with Fabric)	[77]	120	2.3	195	0.0118
Y. Sun et al. (Ecoflex 0030)	[77]	240	0.8	65	0.0123

The evaluation metrics, in this research is based on 4 evaluation parameters, which are discussed above. The bending angle defines the reach and flexibility of the actuator. Increase in bending angle increases reach and flexibility and therefore, design improvements are made in this research to enhance the bending angle. Force exerted by the actuator on an object determines the carrying, holding, pulling, or pushing capabilities. Higher force requires higher pressure and actuator fabricated with harder materials [7, 69]. The force output determines the application of the actuator

38

for example, a gripper with two actuators of 0.8 N force output can lift an object of 500g [77]. As the pressure increases, the power consumption increases, pressure losses increases and efficiency decreases [26]. Effectiveness establishes a relationship between force and pressure, and higher effectiveness is most desirable.

2.10 Conclusion

In this chapter, a detailed literature review was delivered on soft robots with focus on types of soft robotic actuators. The working principles of different types of actuators are also discussed. It was discovered that each type of soft actuator has a particular application. This research focuses on soft pneumatic actuator as it has more versatile applications when compared to other actuators [10]. It was observed from prior art that, design improvement has not been the priority. The current design of the actuator can be improved by changing the profile of the cross-section and improving the design parameters through simulation study. Which will improve the bending angle and output force at given pressure. It was observed that more research has been conducted on the actuator with positive vacuum which performs in only one direction and has one degree of freedom. This is also addressed in this research by implementing vacuum feature which allows the actuator to perform in one more direction, which increases its degree of freedom by 1. When using softer silicone elastomers, the holding force of the actuator tends to be low (approximately 10 g – 250 g carrying capacity [10]). The low capacity restricts the application range of the soft actuator. This issue is also addressed in this research by a novel idea of implementing a granular jamming component to the actuator. The granular jamming gives an active control over the stiffness of the actuator. Apart from terms explained in the summary of Table 2,

Table 6. Comparison of present literature with this research.

Literature	Responsiveness	Displacement	Practicality	Flexibility	Ease Of Control	Economical	Bi-Directional
[15]	✓		✓			✓	✓
[16]	✓		✓				✓
[17]	✓				✓		✓
[18]		✓				✓	
[19]	✓		✓			✓	
[9]	✓	✓	✓		✓		✓
[20]	✓	✓			✓		✓
[21]		✓	✓				✓
[22]	✓				✓		
[23]	✓						
[24]	✓	✓	✓	✓	✓		
[26]	✓		✓			✓	
[27]	✓	✓	✓		✓	✓	
[28]	✓		✓		✓		
[29]	✓		✓	✓	✓	✓	
[30]	✓		✓			✓	
[31]	✓	✓	✓	✓	✓		
[32]	✓	✓	✓				✓
[33]		✓		✓			
[34]		✓	✓	✓			✓
[35]	✓		✓		✓	✓	
[36]	✓	✓	✓				
[37]	✓	✓		✓			✓
This Research	✓	✓	✓	✓	✓	✓	✓

This research aims to implement all the features- responsiveness, displacement, practicality, ease of control, economical and bi-directional as described in Table 6. "Bi-directional" is added to the

comparison Table 6. Bi-directionality is when an actuator can actuate in more than one direction. This can be achieved, in pneumatic soft robotics, by adding multiple sources with multiple chambers or by adding special feature. For example, in this research, the positive pressure moves the actuator in one direction, and vacuum moves the actuator in opposite direction. The fabrication of the soft pneumatic actuator is conducted by simple molding method also known as casting, described in section 2.7.1.3. The mold is manufactured using additive manufacturing with fused layer deposition 3D printing technique.

Chapter 3 Methodology

3.1 Introduction

This research focuses on improving the performance of a soft robotic actuator. The material used for fabricating soft actuators is soft silicone elastomers. It was observed that the soft elastomers tend to bend under their own weight which limits the performance of the actuator [47]. This research is aimed to achieve better bending performance and force characteristics by accomplishing two major objectives:

1. By improving the present design of the conventional actuator for better performance and,

2. By implementing a granular jamming component to increase the stiffness of the actuator.

The design of the actuator is improved by changing the cross-sectional profile of the conventional actuator. Additionally, the design parameters of this new actuator are also improved through simulation studies. Another method applied for achieving better results was by reinforcing the actuator in a way which would not affect the primary characteristics of the actuator. A granular jamming component is added to facilitate this objective. This jamming component can change its stiffness based on the degree of vacuum applied to it. The jamming chambers are attached to the actuator on either side. Experimental study is conducted to evaluate the improvement of the actuator through jamming component. Also, ANOVA is conducted to determine the significance of the input variables on the output-blocking force. An evaluation metrics discussed in Chapter 2, is used to show the significant contributions with significant parameters being bending angle, force, pressure, and effectiveness. A detailed methodology followed in this research is discussed below. Figure 24 shows the outline of the methodology followed in this research.
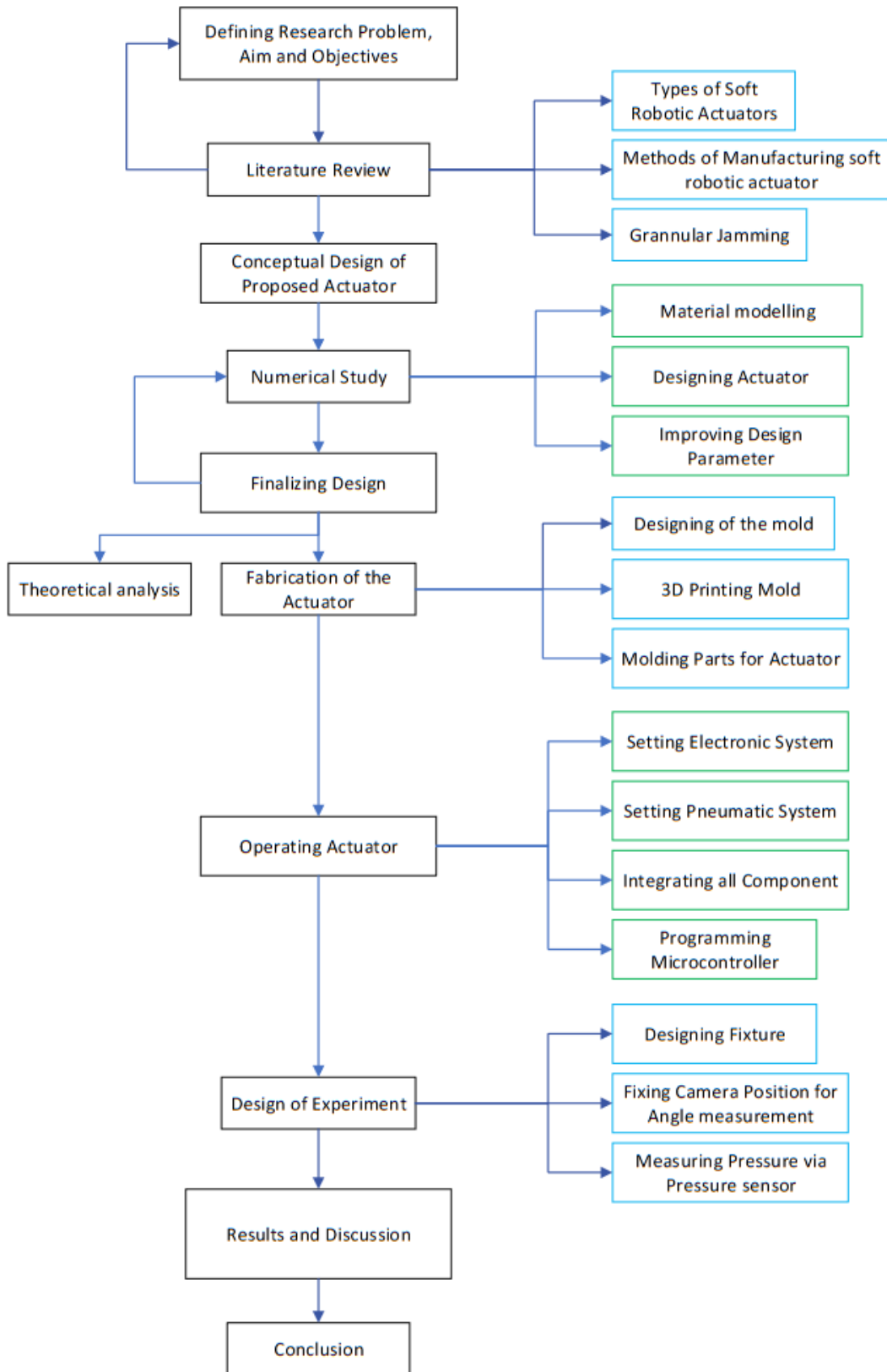
Figure 24. Outline of the methodology

3.2 Conceptual Design of Proposed Actuator

Preliminary design of the pneumatic actuator is performed in CAD software- CATIA. This design is inspired from Mosadegh et al, where the dimensions of the primary design are kept in accordance with present literature [18, 35,49, 56] and handling everyday objects with human hands. This preliminary design involves a new design of the cross-section profile of the pneumatic chamber in the actuator. The conceptual design of the actuator is shown in Figure 25. The design also involves consideration of actuator performing under vacuum and positive pressure as a two-way motion provides more degree of freedom. Also, jamming components are added on either side of the actuator. Vacuum is needed to actuate these chambers, which is provided through an air pump.
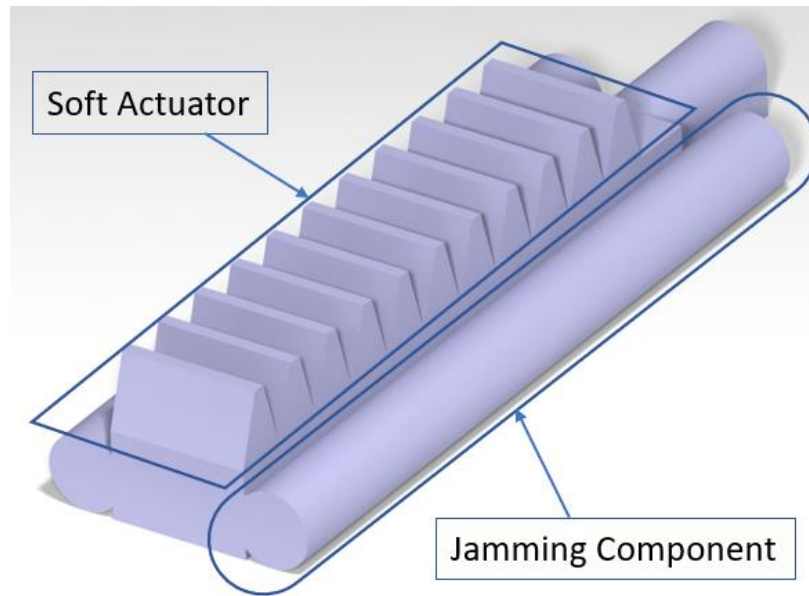
Figure 25. Conceptual design of the actuator

3.3 Material Modelling

To get a better understanding of the actuator design and effect of different parameters on the bending of the actuator, conducting experimental analysis for each case is time consuming and a tedious task overall. A simulation study is more suitable to predict the behavior of the soft actuator. To conduct a simulation of the actuator, the material should be modelled into the simulation

software-ANSYS. Eco-Flex 00-30 is categorized as hyperelastic material [78]. A hyperelastic material is a material which can go under deformations as large as 40% without going through plastic deformation [79]. ANSYS or any other commercially available software cannot simulate a hyperelastic material directly. It requires experimental data of the material. In this study, the material data is obtained from Ghamsari Z.S.N. [78], who have performed an extensive experimental study on the material Eco-Flex 00-30. The obtained data is imported to ANSYS and calibrated to curve-fit on the present hyperelastic models one by one. The best fitting model is selected and assigned to the material to perform simulations. A detailed material modelling is discussed in Chapter 4.

3.4 Numerical Study / Design Optimization

After finalizing a preliminary design for the pneumatic actuator, the CAD file is imported to ANSYS in STEP file format. Material properties of Eco-Flex 00-30 are assigned to the CAD model. A tetrahedron mesh type is used for meshing the part, as the part is moderately complex in nature. Mesh with the element size of 0.01 mm was used in the beginning and reduced to 0.5 mm as the results remain consistent. The input pressure of actuators made from Eco-Flex 00-30 was observed to be 0 to 65 kPa from Y. Sun et al. [77]. A binary search was conducted to find a pressure match for the actuator with a range of 1 kPa and 65 kPa. In this method, the simulation is conducted with highest and lowest parameter (pressure). A failure occurred in the simulation at 65 kPa, which was followed by a simulation with half the value of maximum parameter and so on. This process resulted in 3.5 KPa as the operable pressure for simulation.

Important design factors of the soft actuators such as apex angle and bottom layer thickness (a geometric parameter of the proposed design) are studied in the simulations. These parameters showed a significant effect on bending of the actuator when compared to other parameters during simulation studies. Detailed study is conducted by varying the parameter values and comparing

obtained results. The results are compared based on maximum angle obtained by the actuator as it depicts an efficient design for maximum angle achieved for a given pressure. The design is finalized with these parameters, and it is used for fabricating the actuator.

3.5 Theoretical Analysis

A theoretical analysis is conducted of a soft pneumatic actuator with finalized parameter values. This analysis is performed to understand the behavior of the actuator under positive pressures. The model is based on principle of minimum potential energy and study performed by Cao G et al. This study assumes uniform bending of the actuator which is considered as a beam. It also assumes that the individual chamber of the actuator is inflated in a uniform elliptical cylinder for the ease in volume calculations. The model is developed for bending angle 'θ' as a function of internal pressure. This is further discussed in section 5.5.

3.6 Fabrication of the Actuator

The silicone Eco-Flex 00-30 is packaged as Part A and Part B liquids. When mixed in equal proportion, by weight or by volume, it starts to form polymeric bonds and cure in solid silicone. Therefore, molding is used as a method of fabrication. The molds are made using additive manufacturing technique (3D printing) using FDM technology. The molds are designed on CATIA. The design was made considering the 3D printing manufacturing process. Various iterations are made in the design of the mold to facilitate the safe removal of the mold. The material used for 3D printing was PLA (Polylactic acid). The major reason behind selecting this material is that Eco-Flex 00-30 does not stick to it and the silicone can be removed easily without applying any release agents. The other reasons include availability, ease of operation and affordability. A detailed fabrication process is discussed in Chapter 6.

3.7 Soft Actuator with Granular Jamming

A granular jamming component is added to the designed and fabricated soft actuator. This component is also made of Eco-Flex 00-30. It is effortless to join silicone parts with same material as they form chemical bonds when cured part is in contact with uncured part. The jamming component is a test tube like structure made with Eco-Flex 00-30 with a 3D printed filter-connector. The filter-connector also acts as a cap to retain the granular material into the chamber. This silicone chamber is filled with jamming material which is ground coffee. This chamber is connected to the suction outlet of the pump. When suction is applied to the jamming component, the granular material starts collapsing into each other which increases its stiffness. This increase in stiffness helps in increasing holding capacity of the actuator.

3.8 Operating Actuator
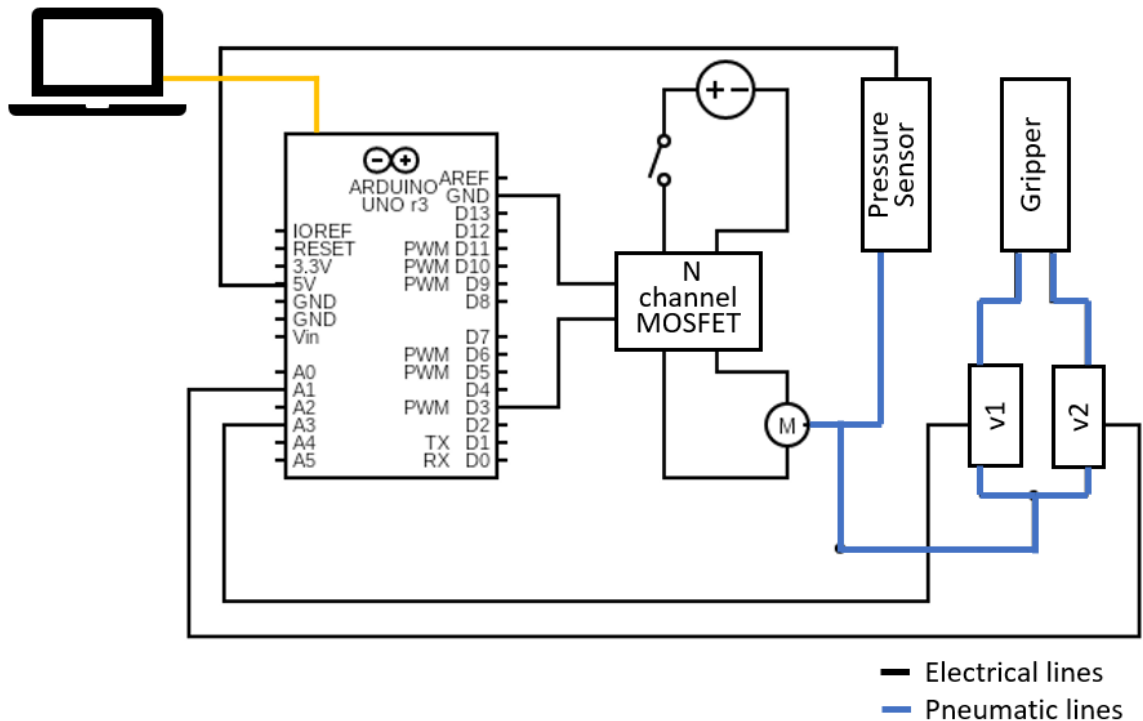
Figure 26. Schematics of Experimental setup

47

Figure 26 shows the schematics of the system used for operating the SPA. A hardware system is designed to operate soft actuator with positive pressure and negative pressure. A pneumatic pump with both capabilities was chosen and shown in the Figure 26 as "M". A simple pneumatic system is put in place with manual valves to adjust the pressure, the pressure data was collected by the pressure sensor attached in the system and Arduino Uno to control the motor driver and read the pressure data of the system. The motor used is operated at 12V and 4 amp and powered with external power supply. SparkFun Qwiic MicroPressure Sensor equipped with Honeywell's 25psi piezoresistive silicon pressure sensor is used to measure pressure in the pneumatic system [80].

3.9 Design of Experiment

An experimental setup is fabricated to measure the bending angle of the actuator as it is pressurized incrementally. The actuator is fixed on a flat surface in a way that the plane in which the bending occurs remain parallel to the ground. The images of this actuator for different angles at different pressures are captured from a fix point. These images are imported into CATIA, and the angles are measured in the software. Another experimental study is carried out for measuring holding force. A holding force is a measure of resistive force that an actuator can resist till it becomes saturated. In this experiment, the actuator is fixed on a platform. The actuator is then actuated with certain pressure which then moved slowly towards the force sensor. The reading on the force sensor increases as the actuator is moved towards it up to a saturation point. After which the force sensor reading does not change. This value is taken as the holding force in Newton.

3.10 Results and Discussion

A comparison of the numerical data, theoretical data, and experimental data of bending angle vs pressure is conducted to understand the bending angle characteristics of the actuator. The results from holding force analysis are also discussed in detail. A two-way ANOVA was conducted to determine the significance of the variables-pressure and vacuum on the force output. An analysis

of cost is also conducted for an actuator. A design of a general-purpose gripper is also proposed with prototype.

Chapter 4 Material Modelling

4.1 Introduction

In the field of soft robotics, the materials used are not very specific. Many applications need these materials to have higher elastic modulus and some of them have lower ranging $1MPa < E < 100MPa$. This variety in material helps in achieving complex locomotion and flexible movements. This also determines how the soft robots interact with external environment and behaves in the environment. Some of the soft robots have applications in surgical robotics and fields related to subcutaneous human interaction, and in such cases the material should be inert and biologically compatible. Silicone polymers are one of the materials to have such properties. The material needed for this research needs to be rubber like, flexible and has above mentioned properties. Rubbers and silicone elastomers possess such properties. These materials are classified into hyperelastic material category.

Hyperelastic is one of the types for modelling elastic materials like rubber and silicone elastomers which has elasticity of returning to original shape and size after 100% to 800%. In this model, the material is considered ideally elastic, also the stress strain relationship is obtained from strain-energy density function [81]. The next section briefly discusses on different types of hyperelastic material models which are all based on strain-energy density function.

Material selection for a soft actuator is an important step. In this chapter, we discuss about selection of the material for the soft robot. Also, we discuss about selection of material for granular jamming component. The soft material used can be categorized as hyper-elastic material. We discuss about different hyper-elastic material models that can be applied to this material and selecting one model for this research. The experimental data required for the material modelling and how to use that data for obtaining material model is also explained.

4.2 Material Selection

As per discussion in Chapter 2, the pneumatically driven actuators are proven to be most effective in terms of applicability, flexibility, ease of control, versatility, and manufacturing cost. This research focuses on pneumatically driven actuator, more precisely, pneumatic network actuators. The pneumatic soft actuator requires material that has high maximum strain value (strain > 500%). Also, soft actuators are developed to be feasible for human interactions, bio-compatibility and toxicity plays a major role. Therefore, the material should also be free from inherent toxins and proved to be bio-compatible. Silicone elastomers are the best example of this type of materials [82]. The pressure requirement for this research is set low (P < 20 kPa) as the material crosses its strain limit for design of an actuator beyond that point [10].

Commercially available silicone elastomer Eco-Flex 00-30 fulfills all the above stated requirements. Not only it is easily procurable, but it is also very easy to handle [83]. The material data is provided in Appendix A. Silicone elastomers are proven to be a good fit for soft actuator fabrication which can be observed in past research [26-31, 34, 65]. To demonstrate the speed of the soft actuators, research was conducted by Mosadegh et al. and achieved a response time of 0.1s [27].

4.3 Material Modelling

The material properties required for the soft actuator developed in this research are similar to conventional pneumatically driven actuators. As per the discussion in Chapter 2, the material used is Eco-flex 00-30. The material properties for this material made available by the manufacturer is described in Hyperelastic Material Models

A hyper elastic material model can be developed by interpreting experimental data into existing model. There are many hyperelastic material models present in ANSYS which can be co-related

with existing experimental data and used to obtain material constants from any particular model. An existing experimental dataset of uniaxial and biaxial test is used for this process. This data is then curve fitted with existing models one by one. Then the graphs are compared to each other to obtain best curve fitting from all material models. Various hyperelastic models used for this method is listed below:

1. Neo-Hookean model
2. Arruda-Boyce model
3. Blatz-Ko model
4. Mooney-Rivlin model
5. Polynomial model
6. Yeoh model
7. Ogden model

All these hyperelastic material models are pre-programmed in ANSYS and can be used to determine material constants. This requires a stress-strain curve of the material which, in turn, is uploaded to Ansys. These models are based on strain-energy function. We have discussed some of them below.

4.3.1.1 Neo-Hookean Model

The Neo-Hookean material model is like Hooke's law, which can be used to predict the stress-strain response of a material. This material model was pitched by Ronald Rivlin in 1948. The connection between applied stress and strain is initially linear, but the stress-strain curve changes at some point. The disadvantage of this model is that it can predict good results only up to 20% of strain and not beyond that. This model is a specific case of the Mooney-Rivlin model where material constant C_{01} is set to zero [84]. The strain energy function is:

$$W = \frac{\mu}{2}(\bar{I} - 3) + \frac{1}{d}(J - 1)^2$$

(2)

Where, μ = initial shear modulus of the material, d = material incompressibility parameter, J = determinant of the elastic deformation gradient.

4.3.1.2 Mooney-Rivlin Model

Hyper elastic models including Mooney-Rivlin model is based on Strain energy function. The function depends on two, three, five, seven and nine parameters. This selection of a particular function is done by curve-fitting of these function on experimental data and comparing best match [85]. This model is widely used and is given by,

$$W = C_{10}(\bar{I}_1 - 3) + C_{01}(\bar{I}_2 - 3) + \frac{1}{d}(J - 1)^2$$

(3)

Where W = strain energy per unit volume, I_1 = first strain invariant, I_2 = second strain invariant, C_{01} and C_{10} = material constant determining deformation of the material.

The three-parameter Mooney-Rivlin model which is considered as generalized model is given by,

$$W = C_{10}(\bar{I}_1 - 3) + C_{01}(\bar{I}_2 - 3) + C_{11}(\bar{I}_1 - 3)(\bar{I}_2 - 3) + \frac{1}{d}(J - 1)^2$$

(4)

The five-parameter Mooney-Rivlin model is given by,

$$W = C_{10}(\bar{I}_1 - 3) + C_{01}(\bar{I}_2 - 3) + C_{20}(\bar{I}_1 - 3)^2 + C_{11}(\bar{I}_1 - 3)(\bar{I}_2 - 3) + C_{02}(\bar{I}_2 - 3)^2 + \frac{1}{d}(J - 1)^2$$

(5)

And the final nine-parameter Mooney-Rivlin model is given by,

$$W = \quad C_{10}(\bar{I}_1 - 3) + C_{01}(\bar{I}_2 - 3) + C_{20}(\bar{I}_1 - 3)^2 + C_{11}(\bar{I}_1 - 3)(\bar{I}_2 - 3) +$$
$$C_{02}(\bar{I}_2 - 3)^2 + C_{30}(\bar{I}_1 - 3)^3 + C_{21}(\bar{I}_1 - 3)^2(\bar{I}_2 - 3) + C_{12}(\bar{I}_2 - 3)(\bar{I}_2 -$$
$$3)^2 + C_{03}(\bar{I}_2 - 3)^3 + \frac{1}{d}(J - 1)^2 \tag{6}$$

4.3.1.3 Arruda-Boyce Model

An Arruda–Boyce model is a hyperelastic constitutive model used to describe the mechanical characteristics of rubber and other polymeric materials in continuum mechanics. This model is based on the statistical mechanics of a material that has a cubic representation with a volumetric element with eight chains running diagonally. It is presumed that the substance is incompressible [86]. The Arruda-Boyce model is given by,

$$W = \quad \mu\left[\frac{1}{2}(\bar{I}_1 - 3) + \frac{1}{20\lambda_L^2}(\bar{I}_1^2 - 9) + \frac{11}{1050\lambda_L^4}(\bar{I}_1^3 - 27) + \frac{19}{7000\lambda_L^6}(\bar{I}_1^4 - 81) +$$
$$\frac{519}{673750\lambda_L^8}(\bar{I}_1^5 - 243)\right] + \frac{1}{d}\left(\frac{J^2 - 1}{2} - \ln J\right) \tag{7}$$

Where, λ_L = the limiting network stretch, μ = initial shear modulus of the material, d = the material incompressibility parameter, and J = the determinant of the elastic deformation gradient.

4.3.1.4 Blatz-Ko Model

Blatz and Ko produced this model for porous rubber material, meaning these are the material that can have large deformation (about 500% in tension and 90% in compression). Sponge is the best example of this material. The model is comprised of lower order form and higher order form, but lower order form is generally used for simulations, which is given by,

$$W = \frac{\mu}{2}\left(\frac{I_2}{I_3} + 2\sqrt{I_3} - 5\right) \tag{8}$$

Though being a very simple material model with just one input parameter, the output relation between stress-strain is only valid for a particular range [87].

4.3.1.5 Polynomial Model

A polynomial hyperelastic material model is in the form of polynomial, modeled for rubber elasticity. Filled elastomers are usually evaluated using this model [88]. The strain energy model is given by,

$$W = \sum_{i+j=1}^{N} C_{ij}(\bar{I}_1 - 3)^i(\bar{I}_2 - 3)^j + \sum_{k=1}^{N} \frac{1}{d_k}(J - 1)^{2k} \tag{9}$$

Where C_{ij}, N, and d_k are material constants.

4.3.1.6 Yeoh Model

Yeoh model, like other hyperelastic model, is also based on strain-energy function. The Yeoh model is very similar to Mooney-Rivlin model as both are polynomial models. On the same order, Yeoh model comes out to be the simpler model compared to Mooney-Rivlin model as the second invariant is not considered in this. The Yeoh model is given by,

$$W = \sum_{i=1}^{N} C_{i0}(\bar{I}_1 - 3)^i + \sum_{k=1}^{N} \frac{1}{d_k}(J - 1)^{2k} \tag{10}$$

This model is simpler as it has a smaller number of parameters when compared to model like Mooney-Rivlin and needs only tensile test experimental data to produce a good prediction. This model can generate prediction for a very wide range of elongations. Not only that, but it can also generate better predictions if the model is simples with low shear stress [89].

4.3.1.7 Ogden Model

Ogden model is widely used model in industry. It was successfully applied in the simulation of o rings, seals, and many industrial products. He believes that using independent strain invariant complicates the model and instead uses principle stretches as independent variable to construct a model. The model is based on left Cauchy-green tensor and is given by,

$$W = \Sigma_{i=1}^{N} \frac{\mu_i}{\alpha_i} \left(\bar{\lambda}_1^{\alpha_i} + \bar{\lambda}_2^{\alpha_i} + \bar{\lambda}_3^{\alpha_i} - 3 \right) + \Sigma_{k=1}^{N} \frac{1}{d_k} (J-1)^{2k} \tag{11}$$

Where, N = order of the model, μ_i and α_i = material constants, λ_1 = principle stretch in x direction, λ_2 = principle stretch in y direction, and λ_3 = principle stretch in z direction.

4.3.2 Experimental Data for Eco-Flex 00-30

To define a material model a relationship between stress strain is very important. The engineering materials are commonly defined with young's modulus. Young's modulus describes the relationship between stress and strain up to a certain point, till this point, the said relationship remains linearly proportional in nature. But, in the case of hyperelastic materials, the linear proportionality does not exist and defining the relationship becomes more complex, which can be simplified with the above discussed hyperelastic material models. All these models require stress strain relationship as input. The mechanical data of stress strain experiment of Eco-Flex 00-30 is obtained from the extensive research conducted by Ghamsari Z.S.N. [78]. According to Ghamsari Z.S.N., to obtain better results for material modelling, two kinds of test are performed on Eco-Flex 00-30 silicone elastomer: uniaxial tensile test and biaxial tensile test.

Uniaxial tests are carried out by applying tensile load in one axis. The shape of the specimen is determined to be bone like. The length to width ratio is determined in such a way that it would not allow any residual shear stress to interfere with the outcome of the test [90]. The experiment was

carried out on ATS universal testing machine. The bulky ends of the bone shaped specimen are clamped to the universal testing machine and an incremental force is applied at certain frequency. A force sensor is attached to one of the clamps in order to measure the tension force and strain. The stain stress curve obtained for uniaxial tensile test is shown in Figure 27.
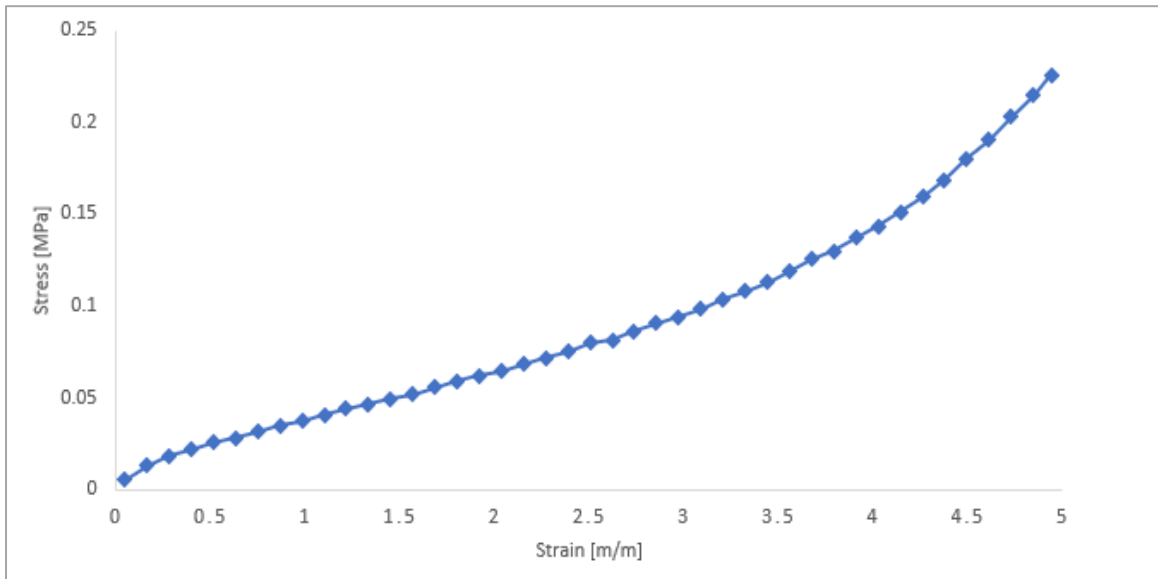
Figure 27. Stress-strain curve of Eco-Flex 00-30 from uniaxial test [78]

Biaxial tensile test is conducted by clamping the specimen in two orthogonal axes. Both axes are in one plane because it guarantees zero twisting of the specimen. A cruciform shaped specimen is used to perform biaxial mechanical test. All four corners of the 'plus' shaped specimen is clamped, and tensile load is applied on it. Biaxial tension is very close to stretching because of inflating a bladder. The stretching of the material when blown with pressure put it under tension from two axis and hence its very close to biaxial test. Because of that, biaxial test is important and has more impact of results of experiments in determining material constants. The stress strain curve obtained from biaxial test of Eco-Flex 00-30 is shown in Figure 28.
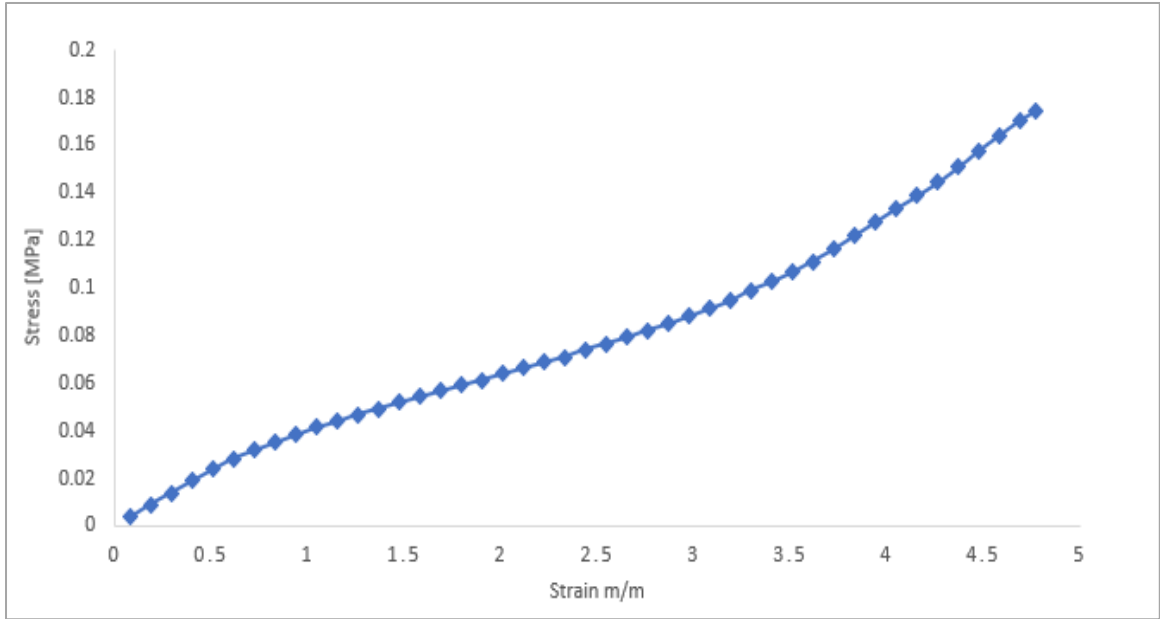
Figure 28. Stress-strain curve of Eco-Flex 00-30 from biaxial test [78]

4.3.3 Selecting Material Model

ANSYS provides a very effective tool to determine the best suitable material model for the hyperelastic material. This tool uses curve fitting technique to fit the function of the pre-existing hyperelastic material model with the experimental data obtained in previous section. The output obtained by this procedure is graphical in nature and different models can be compared visually to determine the best fit. The material constants for each model are also obtained through this method. Below, various models are discussed one by one with their curve-fitting. The plot generated by strain energy function and experimental data are given in Figure 29, Figure 30, Figure 31, Figure 32, Figure 33, Figure 34, and Figure 35. Also, the generated material constants through curve-fitting for all studied hyperelastic material model are listed in Appendix B.
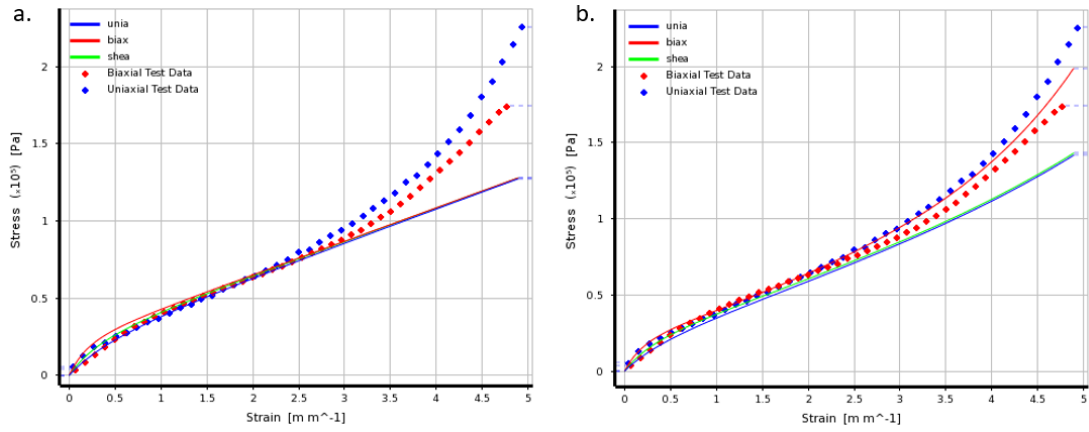
Figure 29. Neo-Hookean and Arruda-Boyce
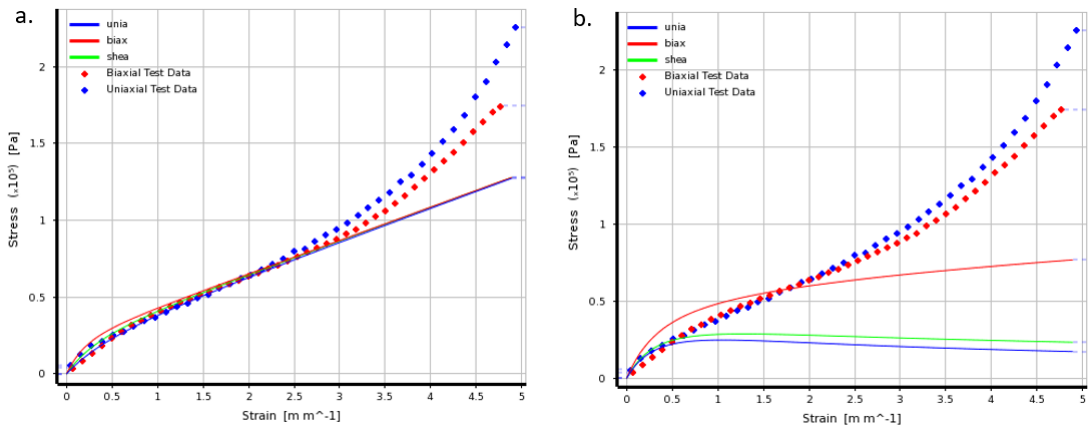
Figure 30. Gent and Blatz-Ko
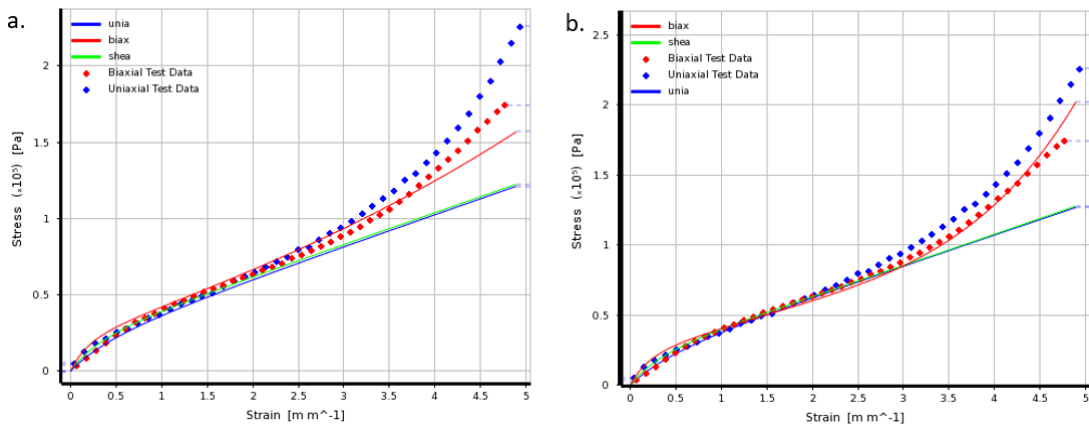
Figure 31. Mooney Rivlin 2 parameter, Mooney Rivlin 3 parameter
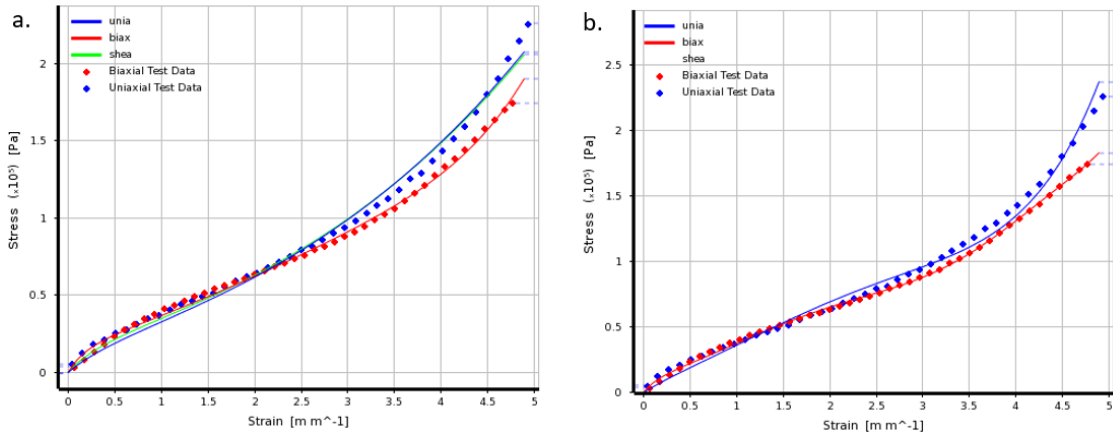
Figure 32. Mooney Rivlin 5 parameter, Mooney Rivlin 9 parameter
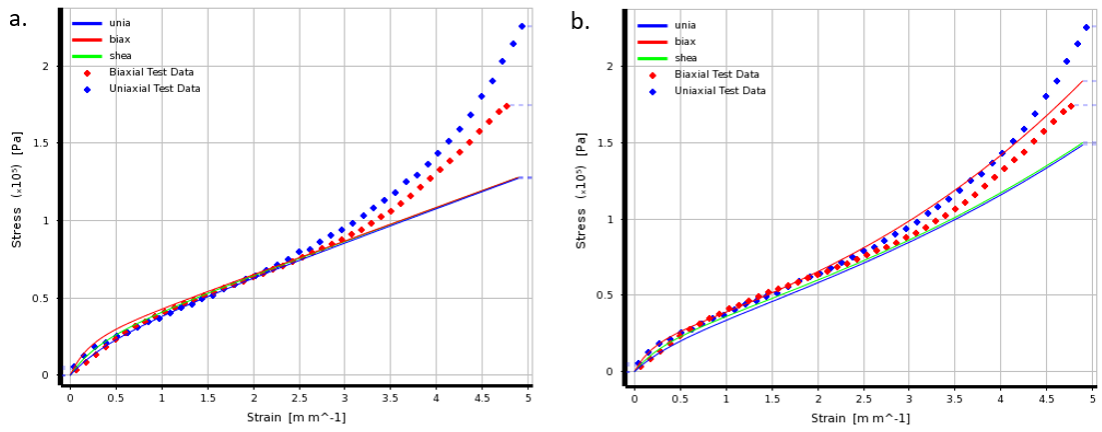
Figure 33. Yeoh 1st Order and Yeoh 2nd order
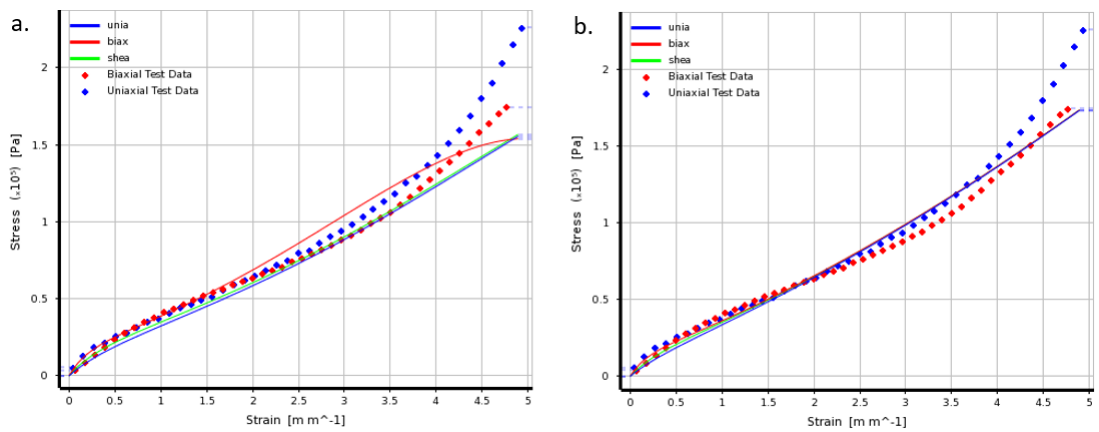
Figure 34. Yeoh 3rd order and Ogden 1st order
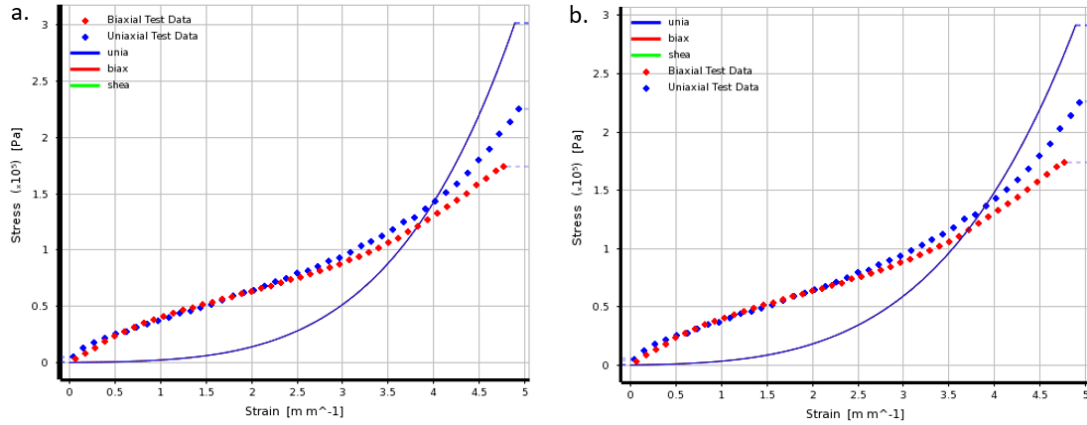
Figure 35. Ogden 2nd order and Ogden 3rd order

4.4 Conclusion

A silicone elastomer, Eco-Flex 00-30 is selected to fabricate the actuator in this study. The material is classified as hyper-elastic material because of its high elastic property (900% strain at breakage) Hyperelastic material models namely Neo-Hookean, Arruda-Boyce, Gent, Blatz-Ko, Mooney Rivlin, Yeoh, and Ogden were studied in this chapter. Compatibility of Eco-flex 00-30 was compared with these models. Relation between stress and strain which was obtained from experimental data is used to curve fit with strain energy functions. The curve fit was done in ANSYS Workbench and different models were compared graphically to find the best fit for the material. Yeoh 2nd order hyperelastic material model was selected to model the silicone elastomer. This model is used for all the simulations conducted in this research.

Chapter 5 Design and Structural optimization of the soft Pneumatic Actuator

5.1 Introduction

A soft pneumatic actuator comes in various sizes and shapes, and determining the preferred design depends completely on the application of the robot. A common attribute found in all soft pneumatic actuators is a degree of deflection. The degree of deflection in all present actuators is significantly high. Furthermore, this high deformation capability facilitates several applications as it represents the reach of the actuator. This actuator's design improves the angle of the actuator when inflated without cutting down on other characteristics. The pattern of folds on the soft actuator makes the difference in movements achieved after inflation. Depending on the pattern, the actuator can achieve linear motion, angular motion in a plane, angular motion out of a plane, expansion, and contraction. The motion also depends on pneumatic network design, the number of pneumatic chambers, and the shape of the pneumatic chambers. This chapter introduces a new design for the soft pneumatic actuator. The design of individual pneumatic chambers is discussed in detail with parameter optimization.

5.2 Geometry of Actuator

The geometry of the soft actuator is taken as a reference to start the process of improving it. The basic design of the actuator before the optimization is 100 mm * 20 mm * 20 mm [3, 91]. The number of pneumatic chambers is kept at 10. The wall thickness is kept at 1.5 mm for all inner walls. Side walls (2 mm) are kept thicker than inner walls to ensure material expansion in inner walls. The expansion of the side wall does not contribute to actuator expansion. The apex angle of the actuator (refer to Figure 42) is kept at 30°.

5.3 Determining Designing Parameters of Pneumatic Actuator

5.3.1 Determining the Shape of Pneumatic Chamber

The design of a pneumatic actuator consists of a series of chambers connected as a single body known as a pneumatic network or PneuNet actuator. The PneuNet design provides the actuator with improved speed and force capabilities [10]. The number of components required to fabricate a pneumatic actuator is much less than the conventional actuators, and they are much simpler in terms of operation and design. This actuator is operated with compressed air. As the air pressure inside one of the chambers increases, it starts to inflate like a balloon and actuates the actuator. Traditional PneuNet soft actuators have a pneumatic chamber with a rectangular cross-section, as shown in Figure 36. The rectangular cross-section provides the simplest design. This design has the minimum number of parameters and facilitates an easy fabrication method. The major advantage of this design is that its rectangular cross-section can inflate very well. Nevertheless, at the same time, under a vacuum, the rectangular cross-section does not perform well.
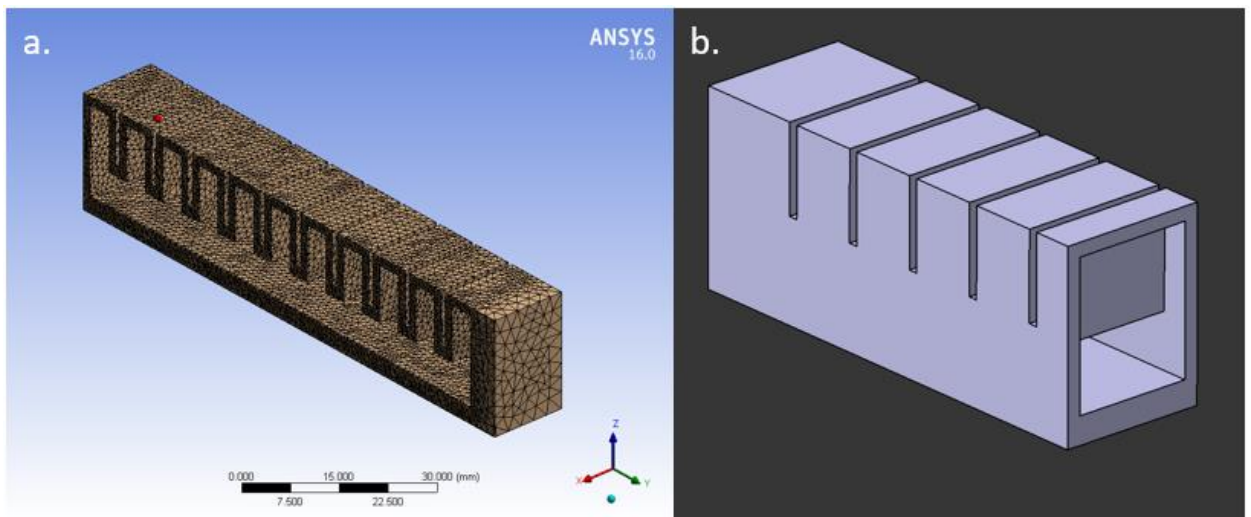
Figure 36. Pneumatic soft actuators with rectangular cross-section a. Section of the actuator along y-z plane, b. Section along x-z plane.

63
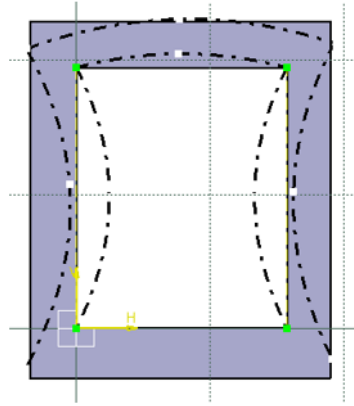
Figure 37. Depiction of rectangular cross-section soft actuator under vacuum

Under vacuum, the rectangular shape does not allow its walls to collapse; hence, the bending achieved in this type of soft actuator is very low. As seen in Figure 37, when the side walls tend to collapse inward, which stops the top wall to collapse inside and forces it to bend outward. Some bending is still achieved, but the geometrical constraints do not allow the top wall to collapse as much, and as a result, significant bending is not achieved. However, this is the case only in vacuum conditions. When under positive pressure, this shape helps a lot. In this research, we aim to find a design suitable for both vacuum and pressure; hence, a new design should be proposed.

The cross-sectional profile for the chamber should have the properties and advantages of the rectangular profile with the additional characteristic of working better under vacuum conditions. The top part can be modified for better performance to eliminate the problem of not collapsing from the rectangular cross-section. Instead, we can introduce a triangle-like structure to the rectangular profile and make a hybrid profile with a triangle on top of a rectangle, as shown in Figure 38. It can be observed from Figure 38 that the proposed design performs very well under a vacuum as the design of the actuator allows the side walls to collapse with negligible geometric resistance. The only obstruction this design has, is undergoing a bi-stable state under a vacuum state. The bi-stable state is a dynamic condition of a mechanism in which the dynamic stability of the material or mechanism can be achieved in one of the two conditions.

Nevertheless, because of the material properties of silicone elastomer, especially Eco-Flex 00-30, this has an insignificant effect on the soft actuator. Therefore, not only this design performs well under vacuum, but it also performs very well under positive pressure, which is presented with evidence in Chapter 6. The simulation results, comparing both the models, with rectangular cross-section and hybrid cross-section, are presented later in this chapter.
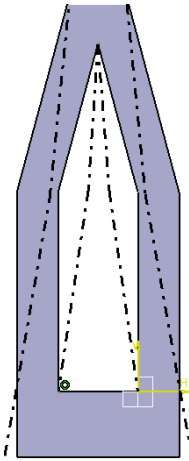
Figure 38. Hybrid profile design of cross-section of the chamber and its condition under vacuum.

Simulation can be conducted to understand the difference in performance between the rectangular cross-section soft actuator and the hybrid profile soft actuator. The design of the soft actuator to be used for the simulation is done in CATIA. The model is then converted into a STEP file format for better compatibility. The model is then meshed more densely than required, leaving no room for error. Boundary conditions are set as required, and calculations are performed. The results of the simulation are as predicted initially. Simulation of a soft actuator with a rectangular cross-section is shown in Figure 39, and simulation of a soft actuator with a hybrid design cross-section is shown in Figure 40. From the results of the simulation, it can be observed that the hybrid cross-section performs significantly better than its counterpart.
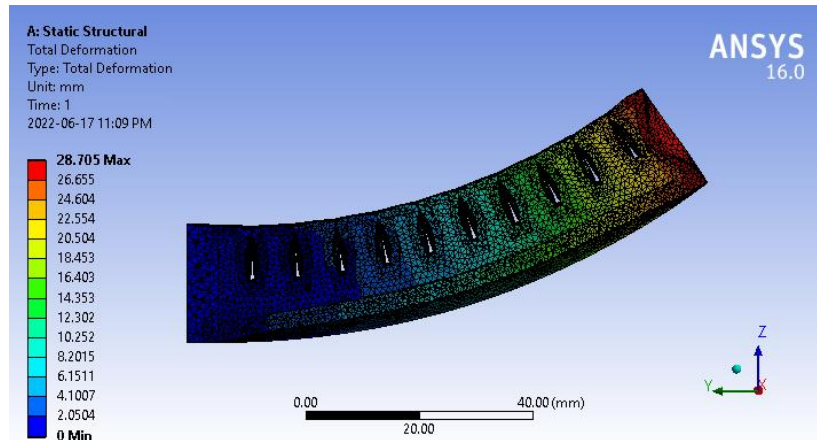
Figure 39. Simulation of soft actuator with rectangular cross-section in ANSYS
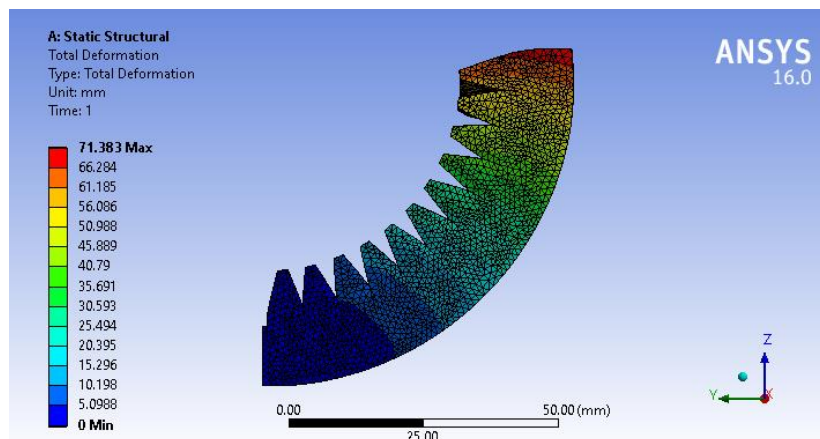
Figure 40. Simulation of soft actuator with hybrid cross-section in ANSYS

Deformation data was collected from ANSYS simulation results which are plotted in Figure 41. Comparison of deformation of soft actuator with rectangular and hybrid cross-section caused under negative pressure. The figure shows the data points of deformation of hybrid design and rectangular cross-section of soft robot with respect to corresponding negative pressure. It can be derived from Figure 39 and Figure 41 that the rectangular soft actuator has bending capacity till the point of saturation, and after that certain point the deformation remains constant even with increase in pressure. The saturation in rectangular soft actuator is due to the hindrance caused by chambers. When the actuator is under vacuum and starts to bend upwards as seen in Figure 39, the chambers

start coming close together from the top and eventually come in contact and that is the point of saturation, as no more bending can be achieved due to structural constraints.
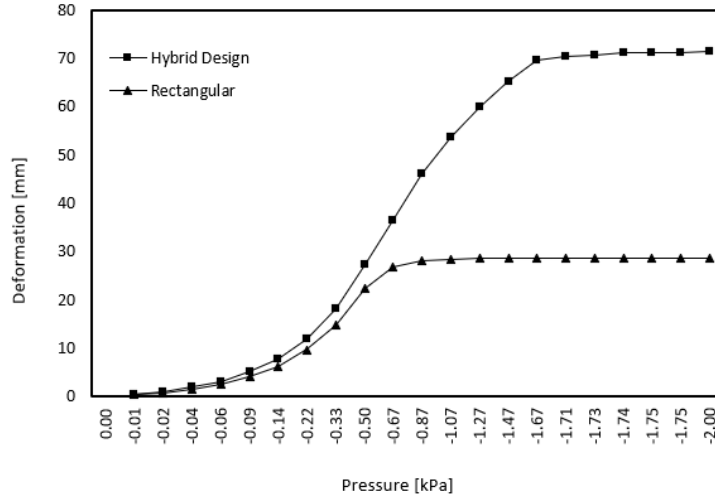
Figure 41. Comparison of deformation of soft actuator with rectangular and hybrid cross-section caused under negative pressure.

The pneumatic network soft actuators are structured as a chain of individual chambers connected together. The design of which determines the design of the soft actuators. So, the hybrid profile design is integrated in the design of the soft actuator. There are a few parameters for the triangle plus rectangle shaped chamber. Figure 42 demonstrates the primary design of the actuator. Where α is the apex angle of the triangular section of the hybrid profile, h_1 is the height of the internal height of the chamber, h_2 is the height of the channel from the base which connects pneumatic network, h_3 is the height of the tringle, t_1 is the thickness of the wall of the chamber, t_2 is the thickness of the base of the actuator, w_1 is the width of the internal chamber and w_2 is the width of the side wall.
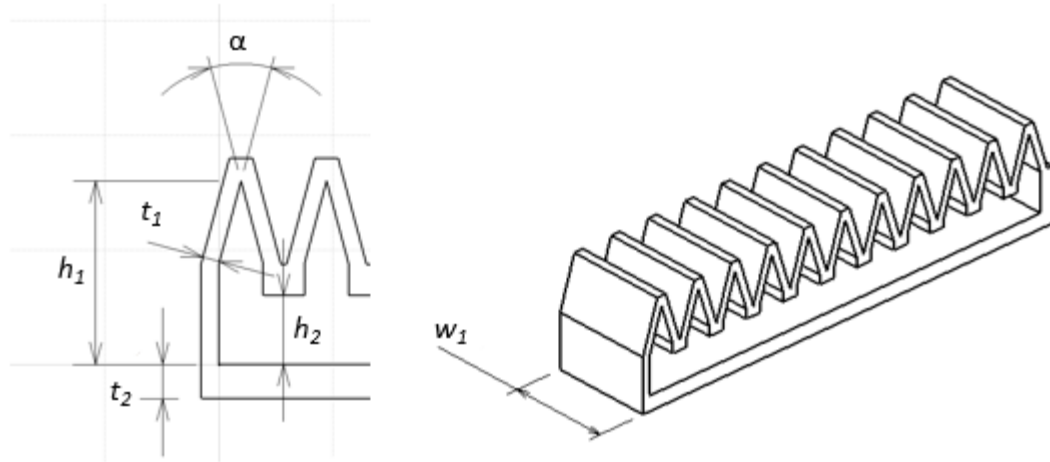
Figure 42. Section view and isometric view of the actuator with dimensional variables.

A study is required to obtain the optimum value of above mentioned parameters. Analyzing all the parameters is significantly time consuming and is out of scope for this research. Hence, only the significant parameters which has the major effect on the actuator are analyzed. The profile of the cross-section of the pneumatic chamber is already decided to be the hybrid shape of triangle on top of the rectangle.

5.3.2 Optimizing the Apex Angle α

In the study of finding the optimum value for the apex angle of the hybrid design number of simulations were performed on ANSYS. All other parameters such as length, wall thickness, bottom layer thickness was kept constant for all simulation cases. The simulations were conducted for every value of apex angle ranging from 20 degrees to 40 degrees with interval of 5 degrees. Figure 44, Figure 45, and Figure 46 shows the simulation results of bending with different apex angles (20°, 25°, 30°, 35° and 40°).

The bending angle is measured by implementing a joint probe into the solution parameters of the Mechanical (ANSYS Multiphysics). The observation point is located at the center of the end face of the actuator and the probe calculated angle with reference to the fixed face of the actuator as shown in Figure 43. The maximum bending angle obtained was 183.1° at 35° of apex angle and 3 kPa. In Figure 47, the trend of the effect of apex angle on the bending angle can be observed.
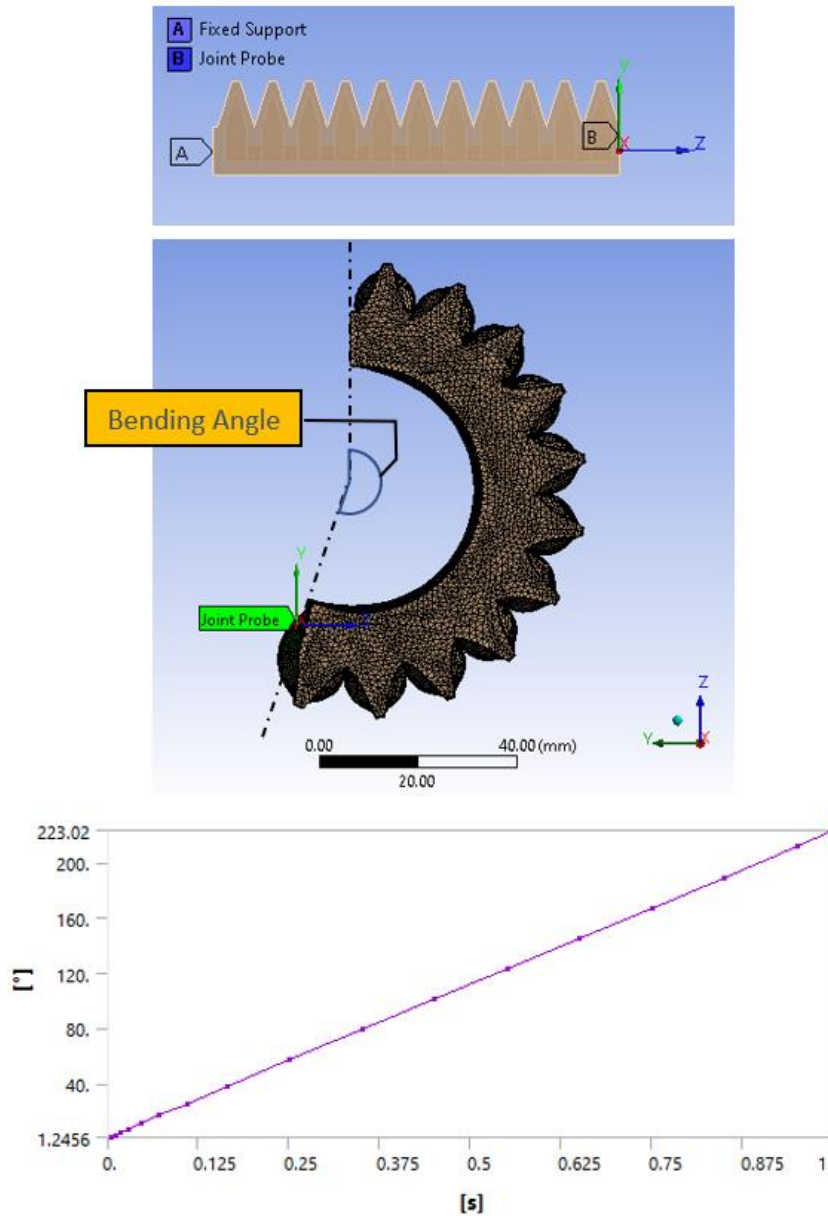
Figure 43. Calculating bending angle of simulated actuator on ANSYS
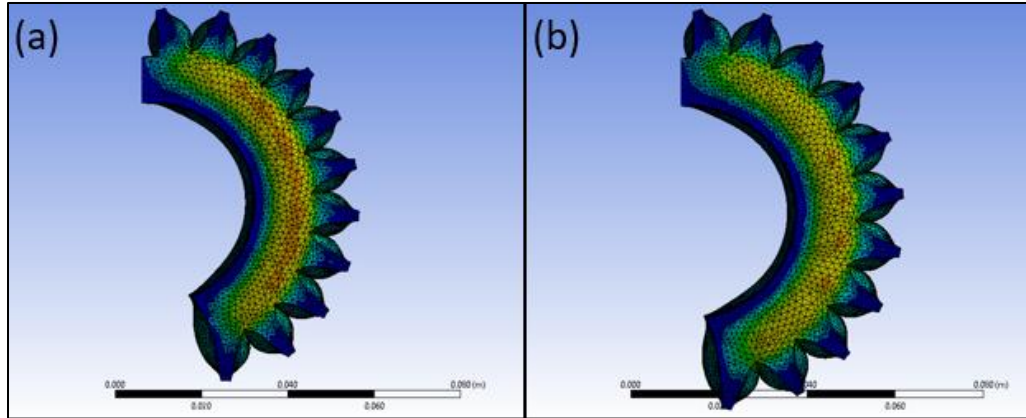
Figure 44. Simulation (ANSYS) result of actuator with apex angle of (a) 20° and (b) 25°
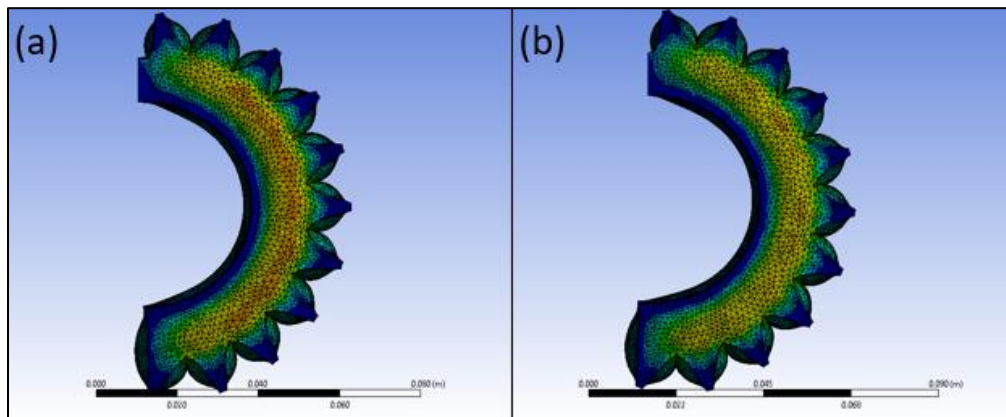
Figure 45. Simulation (ANSYS) result of actuator with apex angle of (a) 30° and (b) 35°
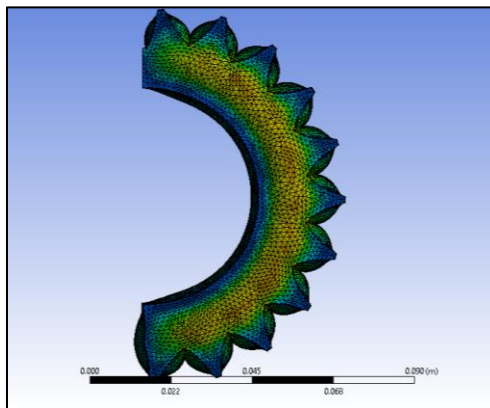
Figure 46. Simulation (ANSYS) result of soft actuator with apex angle of 40°
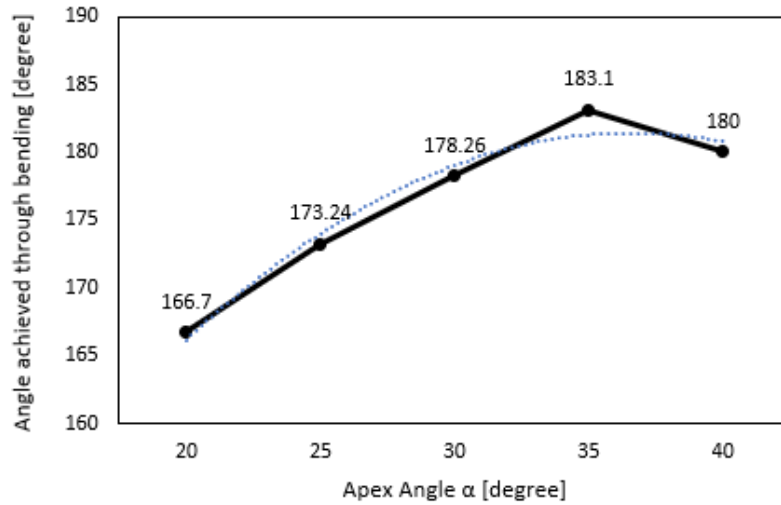
Figure 47. Change in bending angle with apex angle (simulation results).

Figure 47 shows the simulation results with a plot of apex angle vs bending angle. The bending angle of the pneumatic actuator was observed to increase with increase in apex angle but dropped after 35° of apex angle. Therefore, maximum bending angle observed is 183.1°.
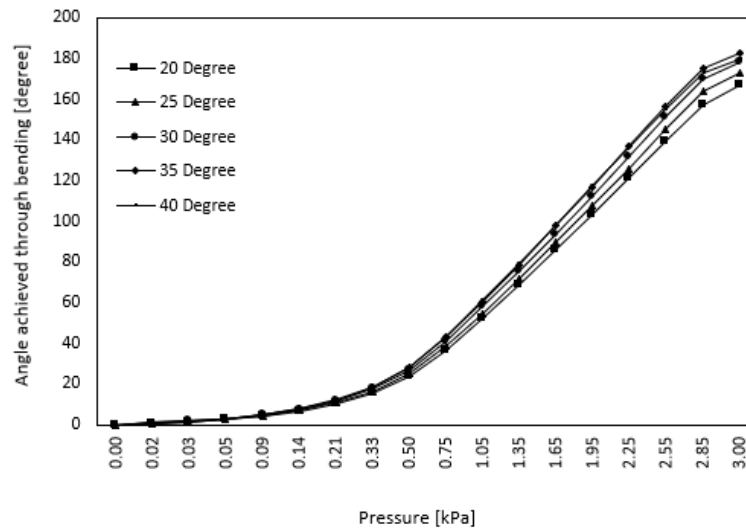
Figure 48. Bending angle at given pressure for actuators with different apex angles
(simulation results)

Figure 48 shows the plot between pressure and bending angle for different apex angles. It was observed that the bending angle response to applied pressure followed similar trend irrespective of the apex angle.

5.3.3 Optimizing the Bottom Layer Thickness

Bottom layer supports the entire actuator. The thickness of bottom layer determines the bending angle and also affects the linear elongation of the actuator. As this part of the actuator needs to be constraint in length in order to achieve maximum bending and transfer of force. Figure 49 shows the change in bending angle with respect to bottom layer thickness. Simulations were conducted for soft actuators for different values of bottom layer thickness keeping all the other values constant. After the simulations, the best value found to be 5 mm.
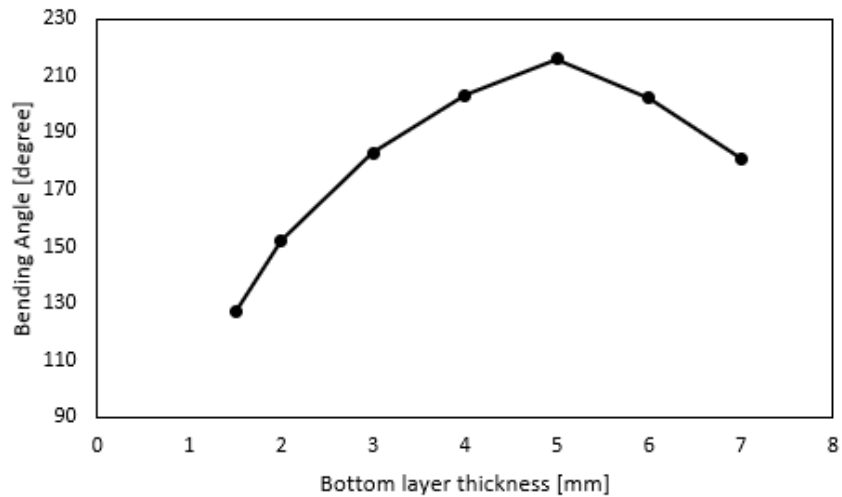
Figure 49. Change in bending angle with bottom layer thickness (simulation results)

In summary, various parameters of the actuators are determined based on simulation. A number of simulations were conducted to find the pattern followed by a parameter concerning bending angle. It was observed that a hybrid triangle design on top of the rectangle is more suitable compared to the conventional rectangle design for a chamber cross-section. The curve of bending angle with change in apex angle was found to achieve the maximum value of bending angle at the apex angle of 35 degrees. Similarly, simulation studies were performed to determine the best bottom layer thickness, and the maximum bending angle was achieved with the bottom layer thickness of 5mm. The study on the width of the actuator resulted in an increasing bending angle with an increase in

the width. However, as the width increases, the actuator becomes more impractical and loses its

structural integrity.

5.4 Design of the Prototype
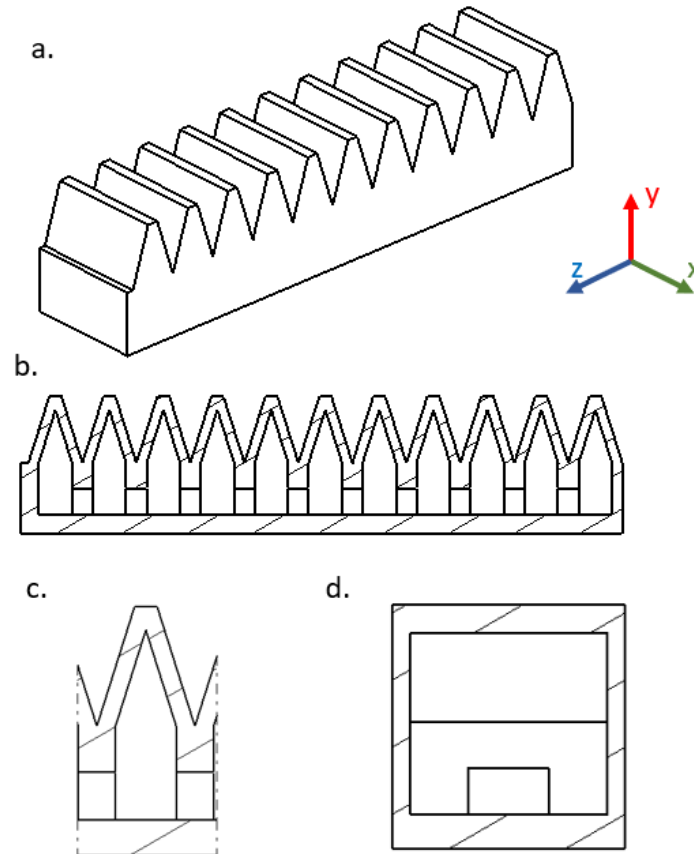
Figure 50. a) Isometric view of the soft actuator and reference co-ordinate system, b)
section view of the actuator in y-z plane, c) enlarged view of the cross-section of the
chamber, and d) cross-section of the actuator in x-y plane

After analyzing and finalizing the parameters, a final design was done using CATIA. Figure 50

shows the isometric and various cross-section of the design for better understanding. After

designing in CATIA the final file is imported to ANSYS for performing simulations. The CATIA

part file is converted to step file and imported to ANSYS. Material properties for Eco-Flex 00-30

were calculated in Chapter 4. The material model selected for the simulation is Yeoh 2nd order. The

material constants were calculated in ANSYS using curve fitting tool. The material constants obtained were C_{10} = 9392.09 Pa, C_{20} = 50.93876 Pa and the material was assumed to be incompressible and hence the incompressibility parameters were assumed null. The meshing was performed in ANSYS with 33309 nodes and 144233 elements for better results and shown in Figure 51. The simulation is then carried out with internal pressure of 3000 Pa with one end of the actuator fixed in space. The simulation results are shown in Figure 52.
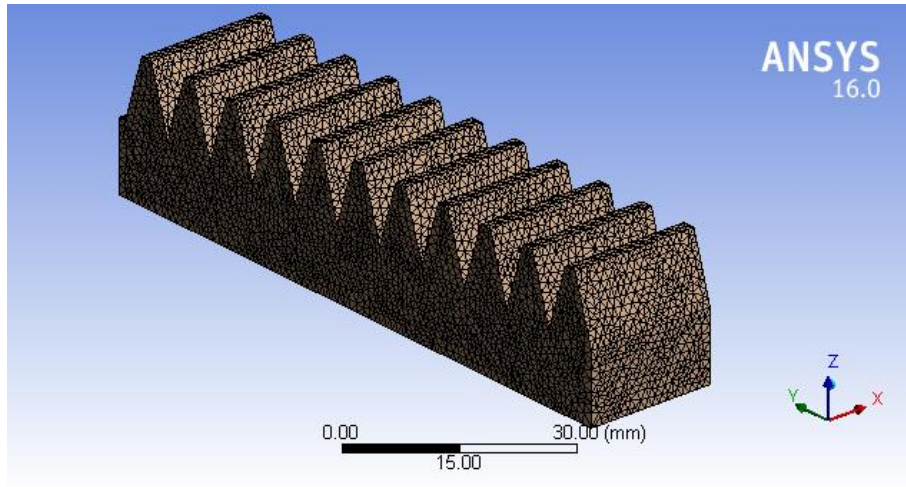
Figure 51. Meshing of the actuator in ANSYS
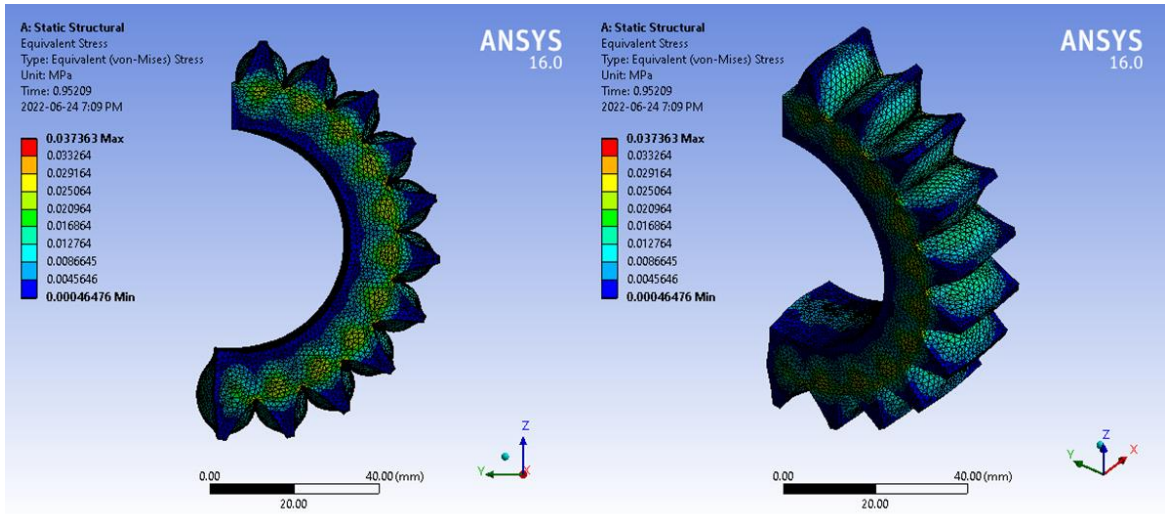
Figure 52. Simulation of the final design of the actuator

With finalizing the design of the actuator and performing simulation, the maximum angle achieved is 223.02 degree. Figure 53 shows the relation between bending angle and pressure which was observed to be linear.
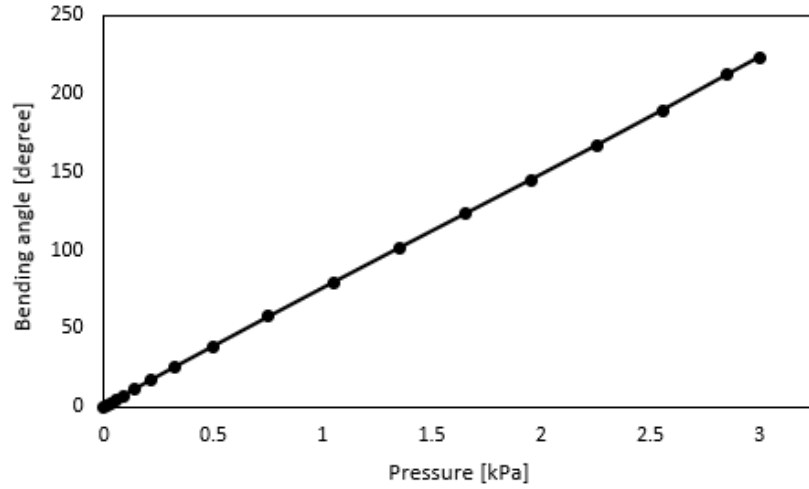
Figure 53. Change in bending angle with pressure

5.5 Theoretical Analysis of the Actuator
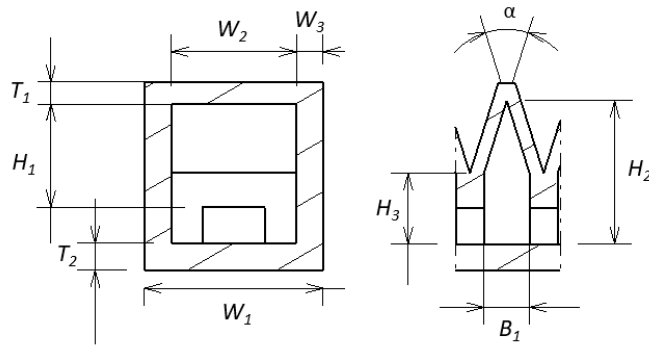
Figure 54. Schematic diagram of cross-section of pneumatic chamber.

In order to understand the behavior of the actuator, in relation to its design parameters, a theoretical model is developed. The hybrid design of triangle on top of rectangle is used to develop the model. the side walls are deliberately kept wider than the top wall so that, the extension would majorly

occur in top wall. This extension leads to better bending performance. To make the model simpler, the actuator is assumed to be a beam with uniform loading. According to Euler-Bernoulli principle,

$$\frac{1}{R} = \frac{M}{EI} \qquad (12)$$

Where R is radius of the curvature, M is bending moment, E is young's modulus, and I is moment of inertia of the chamber when it is inflated. The maximum inflation occurs at the middle of the inflating chamber which is shown in Figure 55 which shows a simplified cross-sectional view of inflated chambers of soft actuator.
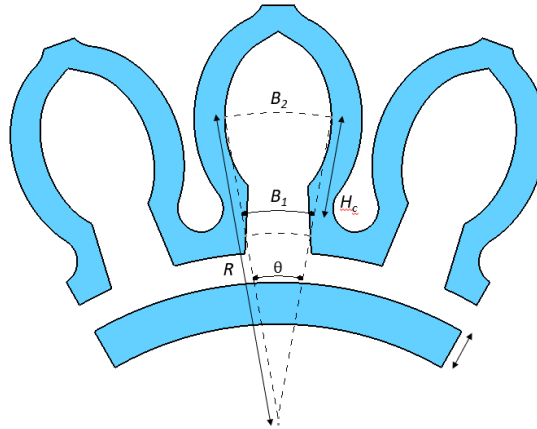
Figure 55. Schematic diagram of inflated chambers (approximate)

For simplification, the inflation of the chamber is assumed to be elliptical and the bending angle for an individual chamber after inflation is shown in Figure 55 and given by,

$$\theta = \frac{B_2}{R}$$

$$\theta = \frac{B_1}{R - H_C} \qquad (13)$$

Where B_2 is maximum width of the elliptical chamber after inflation, R is the radius of the curvature form by bending, B_1 is the initial width of the chamber, and H_C is distance between B_1 and B_2. After inflation, the volume of the inflated elliptical chamber is given by,

$$V = \frac{\pi}{4} H_1 B_2 W_2 \qquad (14)$$

Where H_1 is the height of the inflated part and W_2 is the width of the internal (inflated) part. Solving the state of the soft actuator based on principle of minimum potential energy [91], the total energy (potential) stored in the actuator without any external forces for individual chamber is given by,

$$\Gamma = \frac{1}{2} D B_2 k^2 - pV \qquad (15)$$

Where D is flexural rigidity of the chamber, k is curvature of the individual chamber and p is pressure. D and k are given by,

$$D = EI \qquad (16)$$

$$k = \frac{1}{R} \qquad (17)$$

From (13), (14) and (15),

$$\Gamma = \frac{1}{2} D B^2 \frac{k^2}{(1 - kH_C)} - \frac{\pi}{4} \frac{pH_1 W_C B_2}{(1 - kH_C)} \qquad (18)$$

At equilibrium, the small change in potential energy becomes zero, $\frac{\partial \Gamma}{\partial k} = 0$, therefore,

$$\frac{d}{dk} \left[\frac{B_2 D k^2}{2(1 - Hk)} - \frac{\pi B_2 H_1 W p}{4(1 - Hk)} \right] = 0$$

$$= \frac{B_2 D}{2} \cdot \frac{\mathrm{d}}{\mathrm{d}k}\left[\frac{k^2}{1-Hk}\right] - \frac{\pi B_2 H_1 Wp}{4} \cdot \frac{\mathrm{d}}{\mathrm{d}k}\left[\frac{1}{1-Hk}\right]$$

$$= \frac{\frac{\mathrm{d}}{\mathrm{d}k}[k^2] \cdot (1-Hk) - k^2 \cdot \frac{\mathrm{d}}{\mathrm{d}k}[1-Hk]}{(1-Hk)^2} B_2 D}{2} + \frac{\pi \cdot \frac{\frac{\mathrm{d}}{\mathrm{d}k}[1-Hk]}{(1-Hk)^2} B_2 H_1 Wp}{4}$$

$$= \frac{\left(2k \cdot (1-Hk) - \left(\frac{\mathrm{d}}{\mathrm{d}k}[1] - H \cdot \frac{\mathrm{d}}{\mathrm{d}k}[k]\right)k^2\right) B_2 D}{2(1-Hk)^2}$$

$$+ \frac{\pi \cdot \left(\frac{\mathrm{d}}{\mathrm{d}k}[1] - H \cdot \frac{\mathrm{d}}{\mathrm{d}k}[k]\right) B_2 H_1 Wp}{4(1-Hk)^2}$$

$$= \frac{(2k \cdot (1-Hk) - (0 - H \cdot 1)k^2)B_2 D}{2(1-Hk)^2} + \frac{\pi \cdot (0 - H \cdot 1)B_2 H_1 Wp}{4(1-Hk)^2}$$

$$= \frac{B_2 D \cdot \left(Hk^2 + 2k \cdot (1-Hk)\right)}{2(1-Hk)^2} - \frac{\pi B_2 H H_1 Wp}{4(1-Hk)^2}$$

$$\tag{19}$$

$$= \frac{B_2 Dk}{1-Hk} + \frac{B_2 DHk^2}{2(1-Hk)^2} - \frac{\pi B_2 H H_1 Wp}{4(1-Hk)^2} = 0$$

Solving for k, we get,

$$k = \frac{EI + \left((EI)^2 - \frac{\pi}{2}(EI)H_1 W_c p H_c^2\right)^{1/2}}{EIH_c} \tag{20}$$

From (13), (17), and (20), solving for θ, we get,

$$N\theta = NB_2 \frac{EI - \left[(EI)^2 - \frac{1}{2}\pi EIW_c H_1 H_c^2 p\right]^{1/2}}{H_c\left[(EI)^2 - \frac{1}{2}\pi EIW_c H_1 H_c^2 p\right]^{1/2}} \tag{21}$$

Where, N is the number of chambers and $N\theta$ is the total angle achieved by the actuator. Also, this equation provides the relation between θ and p. From this formulation, we can determine the change in angle with change in input pressure. A plot shown in Figure 56 shows the change in bending angle achieved by the theoretical formulation of soft pneumatic actuator with change in pressure. The plot achieved is parabolic in nature.
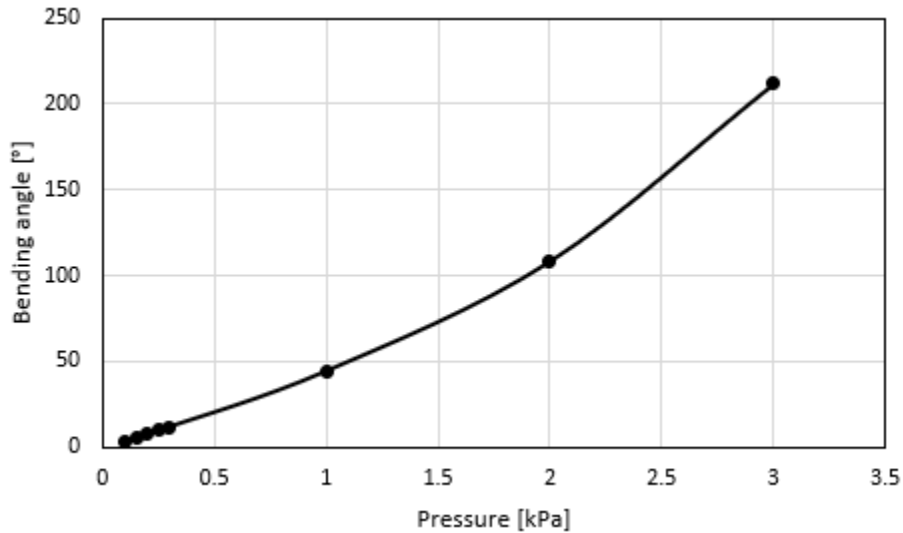
Figure 56. Change in bending angle with change in pressure of theoretical model.

5.6 Conclusion

In this chapter, a basic geometry of the actuator was defined with its outer dimensions of 100 mm * 20 mm * 20 mm and the number of pneumatic chambers to be 10 with a condition of side walls and bottom layer to be thicker than the chamber's lateral walls. A profile comparison was made between the conventional and the proposed hybrid design, resulting in better performance of the hybrid actuator, acquiring 53° more bending angle of the actuator under vacuum. Parameter optimization is performed on various parameters like apex angle and bottom layer thickness. A final design was made on CATIA for prototyping, and numerical studies were conducted through simulation software-ANSYS. A relation between internal pressure and bending is obtained. A theoretical study based on the principle of minimum potential energy was also performed to

understand the behavior of different parameters. A model is developed for bending angle θ as a function of internal pressure p.

Chapter 6 Experimental Study and Results

6.1 Manufacturing of Soft Actuator

6.1.1 Designing of the Mold

Design of a mold is primary goal. The requirements for designing this mold are listed below.

- Primary (conceptual) design of the mold according to the requirements.

- The cured silicone part should be able to come out without requiring much force.

- The removal of part should not damage the actuator.

- The removal process should not do any damage to the mold parts in order to use the mold for multiple times.

- The shrinkage of the material should be considered.

- The feasibility of the product with the molding technique and vice-versa.

- Iterations in the design of mold and the product according to the mold-product requirements.

- Prototyping and testing of the mold.

The primary mold was designed in CATIA, where the design was simple and consisted of only one part mold with one opening for the pouring of uncured silicone. In order to remove the cured silicone, we needed to pull the part with much force or break open the mold, which made the design and manufacturing of this mold very complex. Therefore, the above technique was eliminated. The second method included dividing the molding process into two parts. One is the inner mold or core, and the other is the outer shell. So, we make half of the actuator with a two-part mold, as shown in Figure 57, where there is no flat layer. Then, we dip this half actuator and place it in the molding tray. The function of the molding tray is to incorporate the missing side of the wall of the actuator by gluing. The uncured silicone elastomer can also function as glue and form new chemical bonds

with cured silicone. Therefore, we can superimpose a new mold on the existing silicone actuator by taking advantage of that property. This method is perfect theoretically, but when experimented with, it was observed that while performing the removal of the first half, the cured silicone does stick to the mold partially, and removal of the mold did damage the actuator 3/5 times as it can be observed in Table 7. Also, in one of the case studies, it was required to break the outer shell to remove the silicone part.
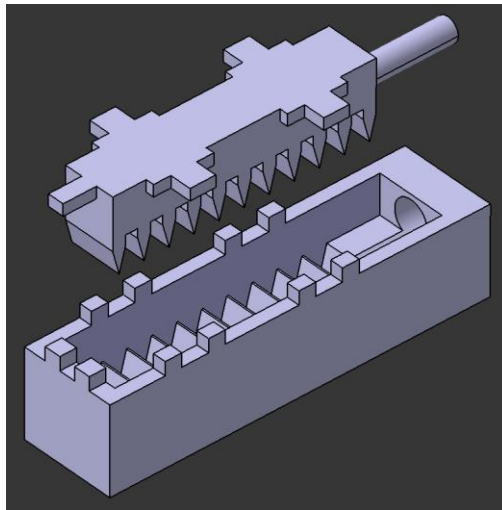
Figure 57. The second version of mold design

Table 7. Mold test for two part mold.

Mold Test	Degree of damage	Damage description
1	minimal	Damage on one tooth.
2	significant	Teer in sidewall
3	No damage	NA
4	insignificant	Cosmetic damage
5	significant	Teer in inlet port

As a result, this method was also rejected, and a new method was put to test. This third method included dividing the mold in three parts, and the two-step molding process was carried forward from the last method. The outer shell was divided in two parts and then joined together with a fastener. The rest of the process remained same. When first half of the actuator was cured, the outer shell was open loose just by unfastening the bolts. This made the removal process quite simple and efficient and there was no damage to the mold. It can be observed in the Figure 58, that upper part is the inner core of the mold and two components at the bottom are the outer shell.
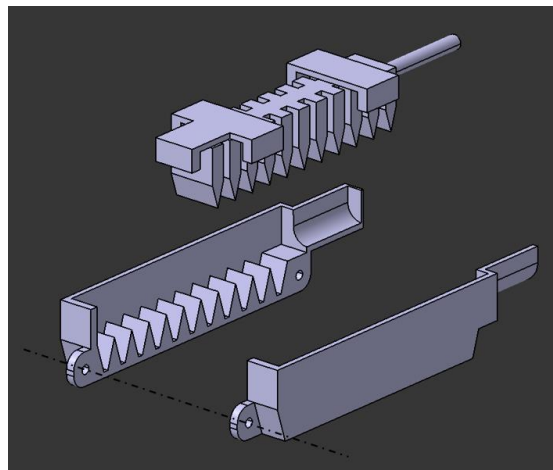
Figure 58. Improved and final version of mold used for fabricating soft actuator

6.1.2 Preparing the Mold

6.1.2.1 Fabrication of the Mold

The designing of the mold is done in CATIA. After the initial design is made in CAD software, the design is improved in for fabricating using 3D printing. A number of components were added to the design in order to incorporate fabricating process. A couple of flanges were added to the design of the shell so that the mold can be aligned and affix together when pouring uncured silicone elastomer. The mold was fabricated using fused deposition modeling (FDM) 3D printing. Polylactic acid or PLA is used as material for 3D printing. PLA is used as the printing material

because it provides almost no adhesion to the silicone elastomer and that help in removal of the mold and eliminates the requirement of mold removal products. CAD model was exported from CATIA as stl file for slicing. Slicing is the process in which the CAD model is divided into multiple layers in such a way that, the printer is able to print a layer at a time. The slicing software used is Ultimaker Cura. Stl files were imported to Cura, and optimal setting were set to get the best quality of print. In output, the slicer returns G-code file for particular 3D print. This gcode file is than run on the 3D printer to obtain the print.

6.1.2.2 Cleaning the Mold

Although the 3D printing with PLA provides particularly good quality of print, a post processing is still needed. The 3D printer prints at 210 °C, and there are cooling fans to reduce the temperature. Still the print does not cool immediately and sometimes forms stringing. Stringing occurs when the printing material is not properly cooled which was followed by printer head travel, which drags the melted PLA in the form of hair like strings. To remove these strings a simple filing is enough. Also, unnecessary sharp edges were also filed. The mold was washed with water and dried completely before used.

6.1.2.3 Preparing Silicone Elastomer Eco-Flex 00-30

The preparation of Eco-Flex 00-30 is quite uncomplicated process. The silicone elastomer comes as two part material from manufacturer, one of them is base material – Part-A and other is curing agent – Part-B. These materials are required to mixed properly in 1:1 ratio. This ratio can be by volume or by weight. The Part A and part B were measured by weight and mixed properly. When mixing this solution, air bubbles get trapped and need to be removed. For that the solution of chemicals is kept into the vacuum chamber. The pot life of this solution is supposed to be 40 minutes according to the manufacturer, but it was observed that pouring it into the mold withing 15 to 20 minutes is optimal.

6.1.3 Fabrication of the Actuator

Fabrication of the actuator is a two-step process. The top part with profile of the chamber is made first with one side open as shown in Figure 59 and Figure 60. The second part is covering up bottom with sealing the entire actuator but one of the openings for air to in and out.

Prepared solution of silicone elastomer is poured into the assembled mold. The elastomer mixture is poured slowly as it has high viscosity and due to high viscosity, the silicone takes longer to reach crevices. After pouring is completed, the mold is placed on a flat surface and let it set for about 4 hours. Which is followed by removal of the elastomer from the mold as shown in Figure 59 and Figure 60. The preparation of silicone elastomer, mixing of part A and part B, degassing it for the removal of suspended gas bubbles and pouring it into the mold takes about 15 minutes altogether.

After finishing first part, the prepared silicone is placed into the second mold of silicone which is at the height equal to the height of base layer as shown in Figure 59-Step 3 and Figure 60 e). A simple rectangular tray with the dimensions, those are equal to the outer dimensions of the actuator, acts as a second mold. Time required for individual stage of fabrication and total time for fabrication is listed in Table 8.

Table 8. Time required for soft actuator during various stages of fabrication.

Process	Time
3D printing Mold	12 hrs.
Assembly of mold	0.25 hrs.
Preparing silicone-1	0.25 hrs.
Mold setting-Part 1	4 hrs.
Removing Part 1	0.25 hrs.
Preparing silicone-2	0.25 hrs.
Mold-Part-2	4 hrs.
Total time	**21 hrs**
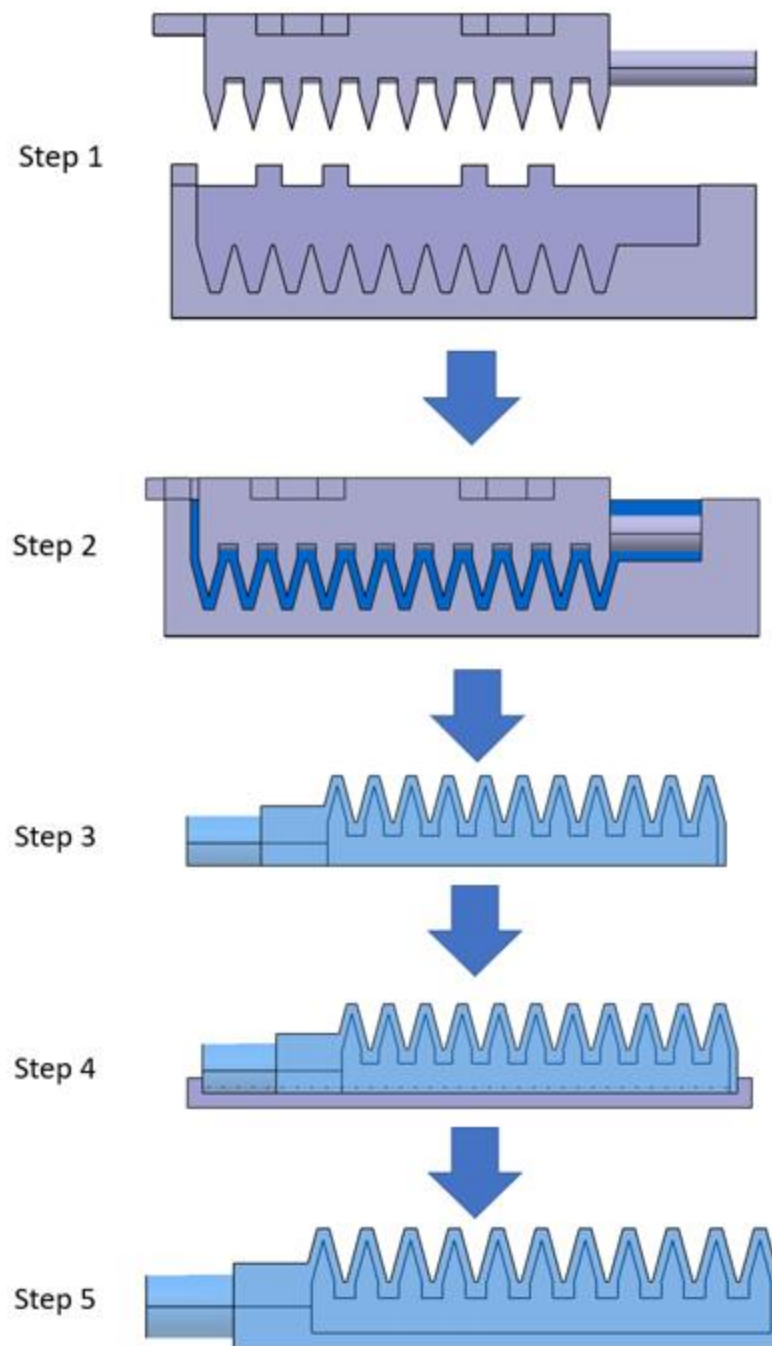
Figure 59. Steps of fabrication process. 1) assembling 3D printed mold, 2) pouring uncured silicone into the mold, 3) removing first part of the mold, 4) setting first part of the mold on second part of the mold to finish bottom layer, 5) removing actuator from the mold.
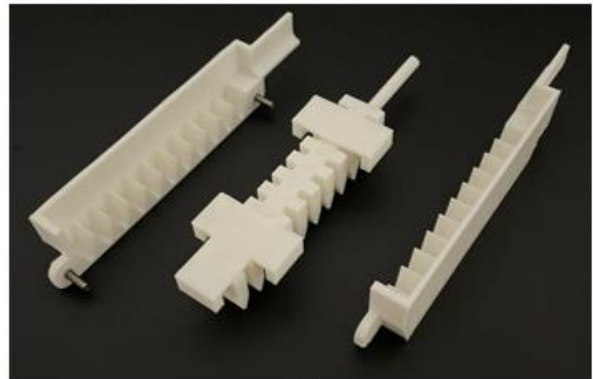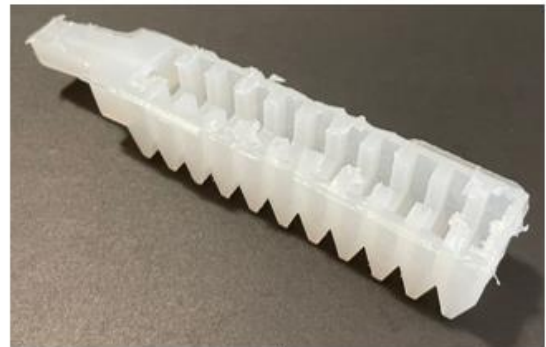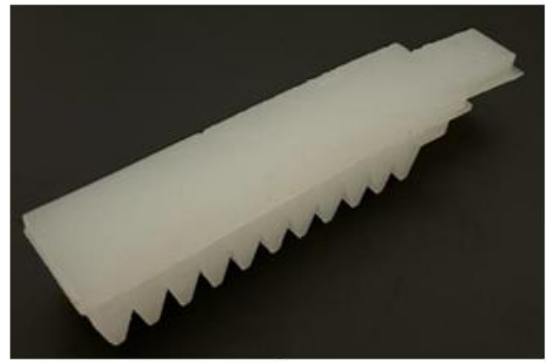
Figure 60. a) pouring and mixing of part A and part B of the Eco-Flex 00-30 in equal parts by weight, b) assembling the 3D printed molds and pouring the silicone elastomer, c) solidified elastomer after curing, d) mold removal-upper half of the actuator, e) attaching the bottom layer and curing it for four hours, f) fabricated actuator with trimmed excess elastomers.

6.2 Granular Jamming Component

When a granular material is stored in a flexible bladder or a sac, and subjected to a vacuum, the particles tend to come close to each other like a bonding force pulling them together. This phenomenon behaves like attraction between molecules and the sac filled with granular particles becomes stiffer and act like solid. This phenomenon is known as particle or granular jamming. The solid like state of the particle in sac can be called pseudo solid.

A stiffness enhancement component is added to the actuator under study which is attached externally to the soft actuator. When deactivated the soft actuator is able to move freely with granular jamming component as moving a sac filled with granular material is relatively easy. Once into position, the granular jamming component can be activated to increase stiffness. This allows the gripper to hold more weight when compared to without jamming component state.
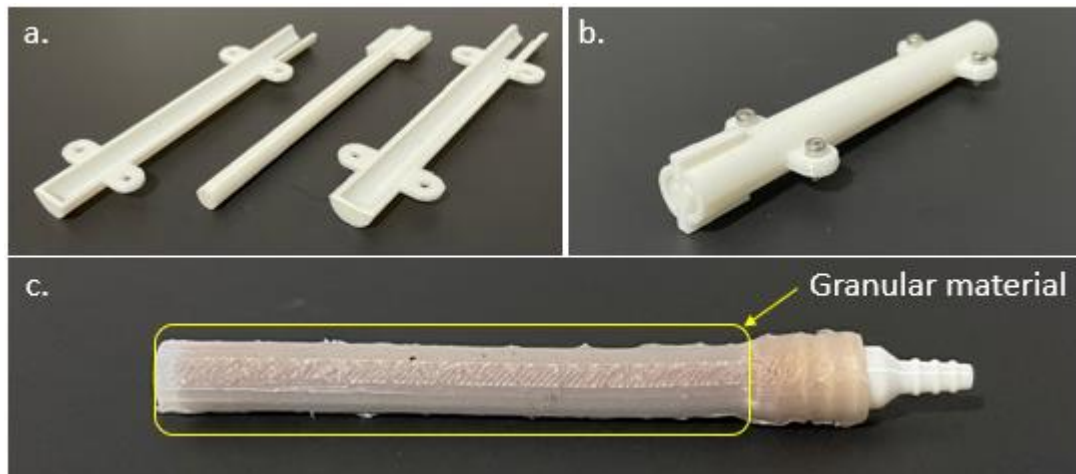
Figure 61. a) 3D printed mold parts for granular sack, b) assembled mold ready for pouring, and c) fabricated silicone bladder filled with granular material (ground coffee).

Granular jamming component are added externally, which consists of a flexible bladder which runs parallelly on either side of the actuator as shown in Figure 62 and Figure 63. These bladders are filled with granular jamming particles. The bladder is fabricated using the same material Eco-Flex

00-30, the material has maximum strain limit of 900%, which makes it ideal material for a vacuum bladder. Using same material also reduces material waste. Also, the silicone has a property to form new bolds even after it has been cured which makes it quite easy to weld the material together.

A 3D printed mold is used to fabricate the bladder. Figure 61 shows the 3D printed mold and its assembly. Figure 61 c) shows the bladder filled with granular jamming material (ground coffee) with a 3D printed connector.
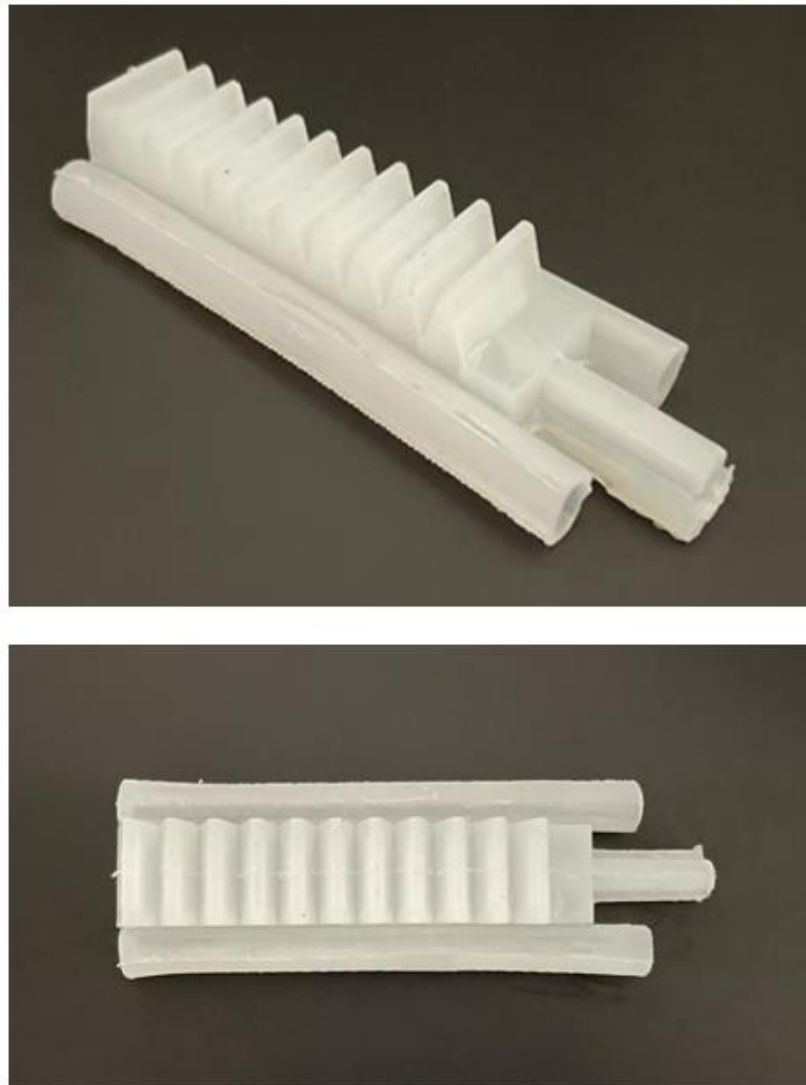
Figure 62. Granular jamming component attached to soft pneumatic component.
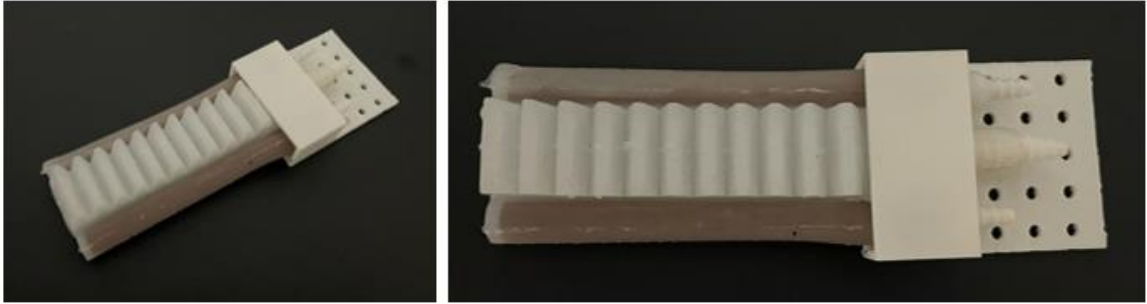
Figure 63. Attached granular jamming component filled with granular material
(Ground Coffee)

6.3 Hardware Setup

After analyzing the performance of the gripper numerically and using commercially available simulation suite, an experimental study is performed to observe how the actuator performs practically. This section discusses on experimental setup for the actuator with and without granular jamming component. It also includes brief on hardware required to run the actuator and its setup.

The hardware unit is setup to provide the actuator with positive and negative pressure and simultaneously record the pressure data. The hardware includes a pneumatic pump, rated at 42 Watts with 12 V. The pump has positive and negative pressure capabilities with one port pushing air out and another one sucking the air in. Both the ports are connected to a valve system which are controlled manually and can be controlled using solenoid valve. The valve system is attached to a pressure sensor (SparkFun Qwiic MicroPressure Sensor equipped with Honeywell's 25psi piezoresistive silicon pressure sensor [80].) which can detect both positive and negative pressures. The pressure sensor is connected to the Arduino to give real time data on the computer. The motor is connected to a motor driver which is controlled by PWM (pulse width modulation) from Arduino. The PWM signal controls the speed of the air pump and powered by external power source of 12V. Figure 64 and Figure 65 shows the hardware setup for operating soft actuator.
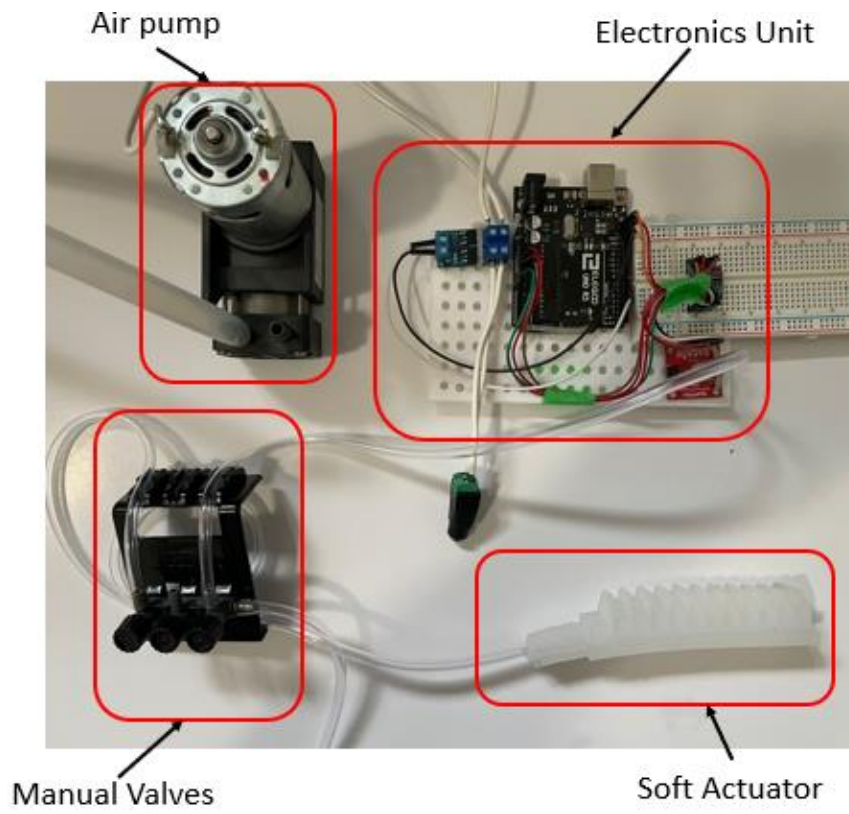
Figure 64. Hardware setup for operating soft actuator
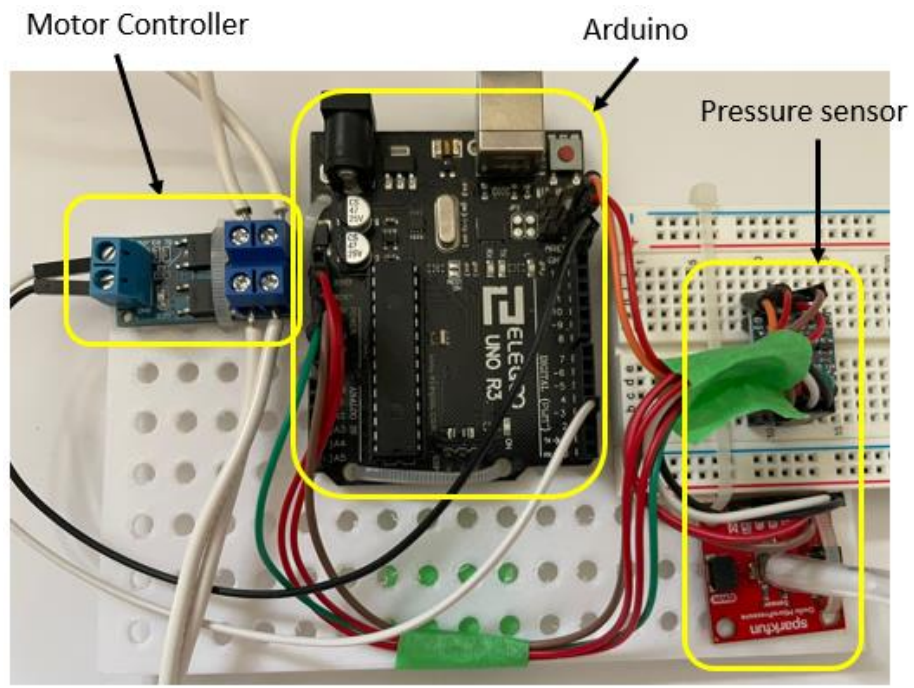
Figure 65. Electronics Unit with Motor controller, Arduino, and Pressure sensor unit.

6.4 Experimental Results and Comparison

The hardware unit, as discussed above is set up. The pump motor is powered by external power source. While operating the motor, a pressure sensor is used to check the corresponding pressure for angle obtained by the soft actuator. Figure 66 shows bending of the soft actuator at different pressure values. The actuator is fixed at one point and then the miniature air pump is powered to inflate the actuator. The actuator takes less than 1 second to inflate and deflate to come to its resting position.
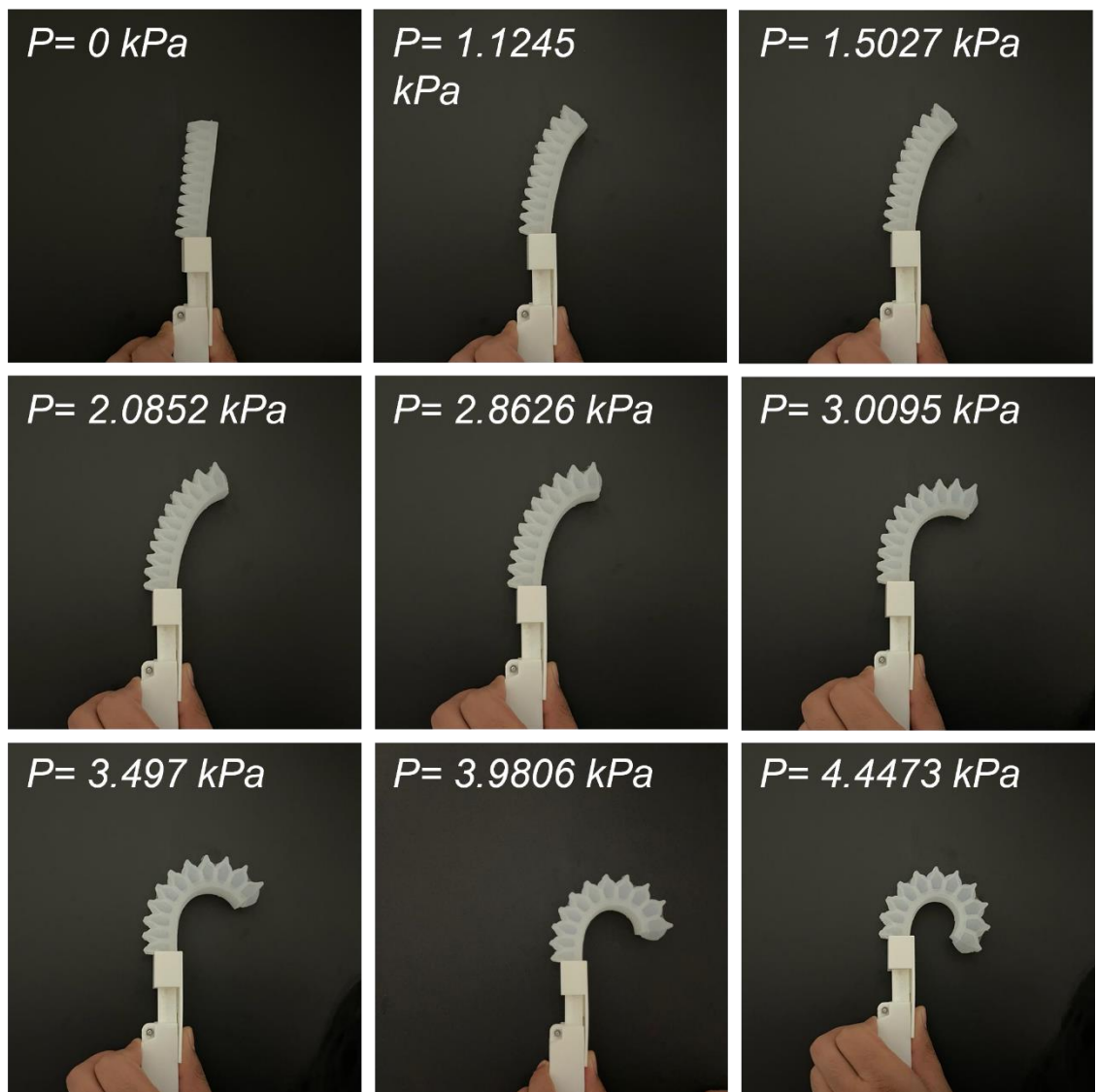
Figure 66. Bending of the soft actuator at different pressure values.

To measure the bending angle, the actuator is fixed with a clamp and the camera is fixed directly on top of the actuator. The data is collected in the form of video and frames are extracted from the video to measure the bending angle. the frames are imported to CATIA individually in the form of image. A grid was placed on the image with origin of the grid at the base of the actuator as shown in Figure 67. A tangent to the base of the actuator is drawn at the end point of the base. The angle between the vertical axis and tangent determined the bending angle.
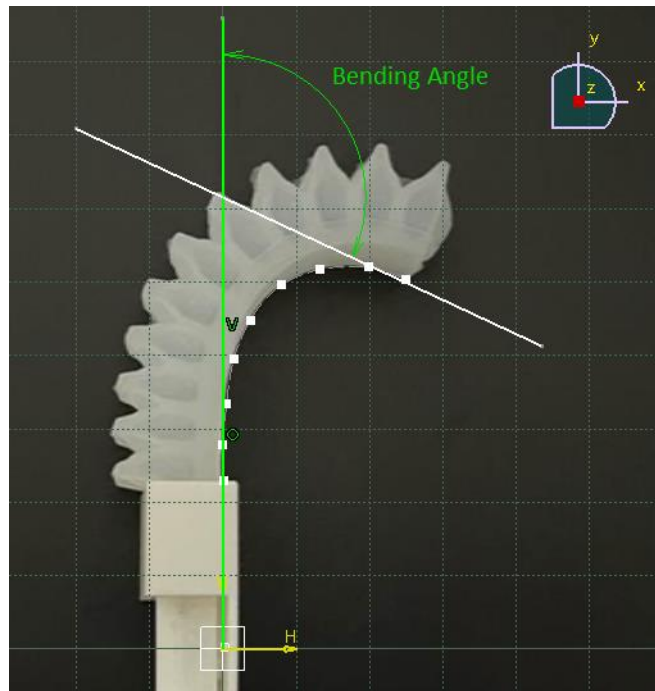
Figure 67. Measurement of bending angle from experiments (screen shot-CATIA).

6.4.1 Comparison of Experimental Results and Simulation Results

The comparison results are shown in Figure 68. The approximate angle obtained by both, experimental and simulation is 223°. In simulation, 223° angle was obtained at a pressure of 3.2 kPa whereas, the fabricated actuator required about 4.4473 kPa to obtain 223° angle and 5.112 kPa for 340° (maximum). A significant difference in the achieved bending angle is observed.
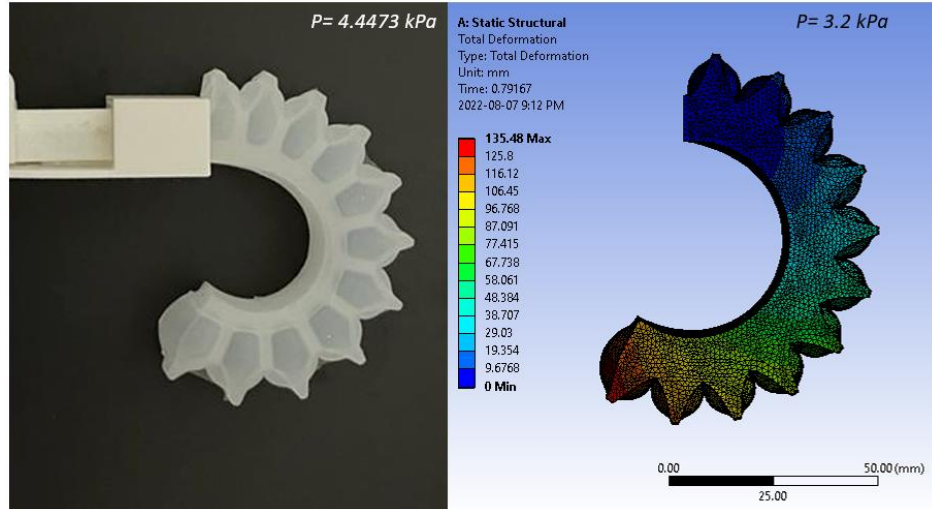
Figure 68. Comparison of experimental result with simulation result for approximately same bending angle.
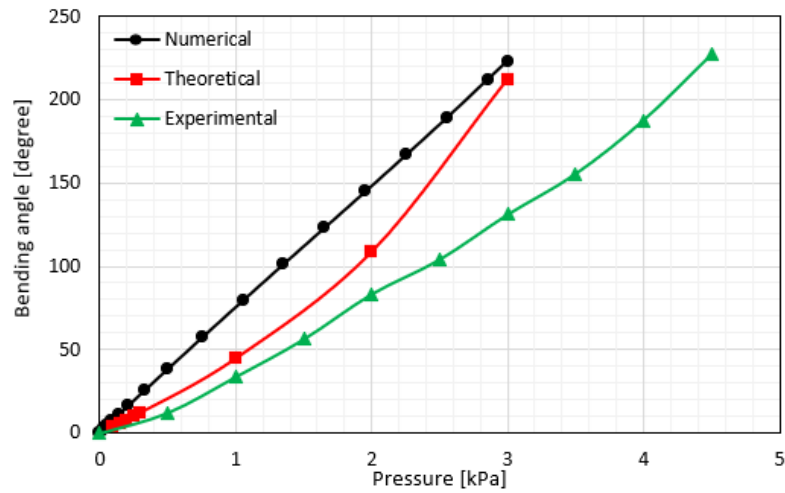
Figure 69. Comparison of numerical, theoretical, and experimental bending angle of the actuator with applied pressure.

Figure 69 shows the comparison of numerical, theoretical, and experimental data of obtained bending angle for a pressure data point. The bending angle increased steadily with increase in input pressure. The numerical model shows a linear relationship between bending angle and pressure whereas, the theoretical model shows a parabolic relation between them. The experimental analysis shows that the bending angle increased linearly at first till 3 kPa but becomes parabolic with increase in pressure. The numerical and theoretical results show a significant similarity whereas

the experimental result have a constant slope difference. This difference indicates that more parameters need to be considered when formulating the theoretical model such as introducing a constant. The curve of the theoretical data has a trendline, which can be modified directly by multiplying it with a constant to fit the experimental data. Studying about this constant is out of scope for this research and can be conducted in future studies. The simulation is conducted with ideal scenario whereas the experiments succumb to various losses. The graph shows non-negligible pressure losses which can be caused by pneumatic network, pneumatic pipes, frictional losses, and experimental errors. These losses are unavoidable in nature and cannot be rectified completely.

6.4.2 Comparison of Bending angle with and without Jamming Component
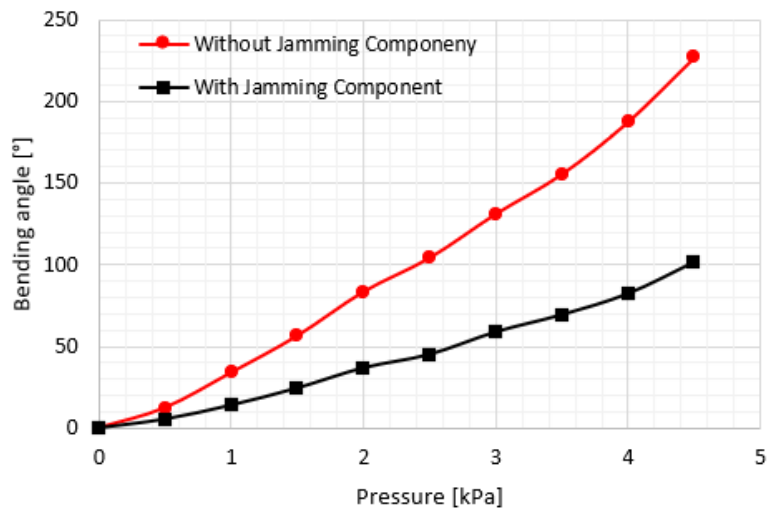
Figure 70. Comparison of bending angle with and without jamming component.

Addition of jamming component adds weight to the original soft actuator. The weight of soft actuator is 29.6 g. The jamming component soft chambers, each weigh around 6.3 g. So, the total weight of the soft actuator becomes 42.2 g. Also, the jamming components are filled with granular material with the weight of approximately 6 g, making the total weight of actuator 48.2 g. The addition of weight affects the bending of the actuator and needs more pressure to actuate the same angle which can be seen in Figure 70.

6.4.3 Holding Force Analysis

The holding force analysis reflects the amount of force transferred by the actuator to lift or push an object. This can also be depicted as the force acquired by the actuator to lift an object. The experimental setup for measuring this parameter is shown in Figure 71. A precision weighing scale was used as a force sensor to calculate a unidirectional force.
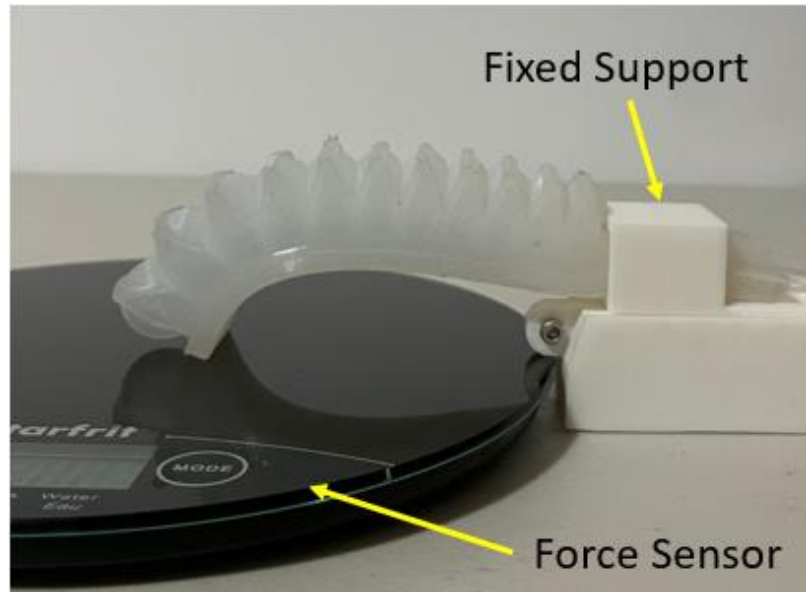
Figure 71. An experimental setup for measuring holding force
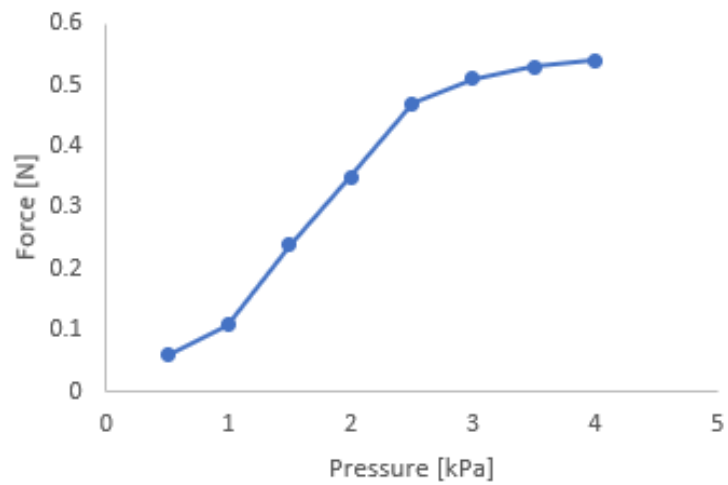
Figure 72. Change in force with change in pressure.

The experimental data shows that the amount of force increases with increase in pressure applied. The curve of force with respect to applied pressure, as shown in Figure 72, is not linear and as the pressure increases the force starts to saturate. A maximum of 0.56 N of force was noted at the pressure of 4 kPa. The saturation occurs as the material is not stiff enough to withhold force > 0.56 N for this design of actuator when the force is applied in the transverse direction (perpendicular to the length of the actuator). It was also observed that the first chamber starts to expand ununiformly which leads to ununiform pressure distribution, and the actuator loses its ability.
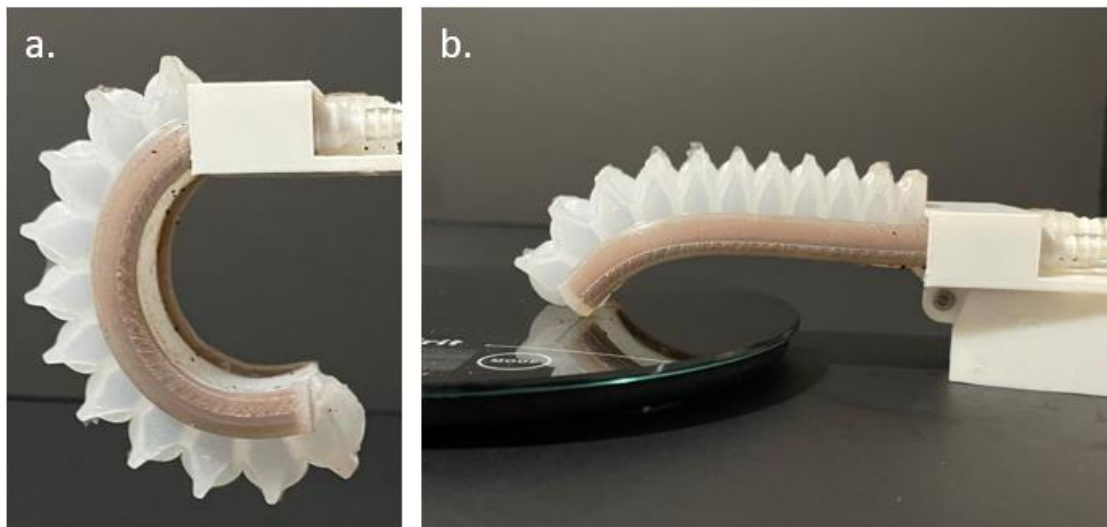
Figure 73. a) Actuator bending in free form at 3.5 kPa, b) holding force setup for modified actuator

The holding force experiment is also conducted with the soft actuator with granular jamming component attached. For performing this experiment, the actuator was first actuated to a certain pressure (1kPa, 1.5kPa, 2kPa and so on) as shown in Figure 73 a), which was followed by depressurization of the granular jamming chambers. The vacuuming process increases the stiffness of the actuator and then the actuator is put to holding force test. This test is performed with different vacuum pressures to study the behavior of the actuator at different stiffness levels.
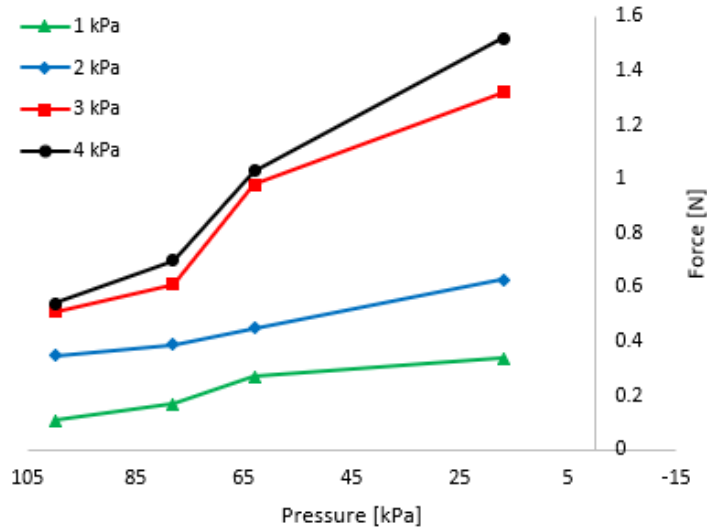
Figure 74. Change in force generated with vacuum pressure (granular jamming) at 1 kPa, 2 kPa, 3 kPa, and 4 kPa (positive pressure for soft actuator)

The relation between vacuum pressure for granular jamming with the force exerted on the force sensor is shown in Figure 74. It describes the plot of vacuum pressures with force output at different internal actuating pressure. It was observed that the holding force of the actuator increases with increase in vacuum pressure. Figure 74 also describes the holding force behavior for different actuator pressure. The actuator pressure also plays a role in holding force variation. The holding force due to vacuum is more prominent when the internal pressure of the actuator is higher, $P > 2.5$ kPa.

Also, it can be observed that the effect of granular jamming component is more prominent in delivering output force at higher actuating pressures with higher degree of vacuum. When internal pressure is low 1 kPa or 2 kPa, implementing vacuum did not provide significant improvement in holding force.
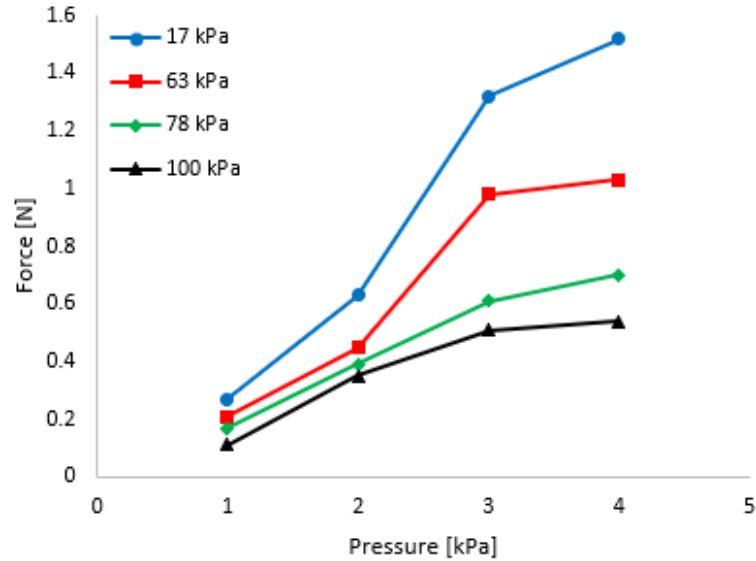
Figure 75. Change in holding force with pressure (soft actuator internal pressure) at 17 kPa, 63 kPa, 78 kPa, and 100 kPa (absolute pressure)

Figure 75 shows the relation between force exerted on a pressure sensor by the actuator with change in soft actuator internal pressure. It can be observed that having a granular jamming component increases the holding force capacity of the actuator. At an internal actuator pressure of 4 kPa (gauge), with vacuum pressure of 17 kPa (absolute) (or -87 kPa), the actuators holding force increases 3 time when compared to simple actuator.

6.4.4 Analysis of Variance (ANOVA)

The output force, obtained from the experimental study, depends on two variables. The first variable is internal positive pressure of the actuator, and another variable is vacuum pressure applied for jamming of the actuator. As there are two variables on which, the output is dependent, a two-factor ANOVA is implemented. This ANOVA test is conducted with a confidence level of 95% using Microsoft Excel's Data Analysis tool. The data used for this analysis is depicted graphically in Figure 74 and Figure 75. In ANOVA, a null hypothesis states that the variables have

no significant outcome on the dependent variable. The null hypothesis is rejected when the *F*-value is greater than the *F-critical*.

Table 9. ANOVA results for output force with pressure and vacuum.

Source of Variation	SS	df	MS	F	P-value	F crit
Rows (Vacuum)	0.7861	3	0.262033	**8.931263**	0.00462	3.862548
Columns (Positive pressure)	1.39085	3	0.463617	**15.80212**	0.000624	3.862548

Table 9 summarizes the results of ANOVA. The *F*-value is a ratio of mean squared sum of a factor (positive pressure and vacuum) to mean squared sum of error. The ANOVA was conducted with 5% significance level. Which means when *P*-value is less than 0.05, the factors will have significant results. The *F*-value for the actuator with vacuum is 8.93 > *F-critical*. This means the vacuum (which is granular jamming) is a very significant factor in increasing force output. *F*-value for positive pressure is 15.8 > *F-critical*, meaning it is also a significant factor affecting the out force of the actuator.

6.5 Discussion

Table 10 contains the comparison of this research with other relevant soft actuators. The maximum bending angle of 340° is achieved by experimentation. The actuators listed in this table are all fabricated with a material with significantly higher material hardness. The Eco-flex 00-30 used in this research has a share hardness of 00-30, whereas other material has 00-70. The comparison of material hardness, tensile strength and tear strength is drawn in Appendix E. As the material used is softer comparatively, the pressure required to actuate it also much smaller. Also, when comparing the force out of the actuator, it produces the least amount of force. To measure how effective the

force produce is, its effectiveness is measured as generated force per unit pressure applied. The comparison of this effectiveness is shown in Figure 76.

Table 10. Comparison of maximum bending angle, maximum force, and pressure of soft actuators.

Author		Max. Bending angle (°)	Force (N)	pressure (kPa)	Force/Pressure (N/kPa)
P. Polygerinos et al.	[73]	320	1.2	45	0.0267
K. M. de Payrebrune et al	[5]	332	0.275	66	0.0042
T. Noritsugu et al	[6]	200	14	500	0.0280
S. Konishi et al.	[74]	75	1.72	80	0.0215
B. Mosadegh et al.	[75]	340	1.4	72	0.0194
H. Li et al.	[70]	270	15	400	0.0375
Y. Li et al.	[7]	45	18	500	0.0360
P. Polygerinos et al.	[69]	300	10	250	0.0400
G. Alici et al. (A1 model)	[76]	270	3.5	120	0.0292
G. Alici et al. (A2 model)	[76]	270	0.9	35	0.0257
J. Wang et al.	[72]	270	0.8	80	0.0100
Z. Sun et al.	[8]	330	2.5	120	0.0208
Y. Sun et al. (with Fabric)	[77]	120	2.3	195	0.0118
Y. Sun et al. (Ecoflex 0030)	[77]	240	0.8	65	0.0123
This research		340	0.56	4	0.14
This research with Jamming		200	1.6	4, -83	0.4
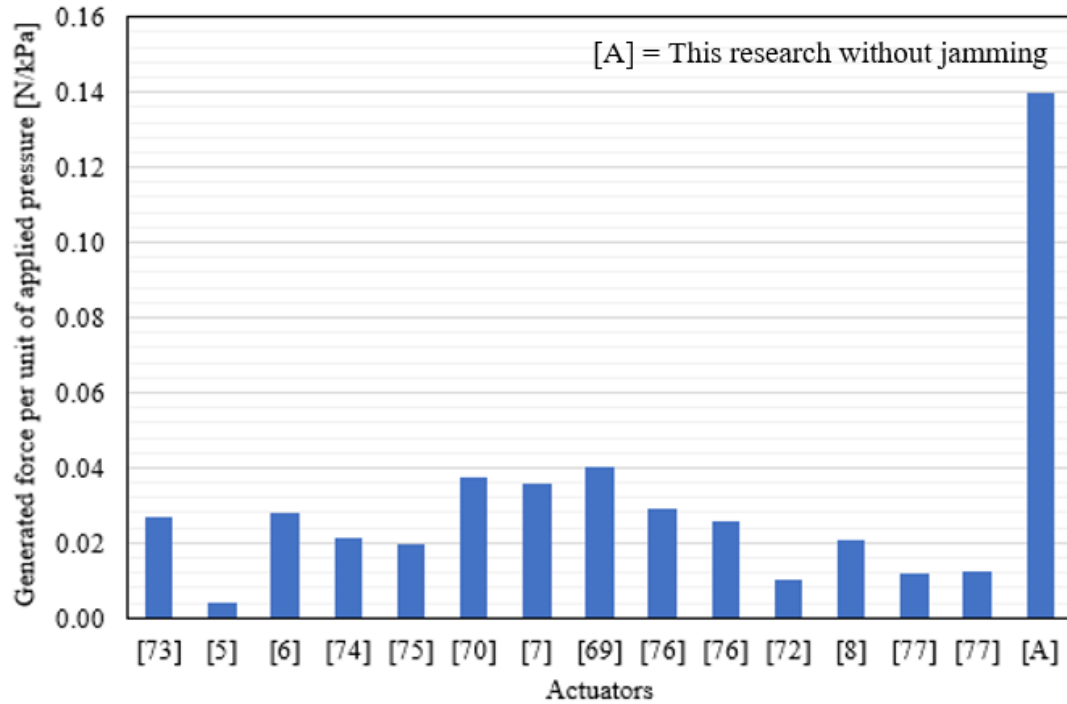
Figure 76. Comparison of effectiveness (generated force per unit of applied pressure)
for different soft actuators ([A] = this research).

The effectiveness of this actuator without jamming component attached to it, is 0.14 whereas the largest value from all other literature is 0.04. This is an increment of 350 %. The reason behind not incorporating actuator with jamming in this comparison is unaccountability of vacuum pressure.

When the theoretical, numerical, and experimental results on bending angle of the actuators were compared, it was observed (refer to Figure 69) that there was much larger difference between experimental and theoretical/numerical models. The main reason of the difference is pressure loss in the pneumatic system. As this research work involves longer pneumatic lines (~1m) with small internal diameter (3mm), there are significant frictional losses. Another factor which could have contributed to the pressure losses is leaks due human error and 3D printed components used for connecting pressure sensor. This research did not go in detail to investigate the cause.
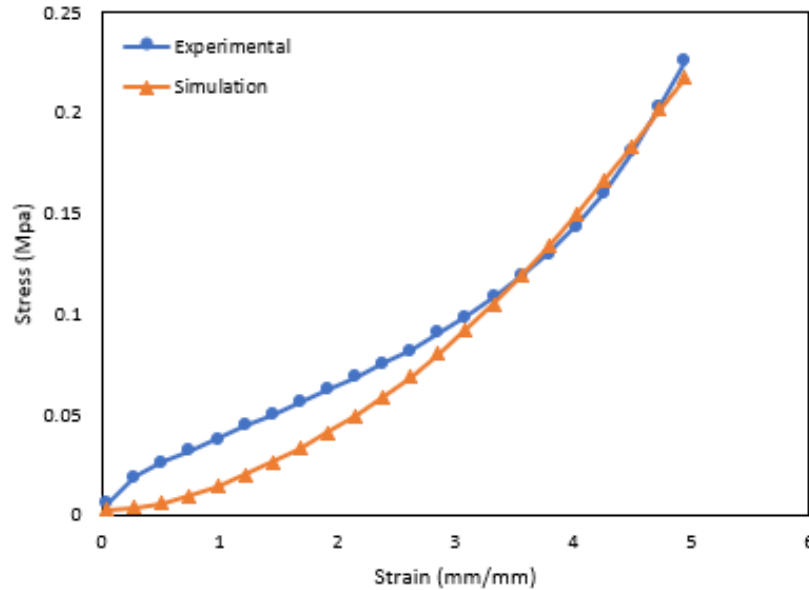
Figure 77. Stress-Strain curve of experimental and simulation study.

One of the notable observations made was the outcome of the simulation results. The graph of bending angle with respect to applied pressure was linear (refer to Figure 53). As the material properties were defined as non-linear in ANSYS, to get a linear outcome is a unique scenario. To investigate whether the ASNSY solver is producing these results due to error, a study was conducted. This study included taking a stress-strain data for an element and comparing it to experimental stress-strain data as shown in Figure 77. The stress-strain curve of simulation study is not linear and getting linear outcome of bending angle simulation can be a co-incidence. An in-depth study can be conducted in future.

6.6 Prototype of the Gripper

A prototype of a gripper (an end effector) for a robotic arm is developed using presented soft actuator. This end effector is made using two actuators. The body of the gripper is manufactured using 3D printing with PLA material. The dimension of the gripper is 200mm * 50mm * 50mm. The weight of the manufactured gripper is 173 g out of which 84.4 g is the weight of actuators. The

prototype of the gripper is shown in Figure 78. The maximum weight, this gripper was able to lift without activating jamming component was 460 g at approximately 4 kPa. After applying jamming component with a vacuum of -67 kPa. The maximum weight carrying increased to 905 g, almost double the amount. This shows that the carrying capacity can be significantly increased by implementing jamming component.
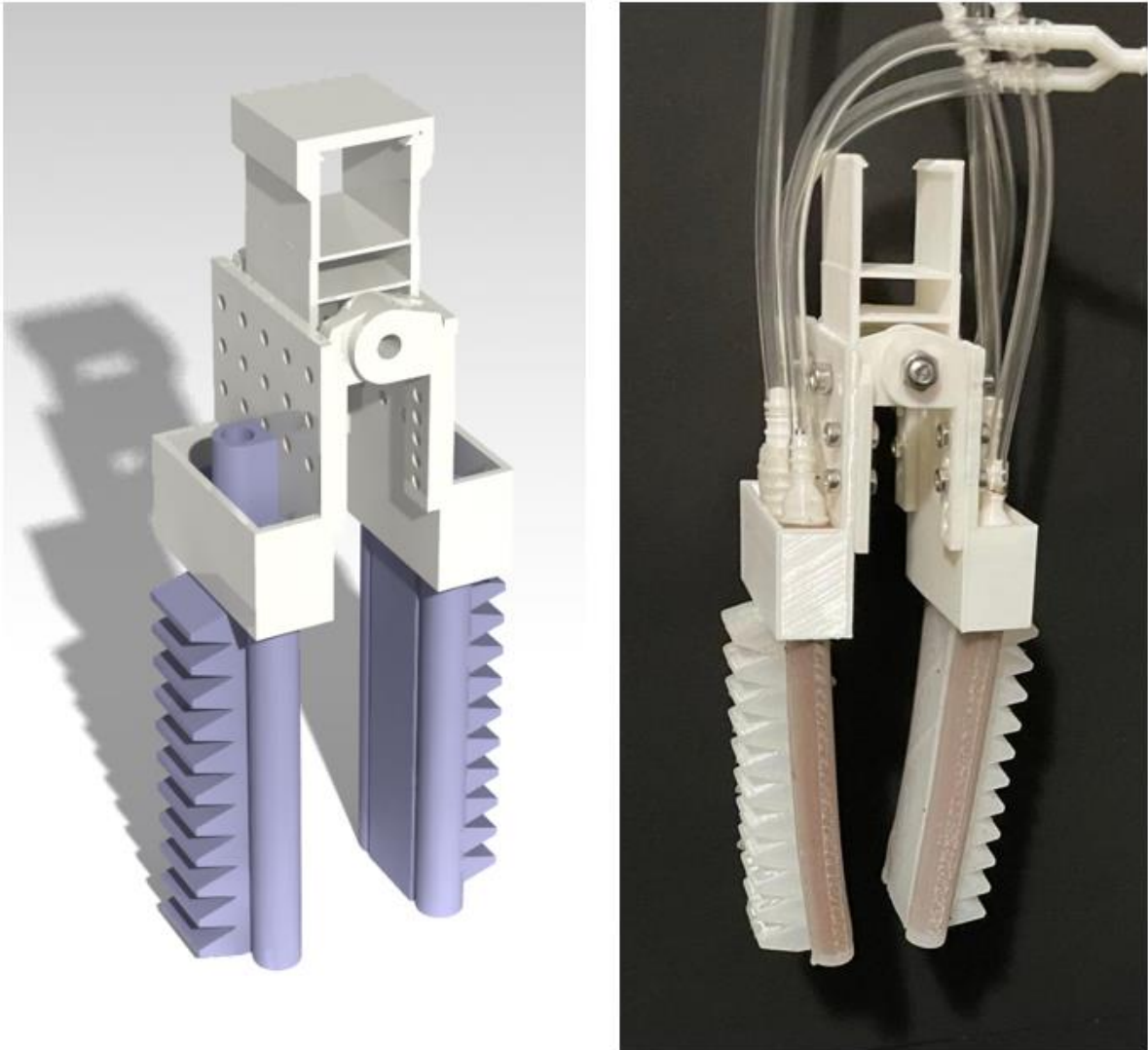
Figure 78. Prototype of the gripper made with proposed actuators (right) and CAD model of the gripper (left)

For this gripper, the positive pressure pneumatic lines are connected with a single source of air pressure and similarly, all four lines of jamming component are connected with a single source of vacuum. This configuration eliminates the need of implementing multiple sources and provides each component with equal pressure. This also allowed us with an easy control of the actuator.

Table 11. Cost estimation for a soft actuator

Component	Weight	Cost (CAD$)
Eco-Flex 00-30	50g	2.8
Mold for actuator	43g	1.1
Mold for Jamming	18g	0.5
Ground Coffee	12g	0.2
Total Cost		4.6

Table 12. Cost estimation of a fabricated gripper

Component	Cost (CAD$)
Actuator	9.2
Pump	50
Motor Driver	2.5
Arduino	25
Pipe and Valve	10
Pressure Sensor	20
Assembly Parts	1.5
Total Cost	118.2

Table 11 shows the total cost estimation of the actuator fabricated shown in Figure 63. The calculation also includes cost of the mold which is reusable. A total cost of mere CAD$ 4.6 is

required to fabricate this component. Table 12 shows the total cost estimation of making a functional gripper, which was totaled to CAD$ 118.2 with a major cost of pump.

Chapter 7 Conclusion and Applicability

7.1 Conclusion

This research was aimed to fulfill two major tasks. One, to improve the conventional design of the soft robotic actuator with parameter optimization to realize the improvement in the bending angle at a given pressure for a silicone elastomer Eco-flex 00-30 when compared to conventional design. The second objective was to improve the force exertion capacity of the actuator on external objects, which has improved the load carrying capacity of a soft robotic gripper fabricated with said soft actuators. To accomplish this, a granular jamming component was implemented in the body of the soft actuator.

After a detailed study of the soft robotic actuator, it was concluded that pneumatically driven soft actuators are more dependable, efficient, versatile, and economical in nature [28-31]. Not only that, but they are also very easy to fabricate as they are fabricated with one of the oldest manufacturing technique-molding. The fabrication process is divided in to two steps: mold making and molding. The technique used in this research relies completely on the additive manufacturing processes. As the mold making is done using 3D printing in this research. This led to minimal material wastage and helped in cost saving.

To study the behavior of the material, a numerical study was performed. As this material is classified as hyper-elastic material, there are no particular methods to implement it in commercially available analysis softwares. To solve for this material, a curve fitting study was required to find the best fitting hyper-elastic model. This study is discussed in Chapter 4. After curve-fitting study the best fitting model was found to be Yeoh's 2nd order hyper-elastic model. The curve fitting data was used to determine material constants, and a material model was ready for simulation study.

A simulation study was conducted to learn the behavior of the actuator with conventional design. In this, it was discovered that, the conventional design with rectangular cross-section for soft actuator delivers excellent performance in positive pressures but performs poorly under negative pressures. A novel hybrid design was implemented which produced a significantly better bending angle under vacuum (almost 3x), through simulations. Geometric parameters which have the most impact on the bending of the actuator were studied and optimized with simulations as well. A theoretical study was performed to calculate the bending angle of the actuator, in which the elastic modulus was assumed to be constant and the expansion of the chamber of the actuator was assumed to be a shape of cylindrical ellipse. A theoretical model was developed in this research, which provided relation between internal pressure of the actuator and bending angle of the actuator.

The final design of the actuator with parameter optimization was made in CATIA. To fabricate this actuator a suitable mold design was also made in CATIA, which was achieved after a few attempts. The molds were manufactured using 3D printing with PLA (Polylactic acid) on Ender 3 Pro (Creality) 3D printer. PLA is used as a filament because it requires no additional mold releasing agent and it is available commercially at low cost. Because of these, the mold is reusable and easy to fabricate. To implement the granular jamming system for variable stiffness, chambers/bladders are attached externally to the actuator. These chambers/bladders are also fabricated using the same silicone elastomer as it is perfect fit for fabricating flexible vacuum chamber with maximum material strain of 900%. Fabricating the chamber with the same material also helps as they can be welded easily.

An experimental rig is setup to study the fabricated actuator. This setup consists of a miniature pump for positive and negative pressure, a motor driver to control the pump, a miniature pressure sensor that give absolute pressure values, a valve system to control the flow manually, and an Arduino as a control board for the system. A set of experiments were carried out to observe bending angle of the actuator at a given pressure and then compared with theoretical and numerical values.

The experimental values followed the same trend as others but produced lower values of bending angle when compared to theoretical and simulation values. It was concluded that the difference occurred because the numerical and theoretical analysis are done in ideal conditions, also there were pressure losses in the experimental setup such as frictional losses in the piping and possible human errors during setup and experimentation.

A series of experiments are conducted to evaluate the holding force of the actuator with and without granular jamming components. This study demonstrated that the holding force of the actuator increases with increase in vacuum pressure. An ANOVA was conducted to determine the importance of the jamming on the actuator, which determined that there is experimental evidence to prove the significance of the jamming on output force. It also showed that, the impact of the jamming is not very effective at lower actuator pressures but becomes significant when the internal pressure is more than 2.5 kPa. Also, at an internal actuator pressure of 4 kPa (gauge), with vacuum pressure of 17 kPa (absolute), the actuators holding force increases 3 time when compared to simple actuator. This is a very significant improvement in the performance of the actuator. The actuator presented in this study was compared with prior art. The evaluation parameters used for this comparison are pressure, bending angle and effectiveness.

7.2 Summary of Contribution

- A pneumatic soft actuator with a new cross-sectional profile is designed and fabricated.
- The simulation study is conducted to improve the design parameters of the soft actuator.
- The new design allowed the actuator to bend in reverse direction with vacuum and increased reverse reach by 280% when compared to conventional design.
- A jamming component is added successfully which increased the blocking force of the actuator by 270%.

- The effectiveness of this actuator when compared to other actuator from literature is 350% more at least.

7.3 Applications

7.3.1 End Effector of a Robotic Arm

The soft actuators are widely used as end effector for robotic arms. Two or more soft actuators are combined to operate as a gripper for pick up and drop operations. Delicate objects are difficult to handle with metallic grippers as they can bruise or damage a delicate object easily, whereas the soft nature of the silicone actuator eliminates that problem.

7.3.2 Food Handling Robot

With increasing automation across all industry platform, need of automation in food industry is also rising. The food handling robots are designed not to damage the food. This task becomes difficult to achieve with conventional robots as it requires very precise force output. But this is eliminated by implementing soft robots. These soft robots cause minimal damage to fresh produce and are very easy to operate. The soft robot developed in this research can perform all these tasks with improved load carrying capacity. The presented gripper can also be used to pick and place marshmallows, cupcakes, and fresh produce.

7.3.3 As Rehabilitation Device

Rehabilitation of fingers can be achieved from such actuators. Completely mechanical devices present a risk factor of damaging patients if gone out of control, whereas the soft devices can cause no such damages. Soft actuator can generate light forces to help achieve folding of fingers with small modification in the design. Also, because of the presence of granular jamming component, which increase the holding force, a finger can be stabilized into a particular position by its

activation. The activation can be easily controlled with the help of a button. The measure of how effective this can prove is one of the possible directions, this research can lead into.

7.4 Future Work

A soft robotic actuator has found applications in numerous fields. With this research, it was determined that a new capability of controlled stiffness can be added to the soft actuators and a method to improve the design and design parameters of any SPA can be implemented. Moving in that direction a list of future work is as follows:

- Improving the jamming component to achieve most effective stiffness, which would result in better use of resources and better force capabilities.

- Trying various silicone elastomers with different hardness index to fabricate soft actuators and study their performance and comparing them.

- Developing and implementing innovative profiles for the cross-section of the soft actuator chambers and studying their behavior.

- Optimizing actuator parameters for the development of a robotic gripper and comparing them for applicability.

References

[1] G. Alici, "Towards soft robotic devices for site-specific drug delivery," *Expert Review of Medical Devices*, vol. 12, no. 6, pp. 703–715, Sep. 2015, doi: 10.1586/17434440.2015.1091722.

[2] M. A. Robertson, H. Sadeghi, J. M. Florez, and J. Paik, "Soft Pneumatic Actuator Fascicles for High Force and Reliability," *Soft Robotics*, vol. 4, no. 1, pp. 23–32, Mar. 2017, doi: 10.1089/soro.2016.0029.

[3] P. Polygerinos *et al.*, "Soft Robotics: Review of Fluid-Driven Intrinsically Soft Devices; Manufacturing, Sensing, Control, and Applications in Human-Robot Interaction," *Advanced Engineering Materials*, vol. 19, no. 12, p. 1700016, May 2017, doi: 10.1002/adem.201700016.

[4] D. Rus and M. T. Tolley, "Design, fabrication and control of soft robots," *Nature*, vol. 521, no. 7553, pp. 467–475, May 2015, doi: 10.1038/nature14543.

[5] K. M. de Payrebrune and O. M. O'Reilly, "On constitutive relations for a rod-based model of a pneu-net bending actuator," *Extreme Mechanics Letters*, vol. 8, pp. 38–46, Sep. 2016, doi: 10.1016/j.eml.2016.02.007.

[6] T. Noritsugu, M. Takaiwa, and D. Sasaki, "Development of Power Assist Wear Using Pneumatic Rubber Artificial Muscles," *Journal of Robotics and Mechatronics*, vol. 21, no. 5, pp. 607–613, Oct. 2009, doi: 10.20965/jrm.2009.p0607.

[7] Y. Li, Y. Chen, Y. Yang, and Y. Li, "Soft Robotic Grippers Based on Particle Transmission," *IEEE/ASME Transactions on Mechatronics*, vol. 24, no. 3, pp. 969–978, Jun. 2019, doi: 10.1109/tmech.2019.2907045.

[8] Z. Sun, Z. Guo, and W. Tang, "Design of wearable hand rehabilitation glove with soft hoop-reinforced pneumatic actuator," *Journal of Central South University*, vol. 26, no. 1, pp. 106–119, Jan. 2019, doi: 10.1007/s11771-019-3986-x.

[9] M. Folgheraiter and G. Gini, "Blackfingers an artificial hand that copies human hand in structure, size, and function," *Proc. IEEE Humanoids*, p. 4, 2000.

[10] J. Shintake, V. Cacucciolo, D. Floreano, and H. Shea, "Soft Robotic Grippers," *Advanced Materials*, vol. 30, no. 29, p. 1707035, May 2018, doi: 10.1002/adma.201707035.

[11] R. F. Shepherd *et al.*, "Multigait soft robot," *Proceedings of the National Academy of Sciences*, vol. 108, no. 51, pp. 20400–20403, Nov. 2011, doi: 10.1073/pnas.1116564108.

[12] H. K. Yap, H. Y. Ng, and C.-H. Yeow, "High-Force Soft Printable Pneumatics for Soft Robotic Applications," *Soft Robotics*, vol. 3, no. 3, pp. 144–158, Sep. 2016, doi: 10.1089/soro.2016.0030.

[13] H. Yuk, S. Lin, C. Ma, M. Takaffoli, N. X. Fang, and X. Zhao, "Hydraulic hydrogel actuators and robots optically and sonically camouflaged in water," *Nature Communications*, vol. 8, no. 1, Feb. 2017, doi: 10.1038/ncomms14230.

[14] F. Daerden, "Conception and realization of pleated pneumatic artificial muscles and their use as compliant actuation elements," PhD Thesis, Vrije Universiteit, Brussels, 1999.

[15] F. Daerden and D. Lefeber, "The Concept and Design of Pleated Pneumatic Artificial Muscles," *International Journal of Fluid Power*, vol. 2, no. 3, pp. 41–50, Jan. 2001, doi: 10.1080/14399776.2001.10781119.

[16] G. K. Klute, J. M. Czerniecki, and B. Hannaford, "McKibben artificial muscles: pneumatic actuators with biomechanical intelligence," *IEEE Xplore*, Sep. 01, 1999. https://ieeexplore.ieee.org/stamp/stamp.jsp?tp=&arnumber=803170

[17] G. Andrikopoulos, G. Nikolakopoulos, and S. Manesis, "Pneumatic artificial muscles: A switching Model Predictive Control approach," *Control Engineering Practice*, vol. 21, no. 12, pp. 1653–1664, Dec. 2013, doi: 10.1016/j.conengprac.2013.09.003.

[18] V. L. Nickel, J. Perry, and A. L. Garrett, "Development of Useful Function in the Severely Paralyzed Hand," *JBJS*, vol. 45, no. 5, pp. 933–952, Jul. 1963, Accessed: Aug. 22, 2021. [Online]. Available: https://pubmed.ncbi.nlm.nih.gov/14047365/

[19] A. H. Morin. Elastic diaphragm. US Patent No. 2,642,091, 1953

[20] T. Noritsugu, M. Takaiwa, and D. Sasaki, "Power Assist Wear Driven with Pneumatic Rubber Artificial Muscles," *2008 15th International Conference on Mechatronics and Machine Vision in Practice*, vol. 21, no. 5, Dec. 2008, doi: 10.1109/mmvip.2008.4749589.

[21] J. S. Martell and G. Gini, "Robotic hands: Design review and proposal of new design process," *World Academy of Science, Engineering and Technology*, vol. 26, pp. 85-90, 2007.

[22] F. Kawai, P. Cusin, and S. Konishi, "Thin flexible end-effector using pneumatic balloon actuator," *Proceedings IEEE Thirteenth Annual International Conference on Micro Electro Mechanical Systems (Cat. No.00CH36308)*, vol. 89, no. 1–2, 2001, doi: 10.1109/memsys.2000.838549.

[23] S. Konishi and H. Kosawa, "High-output bending motion of a soft inflatable microactuator with an actuation conversion mechanism," *Scientific Reports*, vol. 10, no. 1, p. 12038, Jul. 2020, doi: 10.1038/s41598-020-68458-5.

[24] Y. Hwang, O. H. Paydar, and R. N. Candler, "Pneumatic microfinger with balloon fins for linear motion using 3D printed molds," *Sensors and Actuators A: Physical*, vol. 234, pp. 65–71, Oct. 2015, doi: 10.1016/j.sna.2015.08.008.

[25] S. Kusuda, S. Sawano, and S. Konishi, "Fluid-resistive bending sensor having perfect compatibility with flexible pneumatic balloon actuator," *2007 IEEE 20th International Conference on Micro Electromechanical Systems (MEMS)*, 2007, doi: 10.1109/MEMSYS.2007.4433082.

[26] M. T. Tolley *et al.*, "A Resilient, Untethered Soft Robot," *Soft Robotics*, vol. 1, no. 3, pp. 213–223, Sep. 2014, doi: 10.1089/soro.2014.0008.

[27] B. Mosadegh *et al.*, "Pneumatic Networks for Soft Robotics that Actuate Rapidly," *Advanced Functional Materials*, vol. 24, no. 15, pp. 2163–2170, Jan. 2014, doi: 10.1002/adfm.201303288.

[28] H. Li, J. Yao, P. Zhou, X. Chen, Y. Xu, and Y. Zhao, "High-force soft pneumatic actuators based on novel casting method for robotic applications," *Semantic Scholar*, 2020, doi: 10.1016/j.sna.2020.111957.

[29] F. Ilievski, A. D. Mazzeo, R. F. Shepherd, X. Chen, and G. M. Whitesides, "Soft Robotics for Chemists," *Angewandte Chemie International Edition*, vol. 50, no. 8, pp. 1890–1895, Jan. 2011, doi: 10.1002/anie.201006464.

[30] S. A. Morin, R. F. Shepherd, S. W. Kwok, A. A. Stokes, A. Nemiroski, and G. M. Whitesides, "Camouflage and Display for Soft Machines," *Science*, vol. 337, no. 6096, pp. 828–832, Aug. 2012, doi: 10.1126/science.1222149.

[31] "Robotic fingers get touchy-feely," *Nature*, vol. 555, no. 7696, pp. 289–289, Mar. 2018, doi: 10.1038/d41586-018-02778-5.

[32] H. Okayasu, J. Okamoto, M. G. Fujie, M. Umezu, and H. Iseki, "Development of a hydraulic-driven flexible manipulator for neurosurgery," *International Congress Series*, no. 1256, pp. 607–612, Jun. 2003, doi: 10.1016/s0531-5131(03)00324-8.

[33] Z. Shen, J. Na, and Z. Wang, "A Biomimetic Underwater Soft Robot Inspired by Cephalopod Mollusc," *IEEE Robotics and Automation Letters*, vol. 2, no. 4, pp. 2217–2223, Oct. 2017, doi: 10.1109/lra.2017.2724760.

[34] R. K. Katzschmann, A. D. Marchese, and D. Rus, "Hydraulic Autonomous Soft Robotic Fish for 3D Swimming," *Experimental Robotics*, pp. 405–420, Nov. 2015, doi: 10.1007/978-3-319-23778-7_27.

[35] M. Lazeroms *et al.*, "A hydraulic forceps with force-feedback for use in minimally invasive surgery," *Mechatronics*, vol. 6, no. 4, pp. 437–446, Jun. 1996, doi: 10.1016/0957-4158(96)00008-6.

[36] [31]K. Ikuta, H. Ichikawa, K. Suzuki, and T. Yamamoto, "Safety active catheter with multi-segments driven by innovative hydro-pressure micro actuators," *The Sixteenth Annual International Conference on Micro Electro Mechanical Systems, 2003. MEMS-03 Kyoto. IEEE*, 2002, doi: 10.1109/memsys.2003.1189704.

[37] M. Controzzi, C. Cipriani, and M. C. Carrozza, "Design of Artificial Hands: A Review," *Springer Tracts in Advanced Robotics*, pp. 219–246, 2014, doi: 10.1007/978-3-319-03017-3_11.

[38] T. Hassan, M. Manti, G. Passetti, N. d'Elia, M. Cianchetti, and C. Laschi, "Design and development of a bio-inspired, under-actuated soft gripper," *IEEE Xplore*, Aug. 01, 2015. https://ieeexplore.ieee.org/stamp/stamp.jsp?tp=&arnumber=7319176

[39] P. Rao, Q. Peyron, S. Lilge, and J. Burgner-Kahrs, "How to Model Tendon-Driven Continuum Robots and Benchmark Modelling Performance," *Frontiers in Robotics and AI*, vol. 7, Feb. 2021, doi: 10.3389/frobt.2020.630245.

[40] J.-H. Lee, Y. S. Chung, and H. Rodrigue, "Long Shape Memory Alloy Tendon-based Soft Robotic Actuators and Implementation as a Soft Gripper," *Scientific Reports*, vol. 9, no. 1, Aug. 2019, doi: 10.1038/s41598-019-47794-1.

[41] S. Kim, C. Laschi, and B. Trimmer, "Soft robotics: a bioinspired evolution in robotics," *Trends in Biotechnology*, vol. 31, no. 5, pp. 287–294, May 2013, doi: 10.1016/j.tibtech.2013.03.002.

[42] J.-S. Koh and K.-J. Cho, "Omega-Shaped Inchworm-Inspired Crawling Robot With Large-Index-and-Pitch (LIP) SMA Spring Actuators," *IEEE/ASME Transactions on Mechatronics*, vol. 18, no. 2, pp. 419–429, Apr. 2013, doi: 10.1109/tmech.2012.2211033.

[43] I. W. Hunter, S. Lafontaine, P. M. F. Nielsen, P. J. Hunter, and J. M. Hollerbach, "Manipulation and dynamic mechanical testing of microscopic objects using a tele-micro-robot system," *IEEE Control Systems Magazine*, vol. 10, no. 2, pp. 3–9, Feb. 1990, doi: 10.1109/37.45787.

[44] S. Kim, E. Hawkes, K. Choy, M. Joldaz, J. Foleyz, and R. Wood, "Micro artificial muscle fiber using NiTi spring for soft robotics," *2009 IEEE/RSJ International Conference on Intelligent Robots and Systems*, Oct. 2009, doi: 10.1109/iros.2009.5354178.

[45] R. Mutlu, G. Alici, X. Xiang, and W. Li, "Electro-mechanical modelling and identification of electroactive polymer actuators as smart robotic manipulators," *Mechatronics*, vol. 24, no. 3, pp. 241–251, Apr. 2014, doi: 10.1016/j.mechatronics.2014.02.002.

[46] T. Mirfakhrai, J. D. W. Madden, and R. H. Baughman, "Polymer artificial muscles," *Materials Today*, vol. 10, no. 4, pp. 30–38, Apr. 2007, doi: 10.1016/S1369-7021(07)70048-2.

[47] S. Maeda, Y. Hara, T. Sakai, R. Yoshida, and S. Hashimoto, "Self-Walking Gel," *Advanced Materials*, vol. 19, no. 21, pp. 3480–3484, Nov. 2007, doi: 10.1002/adma.200700625.

[48] B. Kim, D.-H. Kim, J. Jung, and J.-O. Park, "A biomimetic undulatory tadpole robot using ionic polymer–metal composite actuators," *Smart Materials and Structures*, vol. 14, no. 6, pp. 1579–1585, Nov. 2005, doi: 10.1088/0964-1726/14/6/051.

[49] S.-W. Yeom and I.-K. Oh, "A biomimetic jellyfish robot based on ionic polymer metal composite actuators," *Smart Materials and Structures*, vol. 18, no. 8, p. 085002, Jun. 2009, doi: 10.1088/0964-1726/18/8/085002.

[50] J. Najem, B. Akle, S. A. Sarles, and D. J. Leo, "Design and Development of a Biomimetic Jellyfish Robot That Features Ionic Polymer Metal Composites Actuators," *ASME 2011 Conference on Smart Materials, Adaptive Structures and Intelligent Systems, Volume 2*, Jan. 2011, doi: 10.1115/smasis2011-5105.

[51] J. Najem, S. A. Sarles, B. Akle, and D. J. Leo, "Biomimetic jellyfish-inspired underwater vehicle actuated by ionic polymer metal composite actuators," *Smart Materials and Structures*, vol. 21, no. 9, p. 094026, Aug. 2012, doi: 10.1088/0964-1726/21/9/094026.

[52] O. Kim, S. J. Kim, and M. J. Park, "Low-voltage-driven soft actuators," *Chemical Communications*, vol. 54, no. 39, pp. 4895–4904, 2018, doi: 10.1039/c8cc01670d.

[53] S. Nemat-Nasser and Y. Wu, "Comparative experimental study of ionic polymer–metal composites with different backbone ionomers and in various cation forms," *Journal of Applied Physics*, vol. 93, no. 9, pp. 5255–5267, May 2003, doi: 10.1063/1.1563300.

[54] W. M. Winslow, "Induced Fibration of Suspensions," *Journal of Applied Physics*, vol. 20, no. 12, pp. 1137–1140, Dec. 1949, doi: 10.1063/1.1698285.

[55] Y. Z. Dong, Y. Seo, and H. J. Choi, "Recent development of electro-responsive smart electrorheological fluids," *Soft Matter*, vol. 15, no. 17, pp. 3473–3486, 2019, doi: 10.1039/c9sm00210c.

[56] R. Tao, H. Tang, K. Tawhid-Al-Islam, E. Du, and J. Kim, "Reply to Smith: Electrorheological technology reduces the chocolate viscosity and fat level," *Proceedings of the National Academy of Sciences*, vol. 113, no. 36, pp. E5255–E5256, Aug. 2016, doi: 10.1073/pnas.1610514113.

[57] T. Mitsumata, K. Sakai, and J. Takimoto, "Giant Reduction in Dynamic Modulus of κ-Carrageenan Magnetic Gels," *The Journal of Physical Chemistry B*, vol. 110, no. 41, pp. 20217–20223, Oct. 2006, doi: 10.1021/jp063494g.

[58] S. Kashima, F. Miyasaka and K. Hirata, "Novel Soft Actuator Using Magnetorheological Elastomer," in IEEE Transactions on Magnetics, vol. 48, no. 4, pp. 1649-1652, April 2012, doi: 10.1109/TMAG.2011.2173669.

[59] F. Putzu, J. Konstantinova, and K. Althoefer, "Soft Particles for Granular Jamming," *Towards Autonomous Robotic Systems*, vol. 11650, pp. 65–74, 2019, doi: 10.1007/978-3-030-25332-5_6.

[60] P. Jiang, Y. Yang, M. Z. Q. Chen, and Y. Chen, "A variable stiffness gripper based on differential drive particle jamming," *Bioinspiration & Biomimetics*, vol. 14, no. 3, p. 036009, Mar. 2019, doi: 10.1088/1748-3190/ab04d1.

[61] Y. Li, Y. Chen and Y. Li, "Distributed design of passive particle jamming based soft grippers," 2018 IEEE International Conference on Soft Robotics (RoboSoft), 2018, pp. 547-552, doi: 10.1109/ROBOSOFT.2018.8405383.

[62] Y. Wei, Y. Chen, Y. Yang, and Y. Li, "A soft robotic spine with tunable stiffness based on integrated ball joint and particle jamming," *Mechatronics*, vol. 33, pp. 84–92, Feb. 2016, doi: 10.1016/j.mechatronics.2015.11.008.

[63] E. Brown *et al.*, "Universal robotic gripper based on the jamming of granular material," *Proceedings of the National Academy of Sciences*, vol. 107, no. 44, pp. 18809–18814, Oct. 2010, doi: 10.1073/pnas.1003250107.

[64] M. Heckele and W. K. Schomburg, "Review on micro molding of thermoplastic polymers," *Journal of Micromechanics and Microengineering*, vol. 14, no. 3, pp. R1–R14, Dec. 2003, doi: 10.1088/0960-1317/14/3/r01.

[65] A. D. Marchese, R. K. Katzschmann, and D. Rus, "A Recipe for Soft Fluidic Elastomer Robots," *Soft Robotics*, vol. 2, no. 1, pp. 7–25, Mar. 2015, doi: 10.1089/soro.2014.0022.

[66] I. Hager, A. Golonka, and R. Putanowicz, "3D Printing of Buildings and Building Components as the Future of Sustainable Construction?," *Procedia Engineering*, vol. 151, pp. 292–299, 2016, doi: 10.1016/j.proeng.2016.07.357.

[67] R. Scopigno, P. Cignoni, N. Pietroni, M. Callieri, and M. Dellepiane, "Digital Fabrication Techniques for Cultural Heritage: A Survey," *Computer Graphics Forum*, vol. 36, no. 1, pp. 6–21, Nov. 2015, doi: 10.1111/cgf.12781.

[68] Wikipedia Contributors, "3D printing," *Wikipedia*, Dec. 03, 2018. https://en.wikipedia.org/wiki/3D_printing

[69] P. Polygerinos *et al.*, "Modeling of Soft Fiber-Reinforced Bending Actuators," *IEEE Transactions on Robotics*, vol. 31, no. 3, pp. 778–789, Jun. 2015, doi: 10.1109/tro.2015.2428504.

[70] H. Li, J. Yao, P. Zhou, X. Chen, Y. Xu, and Y. Zhao, "High-force soft pneumatic actuators based on novel casting method for robotic applications," *Se c Scholar*, 2020, doi: 10.1016/j.sna.2020.111957.

[71] H. K. Yap, J. C. H. Goh, and R. C. H. Yeow, "Design and Characterization of Soft Actuator for Hand Rehabilitation Application," *IFMBE Proceedings*, pp. 367–370, 2015, doi: 10.1007/978-3-319-11128-5_92.

[72] J. Wang, Y. Fei, and W. Pang, "Design, Modeling, and Testing of a Soft Pneumatic Glove With Segmented PneuNets Bending Actuators," *IEEE/ASME Transactions on Mechatronics*, vol. 24, no. 3, pp. 990–1001, Jun. 2019, doi: 10.1109/TMECH.2019.2911992.

[73] P. Polygerinos *et al.*, "Towards a soft pneumatic glove for hand rehabilitation," *2013 IEEE/RSJ International Conference on Intelligent Robots and Systems*, Nov. 2013, doi: 10.1109/iros.2013.6696549.

[74] S. Konishi and H. Kosawa, "High-output bending motion of a soft inflatable microactuator with an actuation conversion mechanism," *Scientific Reports*, vol. 10, no. 1, p. 12038, Jul. 2020, doi: 10.1038/s41598-020-68458-5.

[75] B. Mosadegh *et al.*, "Soft Robotics: Pneumatic Networks for Soft Robotics that Actuate Rapidly (Adv. Funct. Mater. 15/2014)," *Advanced Functional Materials*, vol. 24, no. 15, pp. 2109–2109, Apr. 2014, doi: 10.1002/adfm.201470092.

[76] G. Alici, T. Canty, R. Mutlu, W. Hu, and V. Sencadas, "Modeling and Experimental Evaluation of Bending Behavior of Modeling and Experimental Evaluation of Bending Behavior of Soft Pneumatic Actuators Made of Discrete Actuation Chambers Soft Pneumatic Actuators Made of Discrete Actuation Chambers," 2018. Accessed: Nov. 09, 2022. [Online]. Available: https://ro.uow.edu.au/eispapers1/1149

[77] Y. Sun *et al.*, "Stiffness Customization and Patterning for Property Modulation of Silicone-Based Soft Pneumatic Actuators," *Soft Robotics*, vol. 4, no. 3, pp. 251–260, Sep. 2017, doi: 10.1089/soro.2016.0047.

[78] Z. S. N. Ghamsari, "The Introduction and Analysis of a Novel Soft Actuator for a Soft Continuum Robot Arm," MSc Thesis, University of Minnesota Duluth, 2018.

[79] A. Hayashi, J. Park and B. J. Kuipers, "Toward planning and control of highly redundant manipulators," Proceedings. 5th IEEE International Symposium on Intelligent Control 1990, 1990, pp. 683-688 vol.2, doi: 10.1109/ISIC.1990.128531.

[80] "SparkFun Qwiic MicroPressure Sensor - SEN-16476 - SparkFun Electronics," *www.sparkfun.com*. https://www.sparkfun.com/products/16476

[81] "Hyperelastic material," *Wikipedia*, Jun. 17, 2022. https://en.wikipedia.org/wiki/Hyperelastic_material

[82] D. Trivedi, C. D. Rahn, W. M. Kier, and I. D. Walker, "Soft robotics: Biological inspiration, state of the art, and future research," *Applied Bionics and Biomechanics*, vol. 5, no. 3, pp. 99–117, Dec. 2008, doi: 10.1080/11762320802557865.

[83] "Ecoflex^{TM} 00-30 Product Information," *Smooth-On, Inc.* https://www.smooth-on.com/products/ecoflex-00-30/

[84] "Neo-Hookean hyperelastic model for nonlinear finite element analysis," *Medium*, Jan. 08, 2020. https://getwelsim.medium.com/neo-hookean-hyperelastic-model-for-nonlinear-finite-element-analysis-16ac996aa507

[85] "Mooney-Rivlin hyperelastic model for nonlinear finite element analysis," *Medium*, Jan. 13, 2020. https://getwelsim.medium.com/mooney-rivlin-hyperelastic-model-for-nonlinear-finite-element-analysis-b0a9a0459e98

[86] E. M. Arruda and M. C. Boyce, "A three-dimensional constitutive model for the large stretch behavior of rubber elastic materials," *Journal of the Mechanics and Physics of Solids*, vol. 41, no. 2, pp. 389–412, Feb. 1993, doi: 10.1016/0022-5096(93)90013-6.

[87] "Blatz-Ko hyperelastic model for nonlinear finite element analysis," *Medium*, Jan. 20, 2020. https://getwelsim.medium.com/blatz-ko-hyperelastic-model-for-nonlinear-finite-element-analysis-d8e4fbd56d39

[88] R. S. Rivlin and D. W. Saunders, "Large elastic deformations of isotropic materials VII. Experiments on the deformation of rubber," *Philosophical Transactions of the Royal Society of London. Series A, Mathematical and Physical Sciences*, vol. 243, no. 865, pp. 251–288, Apr. 1951, doi: 10.1098/rsta.1951.0004.

[89] "Yeoh hyperelastic model for nonlinear finite element analysis," *Medium*, Jan. 17, 2020. https://getwelsim.medium.com/yeoh-hyperelastic-model-for-nonlinear-finite-element-analysis-6b45e59d2634

[90] K. Miller, "Testing Elastomers for Hyperelastic Material Models in Finite Element Analysis," in *Int. ANSYS Conf. Proc.*, 2002, pp. 1–13.

[91] G. Cao, B. Chu and Y. Liu, "Analytical Modeling and Control of Soft Fast Pneumatic Networks Actuators," IECON 2020 The 46th Annual Conference of the IEEE Industrial Electronics Society, 2020, pp. 2760-2765, doi: 10.1109/IECON43393.2020.9254517.

[92] Fabrication- Soft Robotics Toolkit. (n.d.). In softroboticstoolkit.com. https://softroboticstoolkit.com/book/pneunets-fabrication

[93] G. M. Whitesides, "Soft Robotics," *Angewandte Chemie International Edition*, vol. 57, no. 16, pp. 4258–4273, Mar. 2018, doi: 10.1002/anie.201800907.

[94] Z. Wang and S. Hirai, "Chamber dimension optimization of a bellow-type soft actuator for food material handling," *2018 IEEE International Conference on Soft Robotics (RoboSoft)*, Apr. 2018, doi: 10.1109/robosoft.2018.8404949.

Appendices

Appendix A: Datasheet for Eco-flex 00-30

Table 13. General properties

Product Type	Silicone Rubber
Appearance	Translucent
Applications/ Recommended for	Appliances and Healthcare / Medical
Labels/Agency Rating	ISO 10993-10
Key Features	Low Viscosity, Low shrinkage

Table 14. Physical Properties

Physical Properties	Value & Unit	Test Condition
Mixed Viscosity	3000 cps	after 7 days, at 23°C
Specific Gravity	1.07 g/cm³	after 7 days, at 23°C
Pot Life	45 min	after 7 days, at 23°C
Linear Mold Shrinkage	< 0.001 in/in	after 7 days, at 23°C
Cure time	4 hr	after 7 days, at 23°C
Specific Volume	26.0 cu.in./lb.	after 7 days, at 23°C

Table 15. Mechanical Properties

Mechanical Properties	Value & Unit	Test Condition
Durometer Hardness	00 - 30	after 7 days, at 23°C
Tensile Strength	200 psi	after 7 days, at 23°C
Tensile Modulus	10 psi	after 7 days, at 23°C
Tensile Elongation	900%	after 7 days, at 23°C

Mechanical Properties	Value & Unit	Test Condition
Tear Strength	38 pli	after 7 days, at 23°C
Maximum Service Temperature	-53 - 232 °C	after 7 days, at 23°C
Dielectric Strength	> 350 volts/mil	after 7 days, at 23°C

Appendix B: Material Constants of Eco-Flex 00-30 derived through material modelling

Table 16. Material coefficients of hyperelastic models obtained from ANSYS

HYPERELASTIC MODELS	COEFFICIENT NAME	CALCULATED VALUES	UNIT
NEO-HOOKEAN	Incompressibility Parameter D1	0	Pa^-1
	Initial Shear Modulus Mu	21712.05	Pa
	Limiting Value	-8.11937E+11	
	Residual	4.960794525	
ARRUDA- BOYCE	Incompressibility Parameter D1	0	Pa^-1
	Initial Shear Modulus Mu	19383.29547	Pa
	Limiting Network Stretch	6.27082607	
	Residual	3.511990628	
GENT	Incompressibility Parameter D1	0	Pa^-1
	Initial Shear Modulus Mu	21712.05	Pa
	Limiting Value	-8.11937E+11	
	Residual	4.960794525	
BLATZ-KO	Initial Shear Modulus Mu	42607.81785	Pa
	Residual	29.10572041	
MOONEY-RIVLIN 2 PARAMETER	Incompressibility Parameter D1	0	Pa^-1
	Material Constant C01	86.30052604	Pa
	Material Constant C10	10315.21126	Pa
	Residual	4.58760969	
MOONEY-RIVLIN 3 PARAMETER	Incompressibility Parameter D1	0	Pa^-1
	Material Constant C01	-161.2265173	Pa
	Material Constant C10	10798.26745	Pa
	Material Constant C11	3.405415914	Pa
	Residual	4.211841109	
MOONEY-RIVLIN 5 PARAMETER	Incompressibility Parameter D1	0	Pa^-1

HYPERELASTIC MODELS	COEFFICIENT NAME	CALCULATED VALUES	UNIT
	Material Constant C01	-204.8220731	Pa
	Material Constant C02	0.162656303	Pa
	Material Constant C10	8929.075303	Pa
	Material Constant C11	-5.032410487	Pa
	Material Constant C20	138.5950589	Pa
	Residual	1.959656398	
MOONEY-RIVLIN 9 PARAMETER	Incompressibility Parameter D1	0	Pa^-1
	Material Constant C01	-1678.878751	Pa
	Material Constant C02	946.0670013	Pa
	Material Constant C03	0.001098034	Pa
	Material Constant C10	9546.512215	Pa
	Material Constant C11	-1654.735597	Pa
	Material Constant C12	-0.072750706	Pa
	Material Constant C20	1343.537247	Pa
	Material Constant C21	-234.700926	Pa
	Material Constant C30	38.64652442	Pa
	Residual	1.477312654	
YEOH 1ST ORDER	Incompressibility Parameter D1	0	Pa^-1
	Material Constant C10	10856.025	Pa
	Residual	4.960794525	
YEOH 2ND ORDER	Incompressibility Parameter D1	0	Pa^-1
	Incompressibility Parameter D2	0	Pa^-1
	Material Constant C10	9392.0915	Pa
	Material Constant C20	50.93876918	Pa
	Residual	3.000602064	
YEOH 3RD ORDER	Incompressibility Parameter D1	0	Pa^-1
	Incompressibility Parameter D2	0	Pa^-1
	Incompressibility Parameter D3	0	Pa^-1
	Material Constant C10	8832.107433	Pa
	Material Constant C20	103.6430112	Pa
	Material Constant C30	-0.721438186	Pa
	Residual	3.001987444	
OGDEN 1ST ORDER	Incompressibility Parameter D1	0	Pa^-1
	Material Constant A1	2.445564396	
	Material Constant MU1	13368.39752	Pa

HYPERELASTIC MODELS	COEFFICIENT NAME	CALCULATED VALUES	UNIT
	Residual	2.005162907	
OGDEN 2ND ORDER	Incompressibility Parameter D1	0	Pa^-1
	Incompressibility Parameter D2	0	Pa^-1
	Material Constant A1	5.532693208	
	Material Constant A2	5.597389809	
	Material Constant MU1	45.98000662	Pa
	Material Constant MU2	45.98005423	Pa
	Residual	40.57315687	
OGDEN 3RD ORDER	Incompressibility Parameter D1	0	Pa^-1
	Incompressibility Parameter D2	0	Pa^-1
	Incompressibility Parameter D3	0	Pa^-1
	Material Constant A1	5.138471606	
	Material Constant A2	5.103681792	
	Material Constant A3	5.094973754	
	Material Constant MU1	66.14269022	Pa
	Material Constant MU2	66.1576383	Pa
	Material Constant MU3	66.16288709	Pa
	Residual	36.14908939	

Appendix C: Datasheet for Ender 3 Pro – FDM 3D Printer

Table 17. Properties of Ender 3 Pro

Property	Value
Brand Name	Creality 3D
Machine Model	Ender 3 Pro
Printing Technology	FDM (Fused Deposition Molding)
Item Weight	6.90 kilograms
Printing Size	220*220*250 mm
Filament Material	PLA, ABS, TPU, wood, copper, etc.
Model Number	BE0276A1
Printing Speed	<= 180mm/s, normal 30-60 mm/s
Printing Precision	±0.1 mm
Nozzle Diameter	Standard 4mm
Machine Size	440*420*465 mm
Hotbed Temperature	≤ 100 °C
File Format	STL, OBF, AMF
Slicing Software	Cura/Repetier-Host/Simplify3D
Power Supply	DC 24V 270W

Appendix D: Datasheet for PLA – 3D Printing Filament

Table 18. Mechanical properties of PLA

Mechanical Property	Value & Unit	Test Condition
Flexural Strength	103 MPa	3D Printing, XY-plane, 0.4 mm, 90% Infill
Flexural Modulus	3150 MPa	3D Printing, XY-plane, 0.4 mm, 90% Infill
Impact Strength, Notched Izod	5.1 kJ/m^2	3D Printing, 23°C, XY-plane, 0.4 mm, 90% Infill
Hardness, Shore D	83	3D Printing, XY-plane, 7 mm Thick Square, 0.4 mm Print core, 100% Infill
Tensile Modulus	2346.5 MPa	3D Printing, 1 mm/min, XY-plane, 0.4 mm, 90% Infill
Tensile Strength, Yield	49.5 MPa	3D Printing, 50 mm/min, XY-plane, 0.4 mm, 90% Infill
Tensile Strength at Break	45.6 MPa	3D Printing, 50 mm/min, XY-plane, 0.4 mm, 90% Infill
Elongation at Yield	3.30%	3D Printing, 50 mm/min, XY-plane, 0.4 mm, 90% Infill
Elongation at Break	5.20%	3D Printing, 50 mm/min, XY-plane, 0.4 mm, 90% Infill

Appendix E: Material used in previous literature and their properties

Table 19. Material used in previous literature for SPAs.

Author		Material	Shore Hardness (00)	Tensile Strength (MPa)	Tear Strength (N/mm)
P. Polygerinos et al.	[81]	Elastosil M 4601	70	6.5	30
K. M. de Payrebrune et al	[82]	Elastosil M 4601	70	6.5	30
T. Noritsugu et al	[83]	Composite	NA	NA	NA
S. Konishi et al.	[84]	KE 1606	70	4.3	12
B. Mosadegh et al.	[85]	Ecoflex 00-30	30	1.38	6.65
H. Li et al.	[86]	Composite	NA	NA	NA
Y. Li et al.	[87]	Composite	NA	NA	NA
P. Polygerinos et al.	[88]	Elastosil M 4601 (fibre reinforced)	70	6.5	30
G. Alici et al. (A1 model)	[89]	Elastosil M 4601	70	6.5	30
G. Alici et al. (A2 model)	[89]	Soft Translucent	54	2.76	NA
J. Wang et al.	[90]	Composite	NA	NA	NA
Z. Sun et al.	[91]	Ecoflex 00-30 (reinforced)	30	1.38	6.65
Y. Sun et al. (with Fabric)	[92]	Ecoflex 00-30 (reinforced)	30	1.38	6.65
Y. Sun et al. (Ecoflex 0030)	[92]	Ecoflex 00-30	30	1.38	6.65
This Research		Ecoflex 00-30	30	1.38	7.65
		Ecoflex 00-30 (Jamming)	30	1.38	8.65

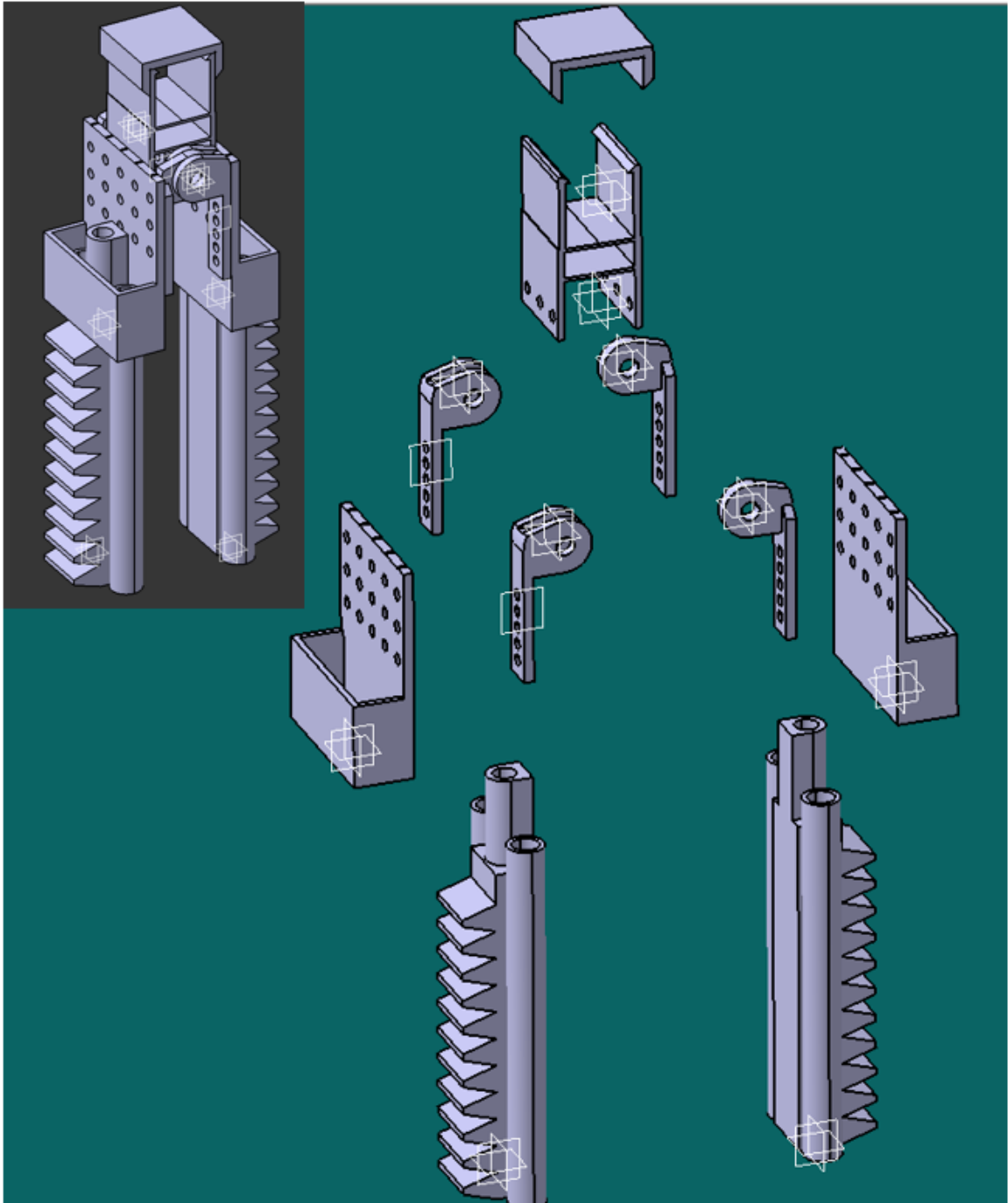**Appendix F: Design of the gripper**

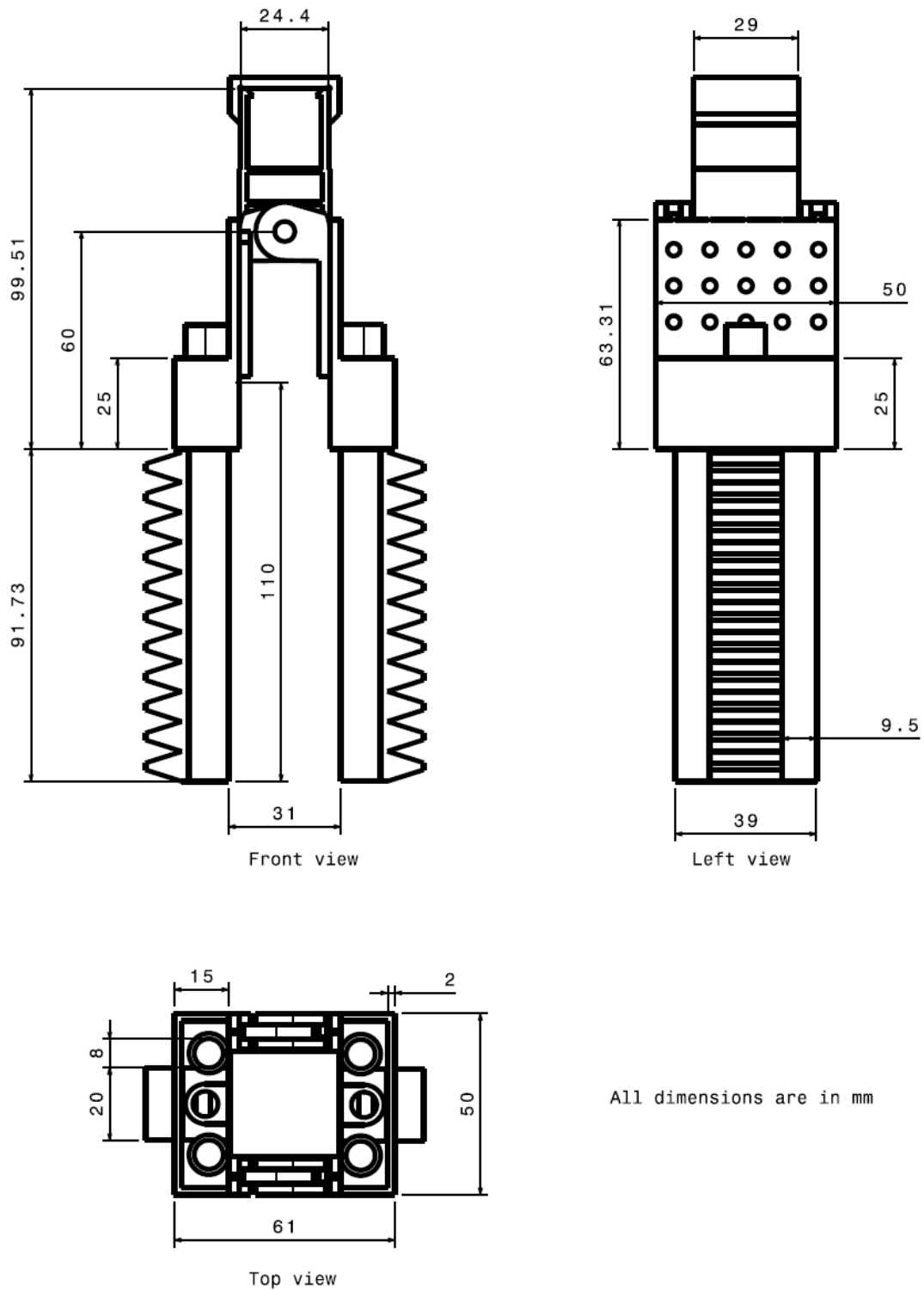Figure 79. Exploded view of gripper assembly

Figure 80. Drafting of the gripper assembly

Vita Auctoris

NAME: Abhishek Manoj Patel

PLACE OF BIRTH: India

YEAR OF BIRTH: 1996

EDUCATION: P. P Savani International School, Surat, India
2014

SRM Institute of Science and Technology, Chennai, India
2018, B. Tech.

University of Windsor, Windsor, ON
2022, M.A.Sc.